The effect of debris-flow sediment composition change on avulsion behavior and debris-flow fan development

MSc. Thesis Earth Science

A.A.J. Deijns

Student number: 4017439

Email: a.a.j.deijns@students.uu.nl

First supervisor: T. De Haas

Second supervisor: S. de Jong

24-05-2018

ABSTRACT

Debris-flow fans are widespread and often densely populated landforms that occur in regions with high relief. Avulsions cause a major risk for inhabitants as they occur sporadic and with current knowledge they are relatively unpredictable. Recent studies on debris-flow fan development and avulsion behavior reveal that the magnitude-frequency distribution and the associated flow-magnitude sequence of a debris-flow fan exerts a significant control on the occurrence of avulsions. Additionally, multiple studies also confirm the influence of debris-flow sediment composition on debris-flow morphology. Here, the effect of a change in debris-flow sediment composition per debris flow on the avulsion behavior and debris-flow fan development is investigated. This is done by creating two experimental fans where debris-flow sediment compositions are randomly extracted from a heavy-tailed double-pareto distribution with an average around 25 volumetric percent gravel. The sequence of volumes is distributed along a thin double-pareto distribution, where the majority of flow volumes cluster around a mean value of 5 kilograms sediment weight, but significantly larger and smaller flow volumes still occur sporadically. Comparing the experimental fans created in this study to a fan in De Haas et al. (*in review*) with similar flow-volume sequence but with uniform composition gives insight into the effect of a change in sediment composition for a debris-flow fan that is simultaneously subjected to a change in volumes. The effect of a sediment composition change on avulsion behavior and debris-flow fan development is best seen on a timescale of a couple of debris-flow events. From this study, three main conclusions can be established. (1) Debris-flow sediment composition is able to enhance or diminish the mobility of a debris flow with a given volume. Here, the volume dictates the main mobility of the debris flow but the mobility is influenced by related debris-flow sediment composition. (2) The influence of debris-flow sediment composition on debris-flow behavior is affected by local topography, where a complex topography diminished the influence of sediment composition, and where a plano-convex surface close to the apex enhances the influence of sediment composition (especially the low mobility of high-gravel debris flows). (3) The increased erosion with high-gravel debris flows is able to effectively enhance channelization. In contrast, gravel-poor debris flows are more likely to create a channel plug or deposit a solid body thereby influencing subsequent debris flows. This study shows that on a timescale of a couple debris-flow events, the effect of a change in sediment composition on debris-flow fan development can be such that it initiates avulsions or enhances the speed of avulsions. Although the debris-flow fan magnitude-frequency distribution seems to be the major controlling factor in fan development, these findings can have important implications for hazard mitigation and therefore an increasing focus on sediment composition during debris-flow fan research is required.

TABLE OF CONTENT

1. INTRODUCTION 1

2. LITERATURE REVIEW 3

2.1. Debris-flow definition and occurrence 3
2.1.1. Internal dynamics and morphological features 3

2.2. Debris-flow fan dynamics 4
2.2.2. Allogenic & autogenic effects. 5
2.2.3. Field observations 6
2.2.4. Experimental observations 9

2.3. Debris flow as a hazard for human life 14

2.4. Knowledge gap, research questions, and hypothesis 15

3. MATERIALS & METHODS 17

3.1. Experimental setup and procedure 17

3.2. Magnitude-frequency– and sediment-size distribution 18
3.2.1. Magnitude-frequency distribution 18
3.2.2. Debris-flow compositions & sediment-size distribution 19

3.3. Single debris-flow reference experiments 20

3.4. Data reduction 20
3.4.1. Reference experiments 20
3.4.2. Spatio-temporal evolution 21
3.4.3. Deposition & erosion patterns 21
3.4.4. Hazard map 22
3.4.5. Surface- and bed roughness 22

4. RESULTS 24

4.1. Reference experiments 24

4.2. Spatio-temporal patterns of development 27
4.2.1. Fan 01 27
4.2.2. Fan 02 37

4.3. Gravel fraction effect 44

4.4. Deposition & erosion patterns 46
4.4.1. Deposition 46
4.4.2. Erosion 47
4.4.3. Deposition-erosion ratio 48

4.5. Hazard map 49

4.6. Roughness 50
4.6.1. Surface roughness evolution 50
4.6.2. Average bed roughness 53
4.6.3. Body-snout comparison 55

5. DISCUSSION 57

5.1. Effects of surface roughness and gravel fraction on avulsion behavior and fan evolution. 57

5.1.1. Gravel fraction 57

5.1.2. Bed roughness 59

5.1.3. Grain-size sequences favoring or inhibiting avulsion. 61

5.1.4. Debris-flow composition affecting avulsion behavior and fan evolution on natural debris-flow fans 63

5.2. Scale effects. 63

5.3. Implications for debris-flow hazard mitigation 64

6. CONCLUSION 66

REFERENCES 67

SUPPLEMENTARY MATERIAL 71

1. INTRODUCTION

Debris flows and debris-flow fans are widespread landforms that occur in regions with steep relief (Iverson, 1997; Larsen et al., 2002; Jakob & Hungr, 2005; De Haas et al., 2015). Debris flows are gravity-driven mixtures of sediment and water that tend to form semi-conical shaped debris-flow fans originating from the mountains through the apex. Debris-flow fans are formed by the consecutive stacking of numerous debris-flow events. Debris flows and the debris-flow fans they deposit on are known for their unpredictability due to the erratic occurrence and behavior of the debris-flow events. They can lead to massive amounts of damage and fatalities, especially on densely populated debris-flow fans (Dowling & Santi, 2005). With an increasing population, the tendency to inhabit debris-flow fans increases (Dowling & Santi, 2005; Pederson, 2015). This leads to the need for understanding the debris-flow fan behavior on both the debris-flow scale as well as on the debris-flow fan scale.

The knowledge about debris-flow fan evolution over time is an important aspect in risk assessment and enhances the ability to predict potential threads. A key feature to debris-flow fan evolution is avulsion behavior, which is a channel shift on the debris-flow fan changing the main locus of activity. Avulsions on a debris-flow fan occur when the debris flow is able to overtop or break the levees of a main channel, thereby creating a new pathway for the sediment. Evidently, these situations can cause major damage to buildings, structures or people close to the main channel. It is therefore of importance to be able to predict avulsion behavior for hazard mitigation. As debris flows tend to occur sporadic, numerous years of monitoring is needed to derive avulsion-related trends (e.g. Marchi et al., 2002; Suwa et al., 2011). Debris-flow fan experiments can therefore be a solution for increasing knowledge on debris-flow fan development, as they are able to create a complete scale-sized fan in a significant lower amount of time. Several experiments are already done to derive debris-flow behavior and spatio-temporal patterns during debris-flow fan development (i.a. Hooke 1967; Iverson 1997, 2003, 2010; De Haas et al., 2015, 2016, *in review*).

De Haas et al. (2016; *in review*) created experimental debris-flow fans to understand their evolution and avulsion behavior. A uniform debris-flow composition was used and the magnitude-frequency distribution was changed per fan. This lead to a conceptual model in which a debris-flow fan is composed of multiple autogenic cycles for which one cycle consists of an avulsion and channelization phase, a backstepping phase and a searching phase. On those fans, the magnitude-frequency distribution and associated volume sequences were able to influence debris-flow fan development and avulsion behavior. Several authors however, also address the fact that not only debris-flow magnitude, but also debris-flow composition is able to affect debris-flow behavior and thus possibly debris-flow fan development (e.g. Whipple & Dunne, 1992; Iverson., 2010; De Haas et al., 2015). This hypothesis however, has not yet been experimentally tested. To be able to correctly predict debris-flow behavior on a debris-flow fan it is necessary to also understand the influence of changing debris-flow sediment compositions on debris-flow fan behavior.

The aim of this study is to find out if a sediment composition change for each consecutive debris flow on an experimental debris-flow fan is able to influence debris-flow fan development and avulsion behavior. To do so, two debris-flow fans are experimentally created where for every consecutive debris flow the sediment composition is changed along a heavy-tailed double-pareto distribution. With the experimental setup from De Haas et al. (2016; *in review*) I aim to reconstruct a scale-size debris-flow fan that is as close as possible to representing a natural debris-flow fan. From the scale-size debris-flow fans, spatio-temporal patterns are quantified to help derive trends of avulsion behavior and debris-flow fan development.

The structure of the thesis is as follows. In the next chapter, a literature review is given where debris-flow morphology, behavior and its hazardous tendency is described, debris-flow fan dynamics based on experimental and field observations are discussed and knowledge gaps and uncertainties are identified. Based on the literature review the research questions and hypotheses are then presented. This is followed by the spatio-temporal extraction and analysis methods. Then the spatio-temporal observations on the experimental debris-flow fan are described and summarized. Finally, the results are discussed and related to other studies (e.g. De Haas et al., 2016; *in review*).

2. LITERATURE REVIEW

2.1. Debris-flow definition and occurrence

Debris flows consist of poorly sorted masses of sediment, mainly composed of sand, gravel and cobbles saturated with water (Beaty 1963; Iverson 1997; Larsen 2002). Sediment concentrations generally exceed 40% (Iverson, 1997). Iverson (1997) mentions the importance of both solid and fluid forces vitally influencing the motion of debris flows, meaning that both fluid and solid material must act in concert to produce a debris flow.

Throughout the years, much discussion about debris-flow classification has occurred leading to a diverse nomenclature (e.g. debris slides, debris torrents, debris floods, mudflows, mudslides) (Iverson, 1997; Jakob & Hungr, 2005). This diversity reflects the diverse origin, composition and appearances of debris flows (Iverson, 1997). Hungr et al. (2001) defined debris flows as follows. "A debris flow is a very rapid to extremely rapid flow of saturated non-plastic debris in a steep channel". Pierson (2005) added that volumetric water content lies between 20% and 60%. Takahashi (2014) similarly mentions that both fluid and solid are important to create a continuous flowing fluid driven by gravity.

To get a general idea about natural debris-flow characteristics, Takahashi (2014) did a survey of debris-flow features in nature based on past records. Natural debris-flow magnitudes in that study ranged from 10^3 to 10^6 m^3. Velocities ranged from 0.5 to 20 m/s and runout distances ranged from 0.2 to 10 km. Although this study gives a good overall idea of debris-flow features in nature, it does not include small-scale experiments, which are also able to produce smaller-sized typically shaped debris flows (e.g. Iverson, 2010; Johnson 2012; De Haas et al., 2015;2016;*in review*).

Although slightly different, all definitions of debris flows emphasize interaction between sediment with a diverse composition and a fluid which saturates the mixture. Due to this interaction, debris flows are able to flow on both steep and shallow slopes (Pierson, 2005) and can carry enormous boulders downstream (Beaty 1963; Beaty 1990).

2.1.1. Internal dynamics and morphological features

Debris flows may form an alluvial- or debris-flow fan. Debris-flow fans are semi-conical depositional landforms, with a confined stream channel originating from a mountain catchment. The semi-conical shape is formed by radial shifting of the geomorphologically active sector by repeated avulsion (Blair & McPherson, 1994; 2009; De Haas et al., 2016). Surface morphology is mainly set by the nature of the channel system, spatial distribution of debris-flow deposits and the interaction between the debris flow and the channels (Whipple & Dunne, 1992). So, to understand processes occurring on the debris-flow fan scale, it is important to know the processes occurring on a single debris-flow scale. In this section, the internal dynamics of a debris flow and the general morphological features after deposition will be reviewed. In the next section, the dynamics causing differences in debris-flow deposition will be elaborated.

Figure 2.1 schematically depicts a debris flow in motion. Debris flows are characterized by a boulder-rich front with a relatively high gravel fraction, depending on the composition of the mixture (De Haas et al., 2015). It is followed by a more dilute tail. Both upward grain segregation of coarse particles and the shear at the bottom of the debris flow causes enhanced transport of coarse material to the flow front (Johnson, 2012). The accumulation of coarse material in the flow front favors inertial grain collision that increases frictional resistance (Iverson, 2010). As an addition to that, the higher pore fluid diffusivity of the coarse-grained flow front causes the high pore pressure generated within the debris

flow to dissipate, subsequently reducing the velocity of the flow front (Johnson, 2012). This decrease in velocity is most apparent on the edges of the debris flow, which results in the pushing aside of coarse debris and the subsequent creation of natural levees (according to experiments done by Jonson, 2012). These levees are able to self-confine the stream and therefore the runout distance increases. This process causes the levees to be mainly composed of coarse material (Whipple & Dunne, 1992; Iverson, 2010; Johnson, 2012; De Haas et al., 2015).

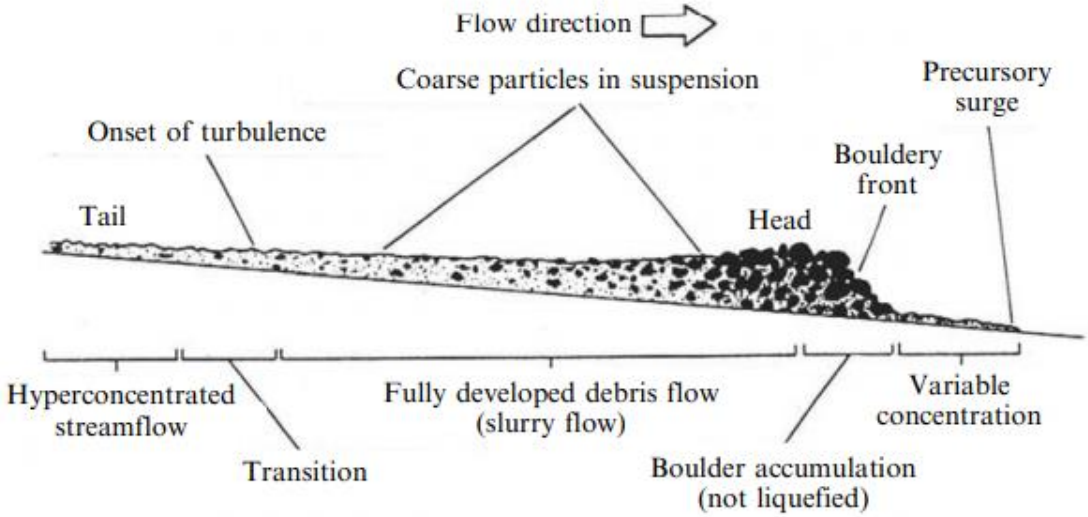

Figure 2.1: Schematic diagram of a debris flow with a boulder front (Jakob & Hungr, 2005).

Debris flows have been extensively studied as summarized in Blair & McPherson (1994). Typical debris-flow deposits are characterized by the presence of coarse grained levees, scoured channels and coarse grained linear debris-flow lobes with a snout (e.g. Beaty, 1963; Addison, 1987; Beaty, 1990; Whipple & Dunne, 1992; Suwa et al. 2009). Variation within the debris-flows deposit are observed as well. Besides the typical debris-flow snout lobes, also flatter headed lobes occur (Suwa & Okuda, 1983; Suwa et al., 2009; De Haas et al., 2015). Debris-flow deposits are mainly non-stratified and extremely poorly sorted. Also, normal and/or inverse grading is common in vertical sections (Pierson, 2005). On the fan scale a difference in slope in the proximal area is visible compared to the distal area (Whipple & Dunne, 1992; Blair & McPherson 1998). Due to the increased spreading and runout distance of less viscous water- and clay-rich debris flows the lower parts of the fan generally consist of a smoother and low-relief surface. On the other hand, this means that closer to the apex an overall increase in grain size may become apparent, with a steeper relief (as observed by Whipple & Dunne, 1992; Blair & McPherson 1998; Staley et al., 2006).

2.2. Debris-flow fan dynamics

To better understand the avulsion behavior and the spatio-temporal development of a debris-flow fan, it is important to understand the process occurring on a debris-flow scale and the debris-flow fan scale. In this section an extensive evaluation of debris-flow origin, trigger, behavior and dynamics is presented.

2.2.1. Origin and trigger of debris flows

A requirement for debris-flow occurrence is sufficient sediment production in the catchment (Blair & McPherson, 2009). Continuous sediment production is caused by incessant weathering and erosion of bedrock in the upper reaches of the catchment (Beaty, 1990; Wohl & Pearthree, 1991; Blair

& McPherson, 2009). This process leads to unconsolidated less stable material overlying bedrock in the source area (Savage & Baum, 2005). Processes causing weathering and erosion in these catchments are physical disintegration, chemical alteration, direct gravity fall, wet mass movements and erosion by running water (Beaty, 1990; Wohl & Pearthree, 1991; Blair & McPherson, 2009). Where an increase in relief increases the mean denudation rate and thus an increase in available unconsolidated material (Ahnert, 1970). A large consensus is present in the literature as to what triggers debris flows. High rainfall intensities during cloudbursts act as the main trigger in multiple studies (Beaty, 1963; Beaty, 1968; Wohl & Peartree, 1991; Helsen et al., 2002; Shieh et al., 2009; Suwa et al., 2011). Suwa et al. (2011) elaborated that high rainstorm intensities raise the subsurface perched-water stage in the deposits. These peaks in perched-water stage coincide with the increase in surface runoff, subsequently initiating debris flows.

The rainfall threshold, meaning the critical rainfall for debris-flow triggering, is variable and is changed by processes such as earthquakes and volcanic eruptions (Suwa et al., 2001; Lin et al., 2004; Shieh et al., 2009). Earthquakes and volcanic eruption trigger landslides, which enhance the amount of sediment material in the initiation area (Shieh et al., 2009). Loose material is taken up easier and thus the rainfall threshold for debris-flow initiation decreases. With time, the loose material is gradually transported downstream resulting in an increasing threshold.

The experimental setups from Iverson (2010) and De Haas et al. (2016) both used slightly different methods of replicating the triggering and release of the debris flow from the source area. In the experiments of Iverson (2010) sediment was deposited in a prism shaped wedge and was manually shoveled to get a homogenous mixture. Then the sediment was watered with subsurface channels and surface sprinklers for 2 to 6 hours before release. During the experiments of De Haas et al. (2016), sediment and water was deposited in a mixing tank. The sediment and water was thoroughly mixed resulting in a coherent homogenous mixture before it was released. The method of Iverson (2010) more closely represented natural circumstances with sprinklers acting as rain and subsurface channels acting as the subsurface perched-water stage, but due to decreased size within the De Haas et al. (2016) setup, the mixture was already thoroughly mixed to make sure that water was completely mixed within the sediment mixture. Although the methods slightly differed, the morphologic debris-flow features typical for natural debris-flows (e.g. levees, channel, coarse-grained snout) were able to form within both setups. It shows that with different methods, similar outcomes can be achieved, for this study the setup of De Haas et al. (2016) works sufficiently regarding origin and trigger.

It must be noted that knowledge on the origin and source area of the debris-flow event is required so that the exact composition of the sediment mixture can be determined.

2.2.2. Allogenic & autogenic effects.

Debris-flow fan dynamics are subjected to both autogenic and allogenic processes. This means that patterns or evolution of debris-flow fans can be accounted to at least one of these processes. Autogenic effects are intrinsic dynamics of the alluvial system that cause them to shift laterally by avulsion (Ventra & Nichols, 2014; De Haas et al., 2016), whereas allogenic effects are extrinsic dynamics such as, plate tectonics, climate and base level change (e.g. Ritter et al., 1995). Ventra & Nichols (2014) emphasize the significance of autogenic effects at large spatial and temporal scales. For a debris-flow fan they attribute the semi-conical form as a direct result of autogenic processes. However, they also state that the role of autogenic effects on alluvial fans is poorly constrained.

In this study the autogenic processes acting on a debris-flow fan will be further elaborated on. As a succession on the study of De Haas et al. (*in review*) where the effect of volume changes on the fan evolution is discussed, in this study the effect of sediment composition on the fan evolution will be

investigated. This will eventually give a more complete and true to nature vision on the autogenic processes acting on a debris-flow fan.

2.2.3. Field observations

Due to the sporadic nature of natural debris flows, quantitative observations of debris-flow dynamics are limited (McCoy et al., 2010). Nonetheless, several authors managed to capture sufficient information on past debris flows to interpret debris-flow fan dynamics (e.g. Marchi et al., 2002; Suwa et al., 2011). Before the presence of advanced techniques observations were based on stories of eyewitnesses. Beaty (1963) gives an example of debris-flow behavior and reconstruction based on the stories of eyewitnesses and aerial photographs (figure 2.2). He concluded that two and a half hours after a heavy thunderstorm, debris flows came advancing down between 2 and 2.5 meter per second in a series of waves and surges accompanied by strong noises likened to "the sound of a thousand freight cars bumping together simultaneously". This lasted for approximately 45 minutes and was followed by high water flow draining from the debris flow for the next 24 to 48 hours. Debris deposition occurred in relatively narrow strips extending radially from the apex.

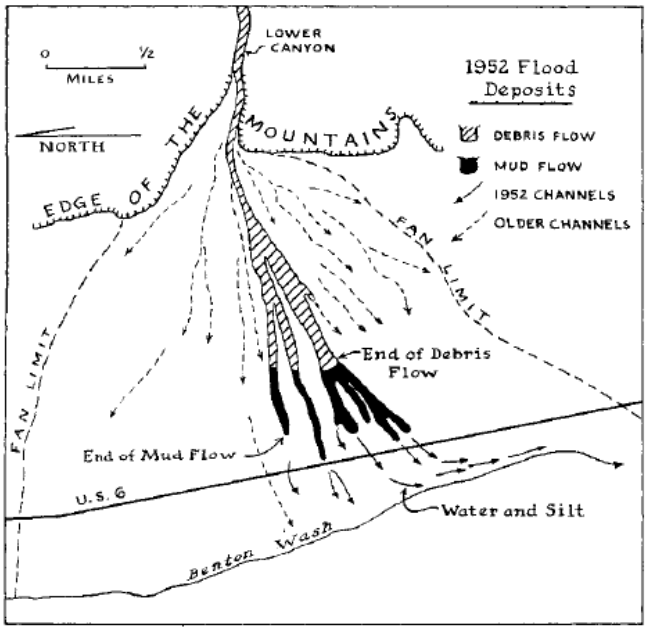

Figure 2.2: Sketch of a typical debris-flow fan, showing the characteristic elongate lobate deposits on a radially extending fan. The debris flows originate from the mountains and flow via the apex onto the debris-flow fan (Image from Beaty, 1963).

Nowadays debris flows are monitored with more advanced techniques (e.g. Marchi et al., 2002; McCoy et al., 2010; Suwa et al., 2011). During a period of twelve years, Suwa & Okuda (1983) monitored debris-flow behavior on the Kamikamihori fan at the eastern foot of Mt. Yakedake, Japan. They discerned periods of channel formation, channel blockage, and avulsion. De Haas et al. (2017) continued monitoring the spatio- temporal patterns of this fan and evaluated the debris-flow fan development with inclusion of the results of Suwa & Okuda (1983) (Figure 2.3). From figure 2.3 it becomes evident that multiple sequences of backstepping and avulsion occurred. For example, a backstepping sequences followed up by an avulsion occurred during 1978 (red debris flows), where debris flows progressively deposited upstream causing an avulsion as a high-volume debris flow was unable to use former channel due to this backstepping sequence. A remarkable sudden shift in channel direction took place from 1980 until 1983 during three subsequent debris flows. The first debris flow had a restricted runout and formed a channel plug. The following debris flows couldn't overtop that channel plug and were forced to make another channel thereby initiating a large avulsion.

As opposed to the gradual backstepping and filling of a newly formed channel, channel filling can also occur within one debris-flow event. McCoy et al. (2010) observed multiple surge events following an initial debris flow. The subsequent surges showed progressively shorter travel distances and thus deposited within the levees of the initial debris flow from the same event.

These observations are in accordance with the conceptual model for debris-flow fan evolution from Whipple and Dunne (1992). They state that debris-flow depositional patterns are controlled by the

channel and the physical properties of the debris flow, meaning that channel avulsion, and the subsequent shift of depositional loci is driven by in- channel deposition of relative immobile debris flows (plug formation). This tendency to avulse is particularly present when the surrounding regions are low relative to the present debris-flow locus (Dühnforth et al., 2007). This tendency is related to compensational stacking, which is defined as the tendency for sediment transport systems to preferentially fill topographic lows (Straub et al., 2009; Pederson et al., 2015). When compensational stacking occurs, the debris-flow fan will laterally display shallow slopes. On the other hand, when no compensational stacking occurs steep slopes will form laterally and no topographic lows will be occupied. When compensational stacking is perfect, avulsions will occur more often.

From field observations, it can be deduced that on both short and long timescales dynamics occur that affect debris-flow fan development. On shorter timescale, channels can be blocked by sediment plugs resulting from several flow surges or large boulders (e.g. McCoy, 2010). These blockages cause subsequent flows to avulse and create a new pathway or locus on the fan. On longer timescales the development of the fan can be influenced by the gradual shifting of the depositional locus to a topographically lower part of the fan (Whipple and Dunne, 1992). De Haas et al. (2017) found similar trends (e.g. figure 2.3). They added that the magnitude-frequency relationship and the flow-volume sequence strongly influence spatio-temporal debris-flow fan patterns. Meaning that on one side large flow volumes are able to overtop channel plugs and maintain channel formation and on the other side, when small flow volumes occur channel plugging is enhanced. The sequence in which these flow volumes occur is important as a series of very large flow volumes will react differently than two small flow volumes followed by a very large one (as also confirmed in small-scale experiments: De Haas et al., *in review*).

Observations show that debris-flow mobility is therefore of importance during debris-flow fan development. Debris-flow volume seems to play an important role in that. However, observations also show that mobility is also dependent on sediment composition. For example, on the Kamikamihori fan a relative matrix-poor boulder-rich debris-flow behaved relatively immobile and thus created a channel plug (Okuda et al., 1981; Suwa et al., 2009). Because debris-flow composition is not easily acquired in the field and the time to derive any trends on a natural debris-flow fan via monitoring is extensive, the effect of composition on avulsion behavior and debris-flow fan development is yet scarcely researched. Experimental observations are therefore a key requirement as exact compositions and volumes of debris flows can be measured and related to their depositional behavior and geometry.

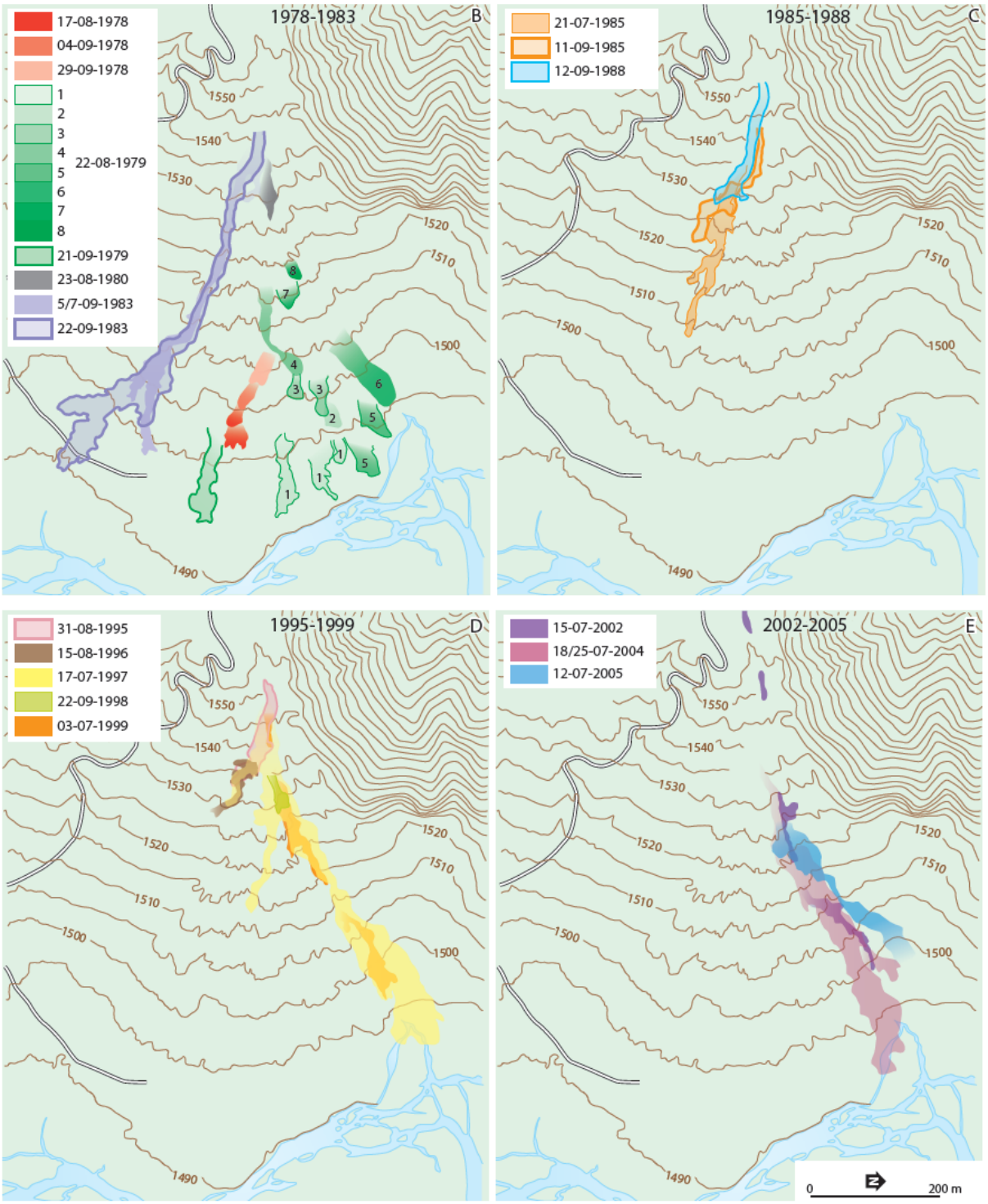

Figure 2.3: Field observations on the Kamikamihori fan from 1978 to 2005. The figure is partially based on observations of Suwa & Okuda (1983). Debris-flow fan development follows a quasi-cyclic pattern of backstepping, channel plugging and avulsion. Image from De Haas et al. (2017).

2.2.4. Experimental observations

Debris-flow experiments can be divided into experiments focusing on properties and behavior of single debris flows (c.f. Iverson, 1997; Iverson et al., 2010; De Haas et al., 2015), and experiments focusing on debris-flow fan spatio-temporal dynamics (c.f. Hooke, 1967; De Haas et al., 2016, *in review*). Both small- and large-scale experiments have been carried out to deduce debris-flow behavior and debris-flow fan dynamics (e.g. Hooke, 1967; Iverson, 1997; Major, 1997; D'agostino et al., 2010; Iverson et al., 2010; Johnson, 2012; De Haas et al., 2015, 2016, *in review*).

Large scale experiments on single debris-flow behavior were carried out in the United States Geological Survey (USGS) debris-flow flume (e.g. Major, 1997; Iverson, 2010). Smaller scaled experiments on both single debris-flow behavior and debris-flow fan dynamics were carried out at the University of Utrecht (respectively De Haas et al., 2015 & De Haas et al., 2016; *In review*). In both flumes the typical debris-flow morphologies (self-formed levees, an elongate depositional lobe and a coarse-grained snout) were created. Although Iverson et al. (2010) suggest that dynamic similarity between natural and small-scale experiments is unattainable due to disproportionally large yield strengths, viscous flow resistance and grain inertia, De Haas et al. (2016; *in review*) managed to simulate quasi-realistic debris-flow fan development patterns comparable to nature by consecutive stacking of small-scale debris flows.

In this section, first the observations on single debris-flow properties and behavior will be discussed and second, this will be followed up by a summarization of results based on the debris-flow fan dynamics experiments.

2.2.4.1. single debris-flow behavior

Understanding the behavior of single debris-flow events is important to be able to interpret patterns and dynamics occurring on natural and experimental debris-flow fans caused by the consecutive stacking of single debris-flow events. Major (1997) emphasizes the importance of water volume within the debris flow as a control on behavior. From his experiment in the USGS flume (figure 2.4), it is concluded that under-saturation of the debris flows leads to relatively thick lobes, with steep and blunt margins. Also, subtle to prominent arcuate ridges dominate surface morphology. On the other hand, saturated debris flows lead to different results. The saturated deposits were longer and thinner, typically had low relief surface morphology and poorly developed levees were visible. Surging behavior was visible within the saturated flow where each surge overrode the former deposit resulting in an increased length.

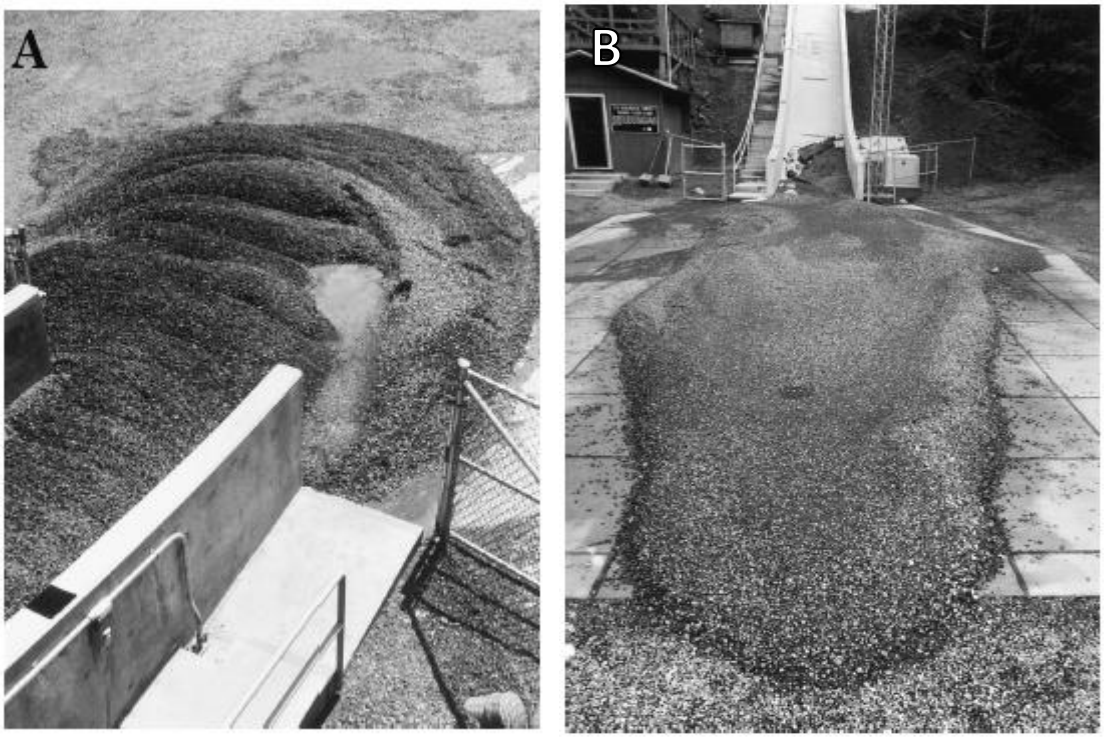

Figure 2.4: USGS large-scale flume experiments. (A) Undersaturated debris flow: low runout distance, thick deposit, no levees, pronounced arcuate ridges. (B) Saturated debris flow: long and thin deposits, levee formation. Image from Major (1997).

Iverson et al. (2010) states that within the USGS flume for any fixed combination of debris-flow composition and bed roughness, debris-flow morphology is reproducible, irrespective of differing details. They carried out 28 large-scale experiments with changing boundary conditions. For these experiments, they used two different sediment mixtures, one consisting of sand-gravel (SG) and the other consisting of sand-gravel-mud (SGM). The outflow plain consisted of a rough bed. Figure 2.5 presents two representable debris flows for each sediment mixture. When solely looking at deposit geomorphology a clear distinction is visible between the two sediment mixtures. The SGM mixture yielded deposits longer, thinner and more tabular than the SG mixture. Also, well-developed gravel-rich lateral levees were formed close to the flume mouth. Lower levees were overtopped by muddy liquefied debris. The SG deposits were half as long and twice as thick as the SGM deposits. Large gravel-rich levees were formed and due to the lack of trailing, liquefied mud, they were rarely overtopped (Iverson et al., 2010). These results give an indication of the different effects of sediment composition on the morphology and behavior of debris flows.

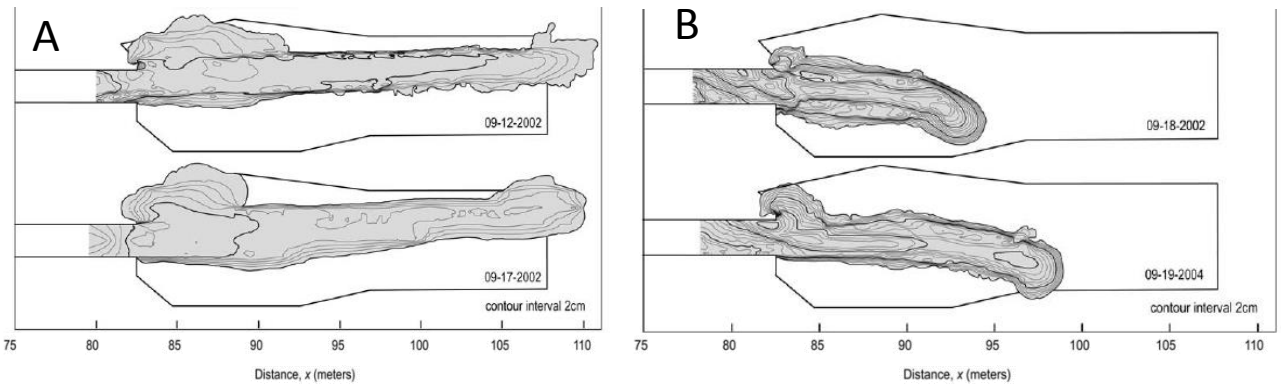

Figure 2.5: USGS experiment: Relative difference dependent on debris-flow sediment composition. A: Sand-Gravel-Mud sediment mixture, longer runout, Gravel-rich levees. B: Sand-Gravel sediment mixture, thicker deposits, shorter runout, large gravel-rich levees. Image from Iverson et al. (2010).

One can thus imagine that on the fan scale differences in debris-flow composition can have a large impact on the evolution of the fan. De Haas et al. (2015) elaborated on this topic and experimented with numerous different sediment compositions. The results of that study can be categorized in debris-flow deposition, runout distance and deposit morphology. According to this study, debris-flow deposition is mainly influenced by the friction at the frontal flow margins, which in its turn is related to the decay of pore fluid pressure. An increase in frontal friction is seen with an increasing gravel fraction and a decrease in clay fraction. An increase in gravel fraction will increase the accumulation of gravel in the frontal part of the debris flow. This leads to increased amounts of diffusivity and friction and thus early deposition. An exception to this rule is found within viscous flows with high clay fractions. During these debris flows, gravel accumulation at the flow front and diffusivity are low, but early deposition occurs as well. In this case they hypothesized deposition to be determined by high effective viscosity and yield strength.

De Haas et al. (2015) concluded that debris-flow runout distance strongly depends on flow momentum. Debris-flow behavior patterns that became apparent were (figure 2.6): (1) Large accumulations of coarse particles at the frontal flow margins decrease runout distance and area, however between 20% & 60% gravel fraction, the runout remained fairly constant. (2) High clay fractions reduce flow velocity and runout above the optimum value of 0.22 volumetric percent clay. (3) Runout distances and runout areas become larger for increasing water fractions. Additional conclusions not visible in figure 2.6 were that increasing debris-flow volume enhances runout and larger channel and outflow plain slopes result in larger runout distances and areas. Regarding deposit morphology, figure 2.6 shows that features such as levee height and lobe thickness are largely controlled by debris-flow composition. Similar results became apparent from the large-scale experiments by Iverson et al. (2010).

The study of De Haas et al. (2015) shows that an increase in gravel results in increasing frontal accumulation of gravel particles, which in its turn results in a decrease in runout and an increased lobe height. Also, an increase in water fraction increases the deposit area because of the increased spreading, but the lobe height is effectively reduced. With an increase in clay fraction up to 0.22 volumetric percent, deposit area increases and lobe height decreases. But, after a clay fraction of 0.22 volumetric percent deposit area started to decrease drastically as well as the lobe height. All of these are examples of debris-flow composition effectively influencing the behavior of debris-flow lobe characteristics. The conclusions of the study of De Haas et al. (2015) therefore strengthen the hypothesis that debris-flow composition has a significant effect on debris-flow behavior and thus debris-flow fan evolution.

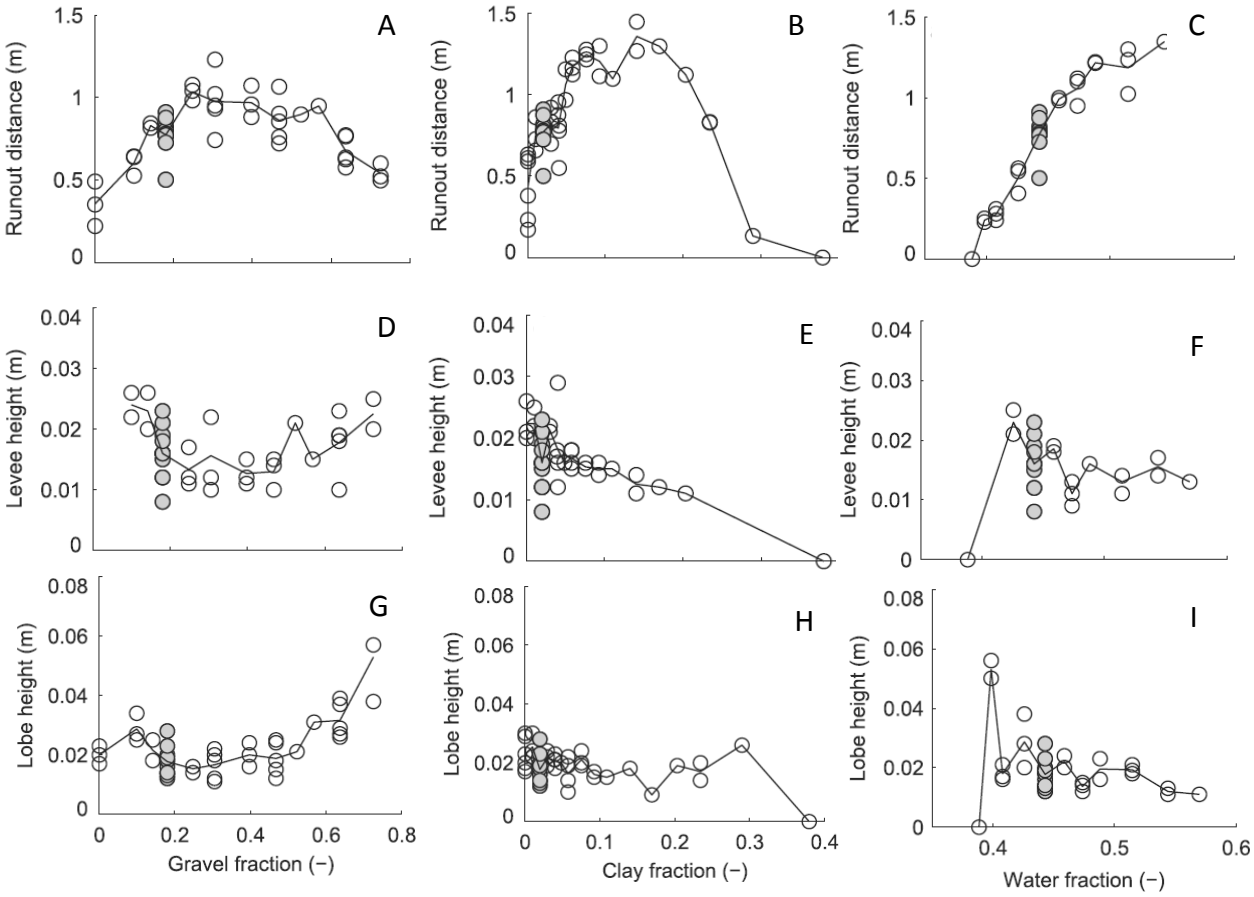

Figure 2.6: Effects of debris-flow composition on runout distance, levee height and lobe thickness A-C: Gravel fraction, D-F: Clay fraction, G-I: Water fraction. Images from de Haas et al. (2015).

Another important, but debated, potential influence on debris-flow runout and morphology is the infiltration of water and sediment from the debris flow within a gravel-rich bed. A process experimentally replicated by Hooke (1967) and Milana and Tietze (2002) and observed in the field by Milana (2010). It is known as the "Sieve Lobe Paradigm". The definition of a sieve lobe as first presented by Hooke (1967) is the percolation of water originating from a debris flow through coarse bed material subsequently inhibiting further transport. Blair & McPherson (1992; 1995; 2009) contested this paradigm repeatedly by denying the occurrence in natural flows. They stated that debris flows represented as sieve lobes originally were matrix-rich due to the production of muds from the catchment bedrock, and that the matrix was removed due to secondary overland flow. This was supported by the fact that matrix-rich deposits were abundant at depth. Milana (2010) observed potential sieve lobes in the field and confirmed the discharge loss due to infiltration when encountering such a lobe.

2.2.4.2. Debris-flow fan evolution and dynamics

Debris-flow fan dynamics have been scarcely reconstructed in physical scale experiments (e.g. Hooke, 1967; De Haas et al., 2016, *In review*). For the purpose of this study, the physical experiments of De Haas et al. (2016; *in review*) will be discussed. De Haas et al. (2016) created a small-scale fan consisting of debris flows, uniform in size with uniform compositions. De Haas et al. (*in review*) varied the volume of each debris flow, while retaining the same composition, and thus changed the magnitude-frequency distribution. This in order to simulate more natural circumstances.

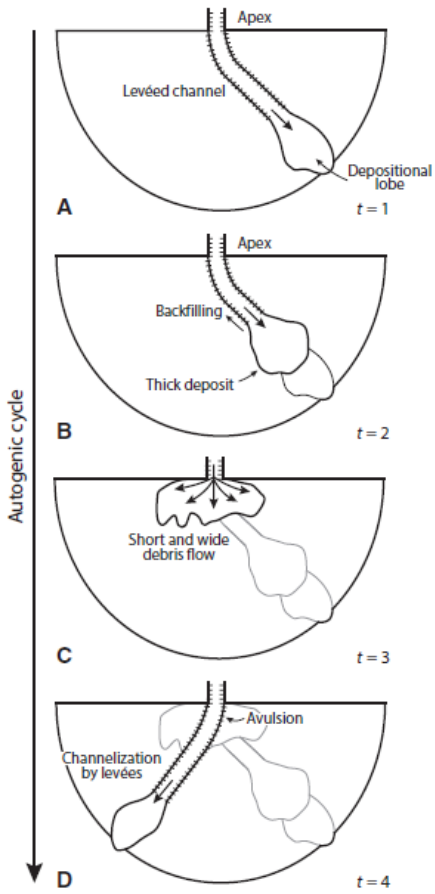

Figure 2.7: Debris-flow fan avulsion cycle model by de Haas et al. (2016). A: Depositional lobe. B: Backfilling sequence. C: Short and wide deposition (searching phase). D: Avulsion and channelization.

The physical scale experiment of De Haas et al. (2016) and De Haas et al. (*in review*) were under constant extrinsic forcing, meaning that the outflow plain and channel slope remained stable and no change in climatic conditions occurred. Based on the results of that experiment, they designed a conceptual model of autogenic dynamics on debris-flow fans (figure 2.7). In this model, the debris-flow fan evolution consists of multiple autogenic cycles. These cycles consisted of sequences of (1) backfilling, (2) searching phase and (3) channelization. During the backfilling phase, sediment is progressively deposited upstream in the present channel. This eventually leads to a situation where the apex cross-profile is plano-convex. This commences the searching phase, where sediment is spread laterally in all directions. Preferential paths receive most of the sediment, initiating avulsion, and channelization commences. During the channelization phase, preferential paths receive most of the sediment and each following debris flow will effectively follow this path, resulting in more effective levee formation. Eventually a channel is formed. From this point the cycle repeats itself again. The occurrence of those cycles is in accordance with field observations on natural debris-flow fans as previously mentioned (e.g. Suwa & Okuda, 1983; Whipple & Dunne, 1992; McCoy et al., 2010).

The occurrence of varying flow magnitudes leads to contrasting avulsion mechanisms as proposed by De Haas et al. (*in review)*. During their experiment, similar phases of the autogenic cycle as seen during the experiment by De Haas et al. (2016) were distinguished. However, clear distinctions were caused by differences in debris-flow magnitude-frequency. One of them being the fact that large volumes were able to overtop channel levees and induce avulsion within one single debris-flow event. Also, rapid channel closure could occur if the volume sequence was favorable. Meaning that when a debris flow consisted of a small volume, it could act as a channel plug, blocking incoming debris flows and force them to overtop channel levees. In the study of De Haas et al. (*in review*), they used two different magnitude-frequency distributions, one being a thin double-pareto distribution and one a wide double-pareto distribution. For the wide double-pareto distribution the variation between volumes is larger, whereas for the thin double-pareto distribution the variation is less and volumes are closer to the mean.

Differences in results were noteworthy. The fan with the thin double pareto-distribution showed more sequences of channel plugging and rapid backstepping than the fan with the wide double-pareto distribution. This can mainly be attributed to the fact that with a wide double-pareto distribution a higher quantity of larger-volume debris flows occur and the effective plugging of the channel decreases. The results of the study lead to the idea that an optimal magnitude-frequency distribution exist for maximizing avulsion frequency. On the other hand, an effective decrease in avulsion frequency is seen when large flows are abundant. This decreases the occurrence of channel plugging and thus the probability of avulsion. Also, with the absence of large flows, the probability of avulsion

decreases, because there are fewer flows which are able to overtop the main channel and create a new channel.

2.3. Debris flow as a hazard for human life

Due to the destructive tendency of fast-moving debris flows, significant damage and fatalities are caused worldwide (Dowling & Santi, 2014). Human population expansion into mountainous regions during the last decades has forced people to live close to debris-flow fans resulting in increased risks (Dowling & Santi, 2014; Pederson et al., 2015). Studies on debris-flow hazard have focused on structural damage (e.g. Totschnig et al., 2011; Jakob et al., 2012) and the actual amount of fatalities (e.g. Dowling & Santi, 2014). Structural damage assessment is based on hazard probability, spatial and temporal probability of impact and vulnerability of the element at risk (Totschnig et al., 2011; Jakob et al., 2012; Van Asch., 2013), whereas the fatalities have been assessed by for example, relating to socio-economic factors (Dowling & Santi, 2014).

In light of this study, only an indication of fatalities is given in order to emphasize the importance of study on this subject. The survey of Dowling and Santi (2014) revealed that during the period from 1950 until 2011, two hundred and thirteen fatal debris flows occurred. These debris flows caused a total of 77,779 human fatalities. The amount of fatalities per debris flow differ greatly ranging from debris flows being fatal to just one person, to one of the largest debris flows being fatal to a large part of a state (figure 2.8).

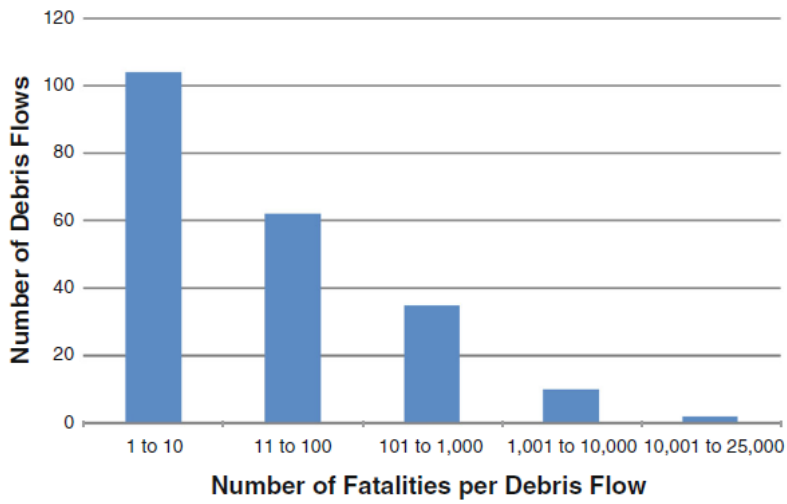

Figure 2.8: Fatalities per Debris flow. Image from Dowling & Santi (2014).

One event of multiple debris flows was able to completely inundate large portions of the state of Vargas in Venezuela, leading to the death of 19.000 people. As part of this event, a large portion of the town of Caraballeda which was constructed on a debris-flow fan got inundated, evidently emphasizing the importance of understanding processes occurring on the debris-flow fan. A conclusion from Dowling and Santi (2014), looking at spatial, temporal, physical and socio-economic factors, is that large differences are seen in the fatalities from debris flows in developing countries opposed to advanced countries. Developing countries were characterized by significant poverty, corrupt governments and weaker healthcare system. All factors emphasizing the inability of a country to cope with such disasters. Figure 2.9 shows this difference between developing and advanced countries.

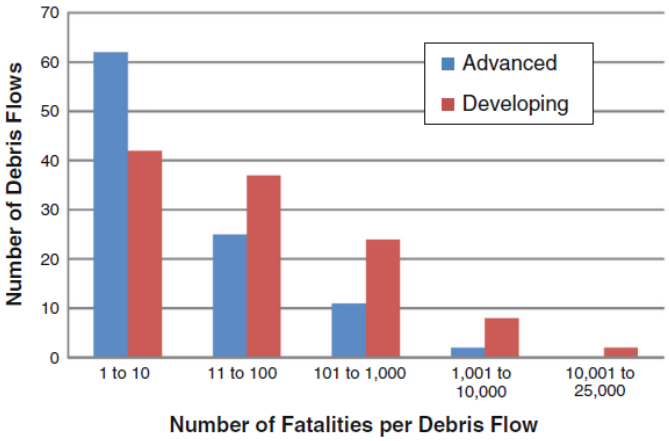

Figure 2.9: Number of Debris flow fatalities of advanced and developing countries. Image from Dowling & Santi (2014).

Santi et al. (2011) mentions the difference in debris-flow risks between different groups within a country. The most vulnerable groups are economically restricted to live in relatively inexpensive and dangerous locations. This leads people to live on landforms such as debris-flow fans. Also, those people are not able to invest in mitigation methods and are therefore extra susceptible to large casualties during such events. So, when increasing knowledge on avulsion behavior and debris-flow fan development the predictability of debris flows increases. Mitigation methods can therefore be made more focused on particular debris-flow events and evacuation strategies can be sharpened.

2.4. Knowledge gap, research questions, and hypothesis

It becomes evident that debris-flow fan dynamics experiments are not abundant. To solely capture internal dynamics of a debris-flow fan, autogenic effects should be thoroughly researched. This will enhance future prediction on the natural occurrence of debris flows. Debris-flow fan dynamics experiments are therefore necessary. Multiple authors address the fact that debris-flow composition significantly changes runout and lobe geometry (Whipple & Dunne 1992; Iverson, 2010; De Haas et al., 2015). However, the significance of this effect on the avulsion behavior and the development of debris-flow fans has not yet been tested within an experimental setup. This study will be a follow up on the De Haas et al. *(in review*) study and will examine the effect of a changing debris-flow gravel content on the debris-flow fan avulsion behavior and spatio- temporal development.

The main question that is going to be addressed in this study is: What is the effect of a change in debris-flow composition on avulsion mechanism and debris-flow fan development? This question arises directly in relation to the studies of De Haas et al. (2015; 2016; *in review*). Various sub-questions will address the main question in more detail.

- What is the effect of debris-flow composition on the behavior of single debris flows and does it influence the evolution of the fan, when using a set magnitude-frequency distribution?
- Is there a noticeable difference in avulsion behavior related to the effect of a debris-flow sediment composition change?
- What is the effect of terrain roughness on debris-flow behavior, does it influence runout distance and is there evidence of the sieve lobe paradigm?
- Is there a series of compositions favoring avulsion as well as a series of composition inhibiting avulsion?

Evidence from field and experimental observations suggest that runout, levee height, lobe height and other geomorphologic features are influenced by a change in sediment composition. These observations suggest that a change in composition may change the dynamics and evolution of a debris-

flow fan. This can thus also change avulsion frequency and behavior. However, it is yet uncertain how much effect it has compared to a change in magnitude-frequency. Experimental observations from De Haas et al. (2015) and Iverson (2010) suggest that bed roughness influences particle segregation and granular agitation within a debris flow. In which a rougher bed promotes particle segregation and granular agitation. This leads to the promotion of gravel-rich lateral levees, which in turn can increase flow runout. However, with the sieve lobe paradigm in mind it might have a negative effect on runout especially in large gravel-rich lobes, where water is able to infiltrate the pore-rich material.

3. MATERIALS & METHODS

Two small-scale debris-flow fans are created during the experiments. Both the methodology and experimental setup are based on the experiments of De Haas et al. (*in review)*. Only now, the sediment composition per debris flows is changed as well. This setup enables the creation of debris flows with their distinct deposit geomorphology such as channels, lobate snouts and levees, similar in shape to debris flows occurring in nature (i.a. Beaty, 1990; Whipple & Dunne, 1992; Suwa et al. 2009). De Haas et al. (2015) extensively tested the experimental setup and concluded that both runout distance and width-to-depth ratio of the experimental debris flows are in range of natural debris flows. Runout distance however, is relatively short due to high friction and an increased yield strength.

3.1. Experimental setup and procedure

The experiments are carried out with the setup depicted in figure 3.1. The experimental setup consists of a mixing tank connected to a 2 m long straight channel inclined with an angle of 30° which in its turn is connected to an outflow plane with an inclination of 10°. In the mixing tank, sediment and water is actively mixed into a coherent mixture for a few seconds before releasing. The channel bed and sidewalls are covered in sandpaper (grade 80; average particle diameter 0.19 mm) to simulate natural bed roughness. The outflow plane is covered in approximately 0.5 cm unconsolidated coarse sand. The coherent mixture of sediment and water is released out of the mixing tank by electromagnetically opening of the gate. Exactly 1.5 seconds after opening of the mixing tank gate a hatch opens 0.76 m above the transition from the channel to the outflow plane. After 1.5 seconds the debris flow already passed the hatch and therefore only the water rich debris-flow tail is diverted. This is done to prevent from excessive amounts of erosion within the debris-flow fan, which is a scale problem within this setup.

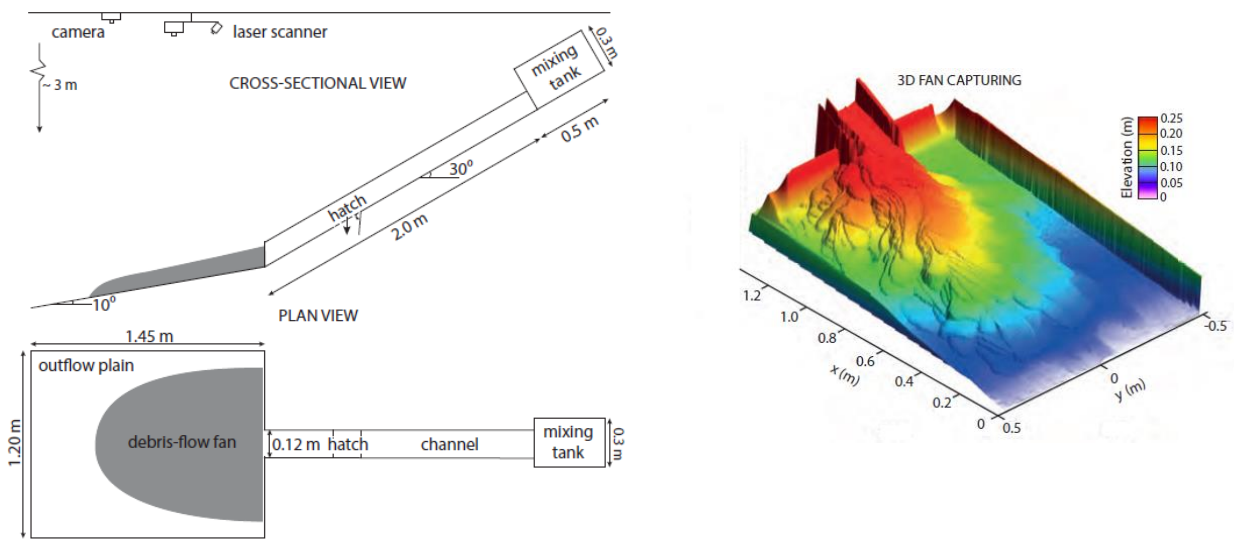

Figure 3.1: Experimental setup with side- and top view (as used in De Haas et al. (2015; 2016; in review)). The 3D fan on the right is the interpolation of the point cloud captured with the Vialux z-Snapper 3D scanner. Image from De Haas et al. (2016).

The debris-flow fans within this setup are created by stacking of consecutive debris flows. After each debris-flow event the fan is dried for at least an hour to inhibit reactivation of previous debris-flow deposits by subsequent debris-flow events. The two debris-flow fans that are created during this experiment consist of 77 and 79 individual debris flows. Outflow plane base level remains on a fixed level to solely investigate autogenic response on debris-flow evolution. The experiments continue until

the feeder channel is severely blocked by the continuous accumulation of sediment, so that debris flows are no longer able to reach the fan.

The setup also consists of two ordinary cameras' and one laser scanner. During every single debris-flow event a video is captured of the movement and deposition of the event. This is done with a Canon Powershot A650 IS on a tripod directed straight on the channel and the fan. A Canon Powershot A640 camera captures images from above the outflow plane to image fan topography. A Vialux z-Snapper 3D scanner (Vialux Messtechnik + Bildverarbeitung GmbH, Chemnitz, Germany) captures deposit morphology at sub-millimeter resolution and accuracy. This 3D scanner creates a 3D point-cloud from a fringe pattern projector (Hoefling, 2004). This point cloud is, via natural neighbor interpolation, converted into a gridded digital elevation model (DEM) of 1 x 1 mm spatial resolution.

3.2. Magnitude-frequency– and sediment-size distribution

3.2.1. Magnitude-frequency distribution

The thin double-pareto magnitude-frequency distribution from De Haas et al. (*in review*) is used during both experimental fans. The exact same magnitude sequence is used during this experiment, which enhances the comparability between the fans so it is possible to evaluate the influence of composition change on debris-flow fan development. The thin double-pareto magnitude-frequency distribution is chosen over the wide double-pareto magnitude-frequency distribution also used in De Haas et al. (*in review*). It becomes evident from test fans leading up to the final created fans that a wide double-pareto magnitude-frequency distribution and thus the occurrence of both very large and very small debris flows inhibits the evolution of the fan within this setup so that after a small amount of debris flows the channel is already filled up and unable to properly route debris flows. The thin double-pareto magnitude-frequency distribution from De Haas et al. (*in review*) only contained 70 debris flows. Because the debris-flow fans turn out to consist of 77 and 79 individual debris flows, extra debris-flow magnitudes are added along the same distribution (figure 3.2).

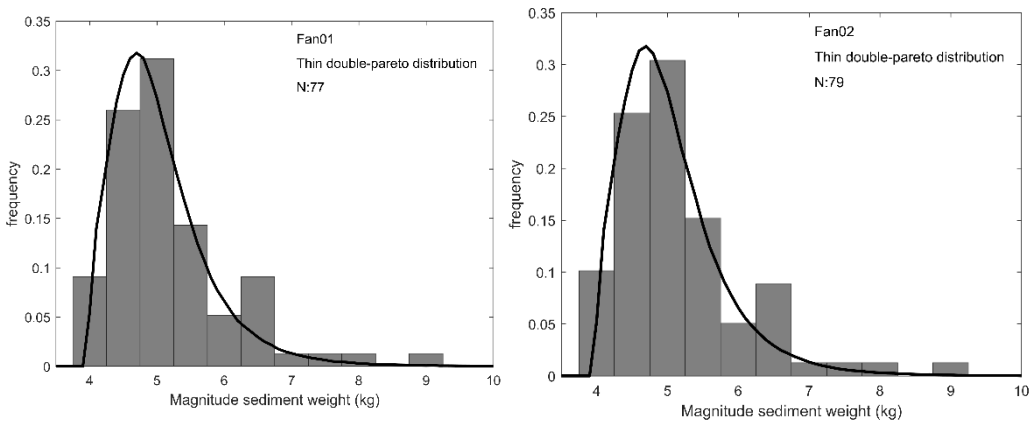

Figure 3.2: Thin double-pareto magnitude-frequency distribution of fan 01 and fan 02. For both the fans the same distribution is used. Mean sediment weight is approximately 5 kg. This magnitude-frequency distribution contains the 70 debris flows from DP02 (De Haas et al., in review). Respectively 7 and 9 flows are added along the same distribution. N = number of debris flows.

To simulate more natural circumstances during the investigation of the influence of sediment composition change on the debris-flow fan development, the use of a magnitude-frequency distribution is favored over the use of a uniform distribution within this experiment (Schürch, 2011; De Haas et al., *in review*).

3.2.2. Debris-flow compositions & sediment-size distribution

The sediment mixture consists of four types of sediment. (1) Angular basalt gravel with sizes ranging from 2-5 mm, (2) coarse sand, (3) fine sand and (4) clay. Similar to the experiments from De Haas et al. (2015; 2016; *in review*) and although scaled, in accordance with observations of e.g. Beaty (1963), Iverson (1997) and Larsen (2002). When changing one component of the sediment mixture the other components are automatically affected. For convenience, the change in sediment composition is indicated by a change in gravel fraction. In this experiment ten different compositions are used (Table 3.1). The debris-flow compositions are derived from De Haas et al. (2015) however, clay fraction is increased (following De Haas et al., *in review*) to increase runout distances and the chance for proper and realistic fan evolution without the early infilling of the chute channel. A standard ratio of 0.36 is taken to distinguish between fine and coarse sand. A volumetric water content of 49% is added after the sediment composition is established. Although De Haas et al. (2016; *in review*) used a volumetric water content of 44%, during this experiment it turns out that a volumetric water content of 49% increases runout distance and therefore channel infilling occurs less rapidly. This enhances the number of possible debris-flow events on one debris-flow fan using this experimental setup.

Table 3.1: Debris-flow compositions per gravel fraction.

Gravel *vol%*	**Coarse sand** *vol%*	**Fine sand** *vol%*	**Clay** *vol%*
0,0	70,0	24,6	5,4
8,0	64,2	22,6	5,2
17,0	57,7	20,3	5,0
25,0	51,9	18,3	4,8
32,0	47,0	16,5	4,4
40,0	41,4	14,6	4,0
48,0	35,8	12,6	3,6
56,0	30,3	10,6	3,1
64,0	24,8	8,7	2,5
72,0	19,3	6,8	1,9

For this experiment the gravel fraction in the sediment is distributed along a heavy-tailed double-pareto distribution (figure 3.3). This distribution is chosen so that there are enough gravel-rich as well as gravel-poor debris-flow events to be able to deduce any relationships between debris-flow fan development and composition change.

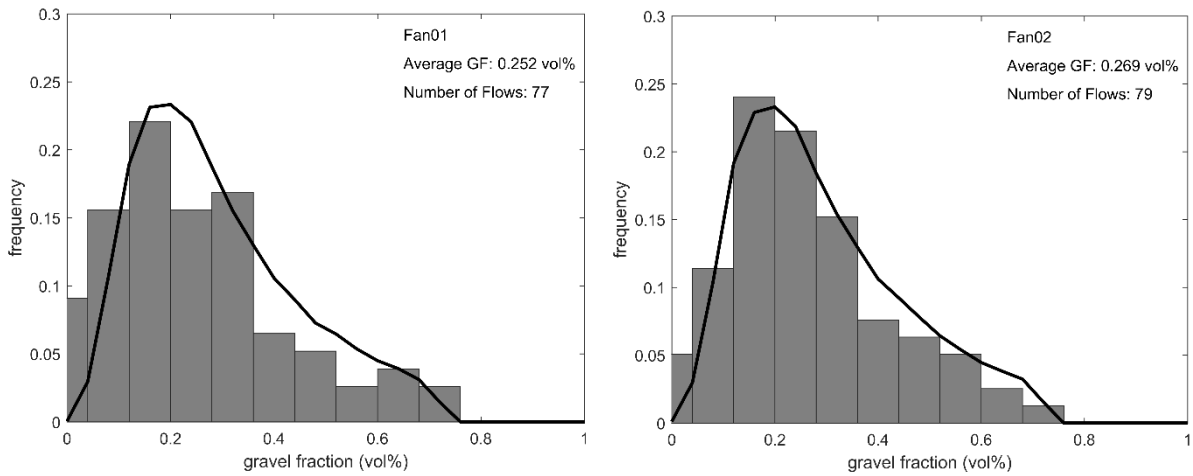

Figure 3.3: Sediment-size distribution of fan 01 (left) and fan 02 (right). Fan 01 contains 77 debris flow events. Fan 02 contains 79 debris-flow events. Average gravel fraction (GF) fan 01: 0.252 vol% and fan 02: 0.269 vol%.

Both distributions are derived from the same double-pareto distribution curve. However, due to random variation, the number of occurrences per gravel fraction differs. This subsequently invokes a small change in the average gravel fraction (average GF). However, the assumption here is that the small change will not significantly affect debris-flow fan development, also in consideration of natural variance during debris-flow deposition.

3.3. Single debris-flow reference experiments

To be able to understand the process occurring on a debris-flow fan scale. First, the mobility and geometry of a single debris flow should be assessed. To do so, the composition in volumetric percentages mentioned in table 3.1 are applied to the mean sediment weight of 5 kg sediment. For every gravel fraction two debris flows in total are run down the chute channel. Per debris flow variables such as runout distance, snout width, snout height and width/height ratio of the lobe are measured. These measurements are then compared to debris flows with similar gravel fraction on the debris-flow fan and therefore give more insight in the processes acting on the debris-flow fan scale.

3.4. Data reduction

3.4.1. Reference experiments

For the reference experiments three different variables are measured. These are the width of the snout, the runout distance of the debris flow and the height of the snout. Figure 3.4 shows the measurement lines for these variables. The lines are dependent on the geometry of the debris flow and therefore have different positions per debris flow. With these measurements the width/height ratio per debris-flow snout is calculated. The width/height ratio might indicate bed roughness influence on the debris-flow morphology (Iverson, 2010; De Haas et al. 2015).

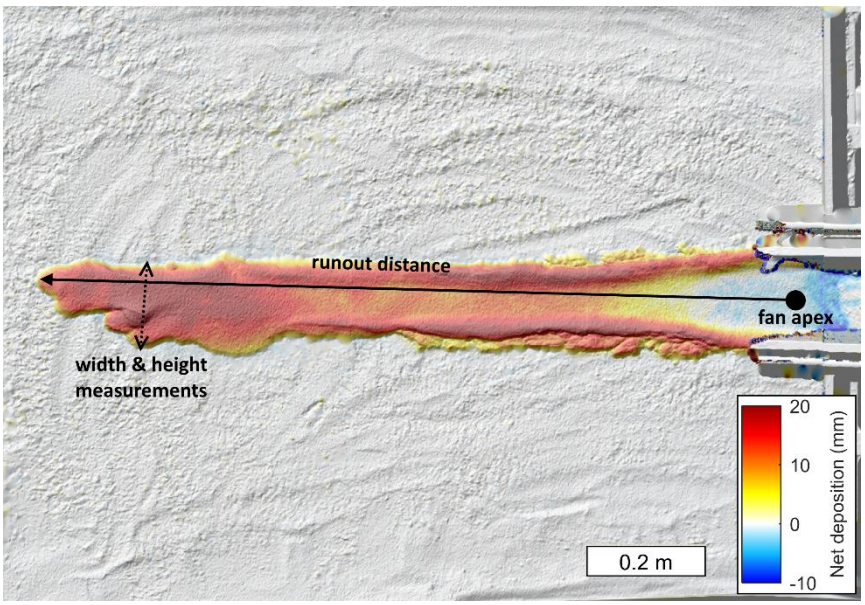

Figure 3.4: Debris flow reference experiments with the measurement lines. Measurements lines are dependent on the outflow of the debris flows. Colors indicate deposition or erosion compared to fan topography after previous debris flow. Warm colors represent deposition. Cold colors represent erosion.

3.4.2. Spatio-temporal evolution

Spatial and temporal evolution of the debris-flow fan is measured by several variables. The same approach is used as in De Haas et al (*in review*). Flow angle, runout distance per debris-flow snout, maximum runout, deposit width, deposit width/depth ratio, apex channel depth, debris-flow fan steepness, snout width and snout height are measured (figure 3.5). Measurements of runout distance, flow angle, debris-flow fan steepness all originate from a set point on the fan midline being the fan apex. Flow angle of a debris-flow snout is defined as the angle between the fan midline and a straight line connecting the fan apex with the debris-flow snout. These variables are then set out to each other, including gravel fraction and debris-flow volume, to be able to deduce any relationships.

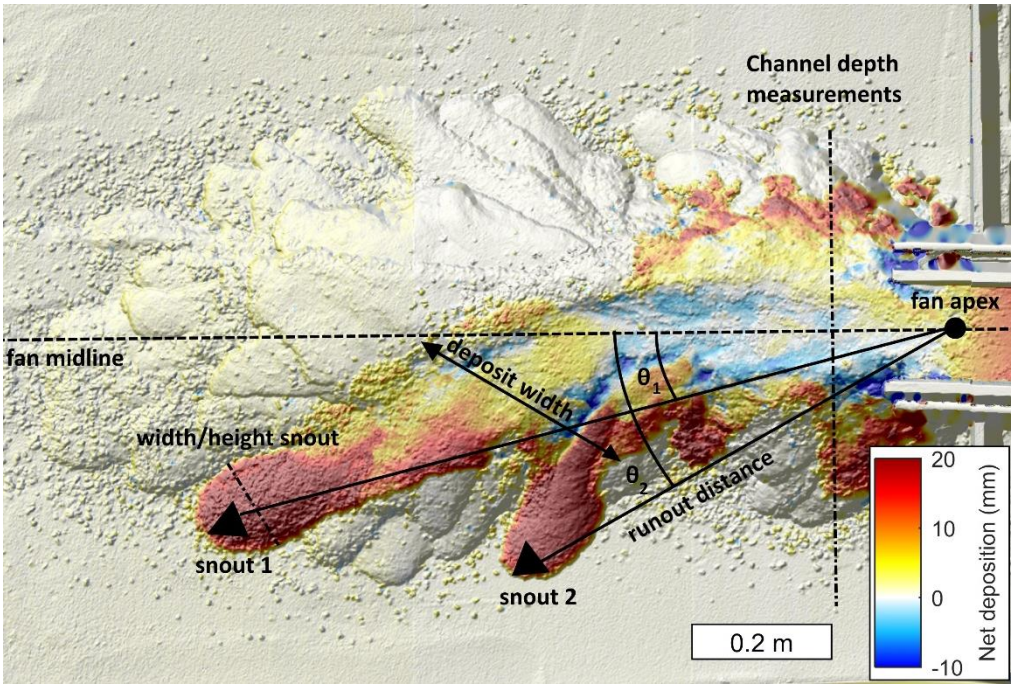

Figure 3.5: Depositional geometry and spatio-temporal pattern measurement. Lines dependent on outflow of debris flow. Colors indicate deposition or erosion compared to fan topography after previous debris flow. Warm colors represent net deposition. Cold colors represent erosion

3.4.3. Deposition & erosion patterns

Deposition and erosion patterns potentially show differences with a change in gravel fraction. To derive deposition and erosion patterns based on the DEMs, the difference in DEMS (diffDEM) is calculated. When the debris-flow fan DEM with current debris-flow deposit is subtracted from the debris-flow fan DEM with previous debris-flow deposit. A map remains where positive values indicate deposition and negative values indicate erosion (diffDEM).

Next, the area of the debris-flow deposit is calculated. Roughly, the area is derived from the DEM by using the diffDEM. This map with deposition and erosion values is then turned into a binary map with 1 for gridcells were either deposition or erosion took place and 0 for gridcells where neither of them took place. Because the Vialux z-Snapper 3D scanner does not have a 100 % accuracy the two DEMs differ slightly from each other, so by creating the diffDEM nearly every gridcell indicates a certain change in height. This subsequently distorts the calculation. To circumvent this problem a threshold value is added with the making of this binary map so slight changes are excluded and only the real debris-flow dimensions remain.
In general, the binary maps are representable for the debris-flow deposit dimension, however this method can introduce a slight error, especially within areas where deposition and erosion even each

other out so the difference in DEM has a value underneath the threshold, which should in fact be included.

Because 1 gridcell is 1 mm by 1 mm, adding all the 1's will result in the total area of the debris-flow deposit in mm^2.

To derive the deposition per area all the values higher than 0 on the diffDEM are added to each other within the dimensions of the debris flow. Then the total deposition is divided by the total area of the debris-flow deposit, resulting in a single value indicating the average deposition per mm^2 for the complete debris-flow deposit. This is done for each debris flow.

To derive the erosion per area, the same method as with deposition per area is used, however now, values lower than 0 on the diffDEM are added to each other and then divided by the total debris-flow deposit area. This results in a single value indicating the average erosion per mm^2 for the complete debris-flow deposit. Again, this is done for each debris flow.

Finally, to derive the ratio of deposition over erosion in m/m for current debris flow, the total deposition is divided by absolute value of the total erosion. Values higher than 1 indicate more deposition than erosion and vice versa.

To visualize the effect of gravel fraction on each of the deposition and erosion patterns, the deposition per area, erosion per area and deposition/erosion ratio is put against gravel fraction.

3.4.4. Hazard map

Next, a hazard map, containing 1 by 1 mm gridcells, is created and indicates the number of times a debris flow has passed each single gridcell after completion of the debris-flow fan. For every time a debris flow has passed a single gridcell, a value of one is added. The binary maps as explained in previous section are used for this calculation. For both debris-flow fans, this hazard map will most likely show high values close to the apex and lower values on more distal parts of the fan distributed in a radial pattern. However, interesting patterns might occur.

3.4.5. Surface- and bed roughness

Surface and bed roughness is derived from the DEM with use of the roughness tool in the topotoolbox package (Schwanghart, 2010). This tool follows the approach of Olaya (2009) and Hobson (1972). These roughness maps are used to evaluate the effect of bed and surface roughness on fan evolution. The standard kernel size of 3 mm by 3 mm for deriving bed roughness is used for the roughness maps. This corresponds with roughness present on a grain level. Roughness maps therefore indicate high roughness's where a lot of gravel is present and low roughness were less gravel is present.

From this map a 2D surface roughness plot, ranging from apex to the most distal part of the debris-flow fan, can be derived after each subsequent debris flow. Hereby it becomes possible to distinguish bed roughness evolution after a number of debris-flow events. For every x value (parallel to the fan midline), the average of all corresponding y values (perpendicular to the fan midline) ranging until the outer extents (above and under the fan midline) of the debris-flow fan are taken. Although it becomes a simplification of reality, it potentially gives good details on roughness evolution. It might show differential grain-size distribution along the fan surface if distal surface roughness is controlled by debris-flow events with gravel fractions that are more mobile, and proximal surface roughness is controlled by debris-flow events with gravel fractions that are less mobile.

To investigate if debris-flow fan roughness influences debris-flow runout distance, two methods are applied. In the first method, the average roughness value of the encountered bed on which a debris-

flow event is deposited, is compared to the runout distance and the width/height ratio of that debris-flow event. This is done for every debris-flow event. Plotting the bed roughness to the runout distance hypothetically gives a relationship where a higher bed roughness influences runout distance (Iverson, 2010; De Haas et al., 2015).

In the second method, the bed roughness underneath the snout is compared to the bed roughness underneath the body of the debris flow as visualized in figure 3.6. This method aims to address the question if rougher bed enhances the friction on the debris flow and thus has a decreasing effect on debris-flow runout. The average bed roughness underneath de snout is divided by the average bed roughness underneath corresponding body. When this value is larger than 1 it means that the bed underneath the snout is rougher than underneath the body. If this holds for most of the debris flows it might be assumed that a rough bed is able to effectively reduce runout distance.

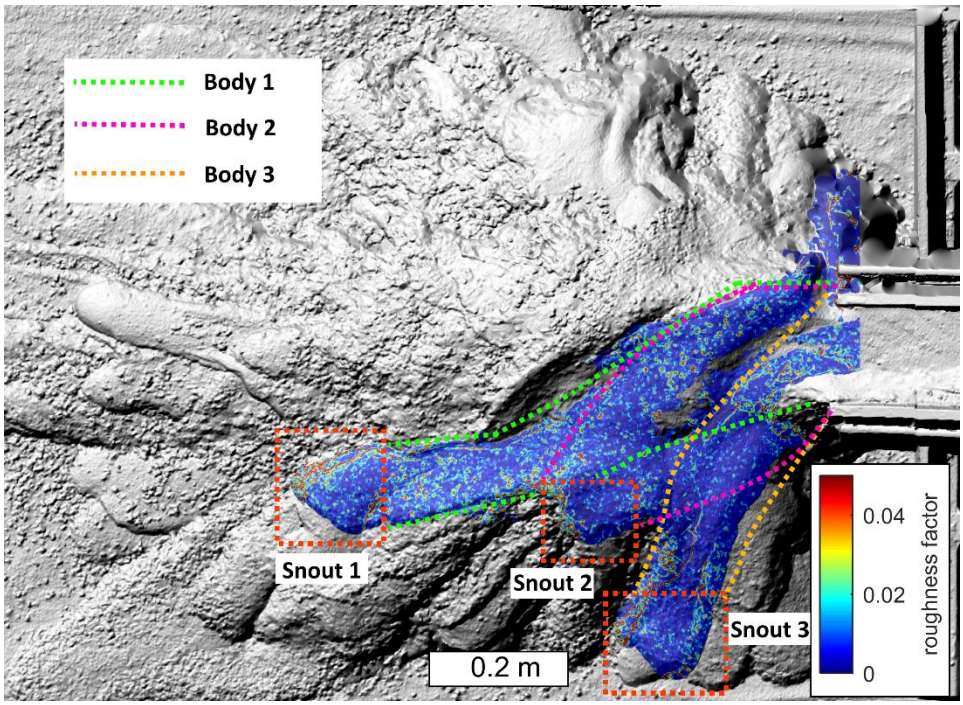

Figure 3.6: Visualization of the second method for bed roughness effect measurement. The colored layer above the gray hillshade debris-flow fan map, represents bed roughness under current debris flow. Warm colors indicate higher roughness values. Cold colors indicate lower bed roughness values. The average bed roughness value of one snout is divided by the average bed roughness value of corresponding body.

4. RESULTS

In this section the processes that occurred during the experiments are summarized. First the reference experiments are discussed. This will be followed-up by an extensive summarization of the spatio-temporal patterns occurring on fan 01 and fan 02. An extensive discussion on the processes occurring and their relation to nature and other experiments is placed in the next chapter.

4.1. Reference experiments

Figure 4.1 depicts the results of the reference experiments. For these experiments the sediment compositions presented in table 3.1 are used. An additional 49 vol% water is then added to this mixture. Per composition, two debris flows are created. Therefore, the mean value depicted as a red line holds the mean value for only two points with a straight line connecting the mean values of different compositions (figure 4.1). Figure 4.2 shows photo images and measured erosion and deposition images of three debris flows respectively having a gravel fraction of 8 vol%, 32 vol% and 56 vol%. Each debris-flow event shows similar typical debris-flow behavior as observed during natural debris-flows (e.g. Sharp & Nobles, 1953), where a channel was present bordered by self-formed coarser-grained lateral levees, and a coarser-grained snout (if any coarse material was present within the sediment mixture). The bottom images depict the measured erosion and deposition based on the difference between the bed topography prior to the debris flow and the topography after the debris-flow event. From these images it becomes evident that lateral levees are present due to increased deposition at the sides, as well as the accumulation of material in and close to the snout.

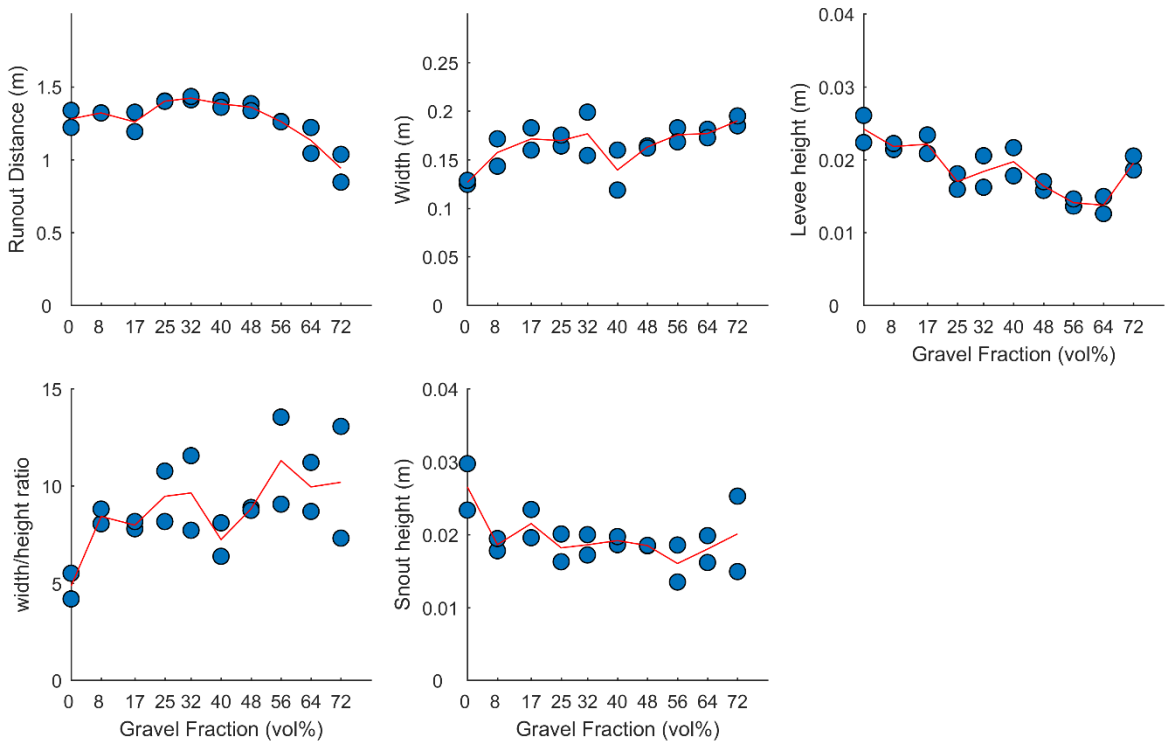

Figure 4.10: summary of measurements for the reference experiment debris flows (following figure 3.4). Runout distance, lobe width, maximum levee height and snout height were measured after each debris flow. The width/height ratio is the width of a debris-flow snout divided by its maximum snout height. Gravel fractions are in volumetric percentages.

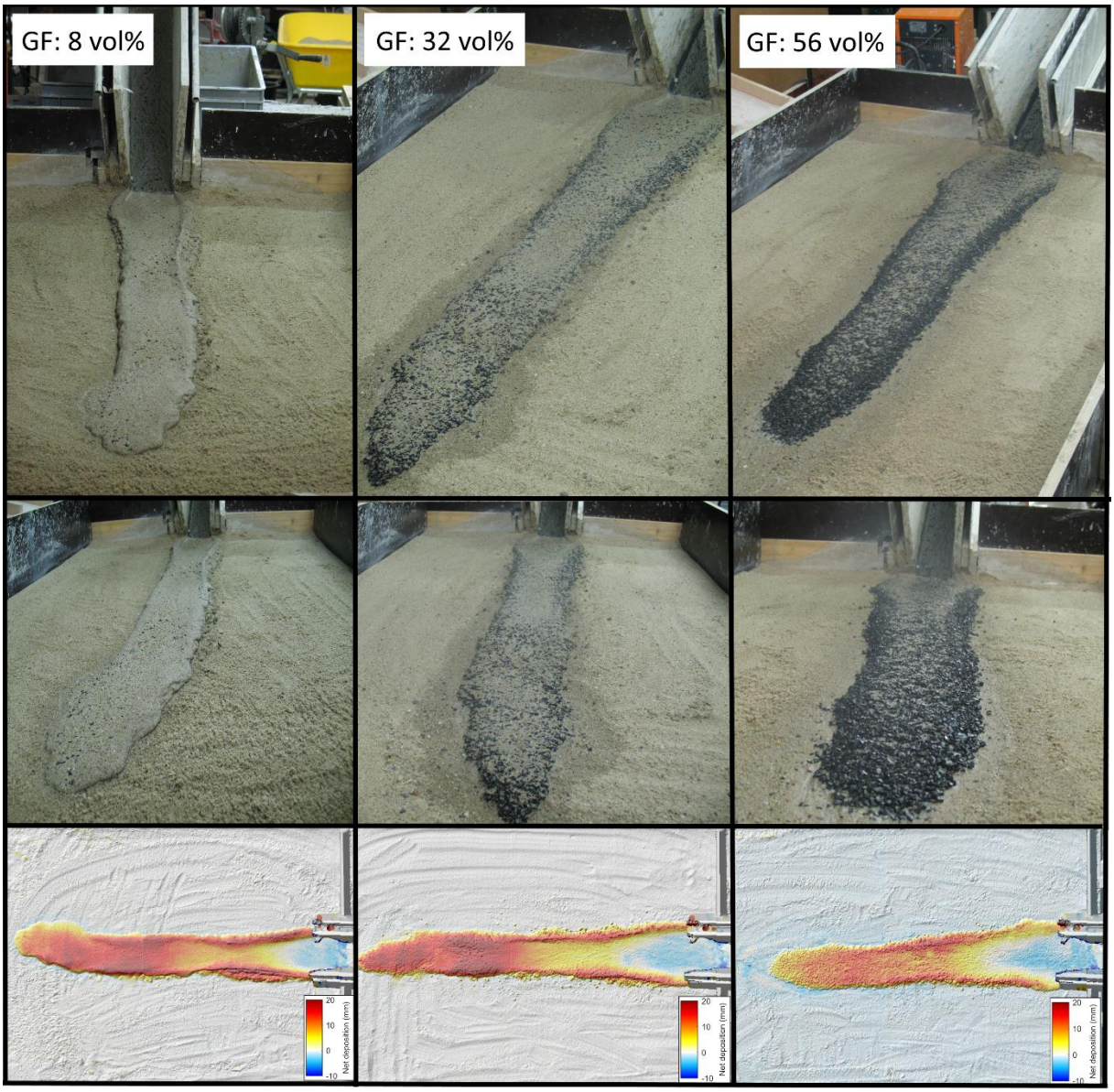

Figure 4.2: Pictures and images of three debris flows. From left to right the sediment mixtures of the debris flow contained 8, 32 and 56 vol% gravel. The bottom images depict measured deposition and erosion. Warm colors denote deposition and cold colors denote erosion.

During this summary of results, comparisons will occasionally be made to the experiments from De Haas et al. (2015). It must be mentioned that the main difference with those experiments lie in the fact that a water fraction of only 44 vol% is used. Whereas in this experiment a water fraction of 49% is used.

Runout distances vary between 1.43 and 0.85 meters. Maximum runout is achieved with a gravel fraction of 32 vol%. Towards higher gravel fractions a significant decrease in runout distance occurs. Towards lower gravel fractions the trend also shows a decrease in runout distance. However, this trend is much less significant. Evidently, a gravel fraction of 0 vol% shows an average runout distance of 1,28 meter, whereas a gravel fraction of 72 vol% shows an average runout distance of 0.94 meter. In comparison with De Haas et al. (2015) this trend towards lower gravel fractions is much less significant.

Lobe width shows a steady but small increase, from 0,125 m to 0,195 m towards higher gravel fractions. A relative smaller lobe width is seen at a gravel fraction of 40 vol%. This might be related to the fact that levee height is somewhat increased, which potentially shows that a sediment mixture

with a gravel fraction of 40 vol% causes more effective grain size segregation and therefore enhances levee creation (Johnson 2012; De Haas et al., 2015). With increased levee formation lateral spreading is reduced subsequently reducing lobe width (Iverson, 2003). In accordance with this process and the widths of the debris-flow lobes, in this experiment levee height is at its largest with low gravel fractions and decreases gradually with increasing gravel fraction. This is in contrast to the results of De Haas et al. (2015), where low gravel fractions lacked the ability to create levees and therefore were able to spread laterally creating lobes with large widths. An increase in levee height is again seen with a gravel fraction of 72 vol%, however this does, remarkable, not initiate a decrease in width, possibly to the significant reduction in runout distance.

Snout height is generally around 0.02 m for every gravel fraction except for the lower gravel fractions. This is in accordance with the lower width, the higher levee height and the somewhat smaller than optimal runout distance which indicate that all material accumulates in a small lobe subsequently increasing the height. Because the snout height remains fairly equal and the lobe width shows a steady but small increase towards higher gravel fractions, the width/height ratio in general shows the same pattern as the lobe width, also containing the dip at 40 vol% gravel. Due to the relative lower width and larger height at 0 vol% gravel the width/height ratio is significantly lower than the rest of the debris flows. The width/height ratio shows a large spread increasing uncertainty in the trend.

4.2. Spatio-temporal patterns of development

In this section, the complete fan evolution will be discussed of both fan 01 and fan 02 and interesting sequences of debris-flow behavior will be pointed out. Photos, images depicting erosion and deposition after each debris-flow event, and synthetic cross-profiles will aid this discussion. Extra focus lies on the effect of gravel fraction in regards of fan behavior. The sediment-size distribution and the magnitude-frequency distribution of fan 01 and fan 02 are given in figure 3.2 and figure 3.3.

4.2.1. Fan 01

Figure 4.3 is the summary of measurements as done following the method depicted in figure 3.5.

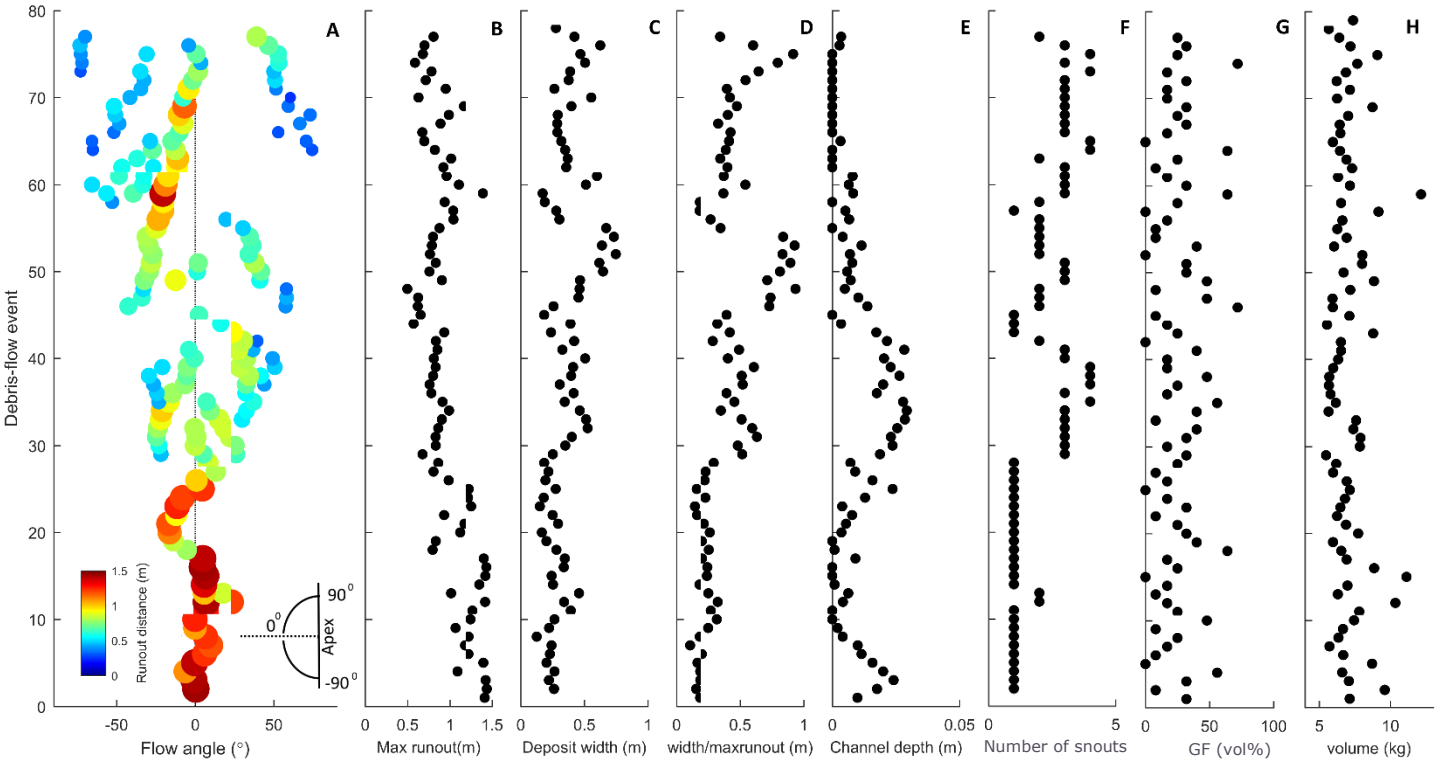

Figure 4.3: Summary of spatio- temporal measurements on fan 01. The y-axis values represent the debris flow events for every plot whereas x-axis values differ per plot. (a) Flow angle and runout distance per snout against the debris flow event. Multiple data points during one debris-flow event indicate multiple snouts. Warm colors denote high runout values whereas cold colors denote lower runout values. (b) Maximum runout (m) for each debris flow indicating the debris-flow snout with the largest length. (c) Deposit width (m) for each debris flow. (d) Width of the deposit divided by the maximum runout. (e) Channel depth close to the apex in order to derive sequences of backfilling and channelization. (f) Number of snouts of each debris flow. (g) The gravel fraction (vol%) of the debris flow sediment mixture. (h) Debris flow volumes (kg).

For the first ten debris-flow events the main direction is along the fan midline. Apex channel depth significantly increases during the first three debris flows, due to the formation and amplification of levees and the subsequent channelization of the debris flow (from now on referred to as DF). Up until DF 9 a sequence of channel backfilling occurs, mainly due to a sequence of relatively smaller-sized debris flows (5.7 to 6.7 kg). DF 3 to 5 show an interesting sequence regarding gravel fraction. DF 3 extends up until the maximum extent of the setup creating levees on either side. Due to channelization it is expected that the next debris flow is able to route through this channel potentially showing an increased runout. However, the next debris flow contains a gravel fraction of 56% and is not able to flow relatively far whereas it has comparable volume. Comparing it to the reference runout from figure 4.1 this might be interpreted as influence due to gravel fraction change. Next flow, containing 0 vol% gravel and having a larger magnitude (8.7 kg) is able to overtop this coarse-grained debris flow and

partially erode the snout. It shows no signs of decreased runout due to a coarse bed as it is able to reach maximum fan extent.

After DF 9 the terrain close to the apex shows a plano-convex profile. This due to the infilling of the accommodation space between the levees within the main channel (figure 4.4). In accordance with the model presented by De Haas et al. (2016), this commenced the searching phase as predecessor of an avulsion. Figure 4.4 shows clear evidence for two phases where first channel deepening occurs due to increased channelization and subsequent accumulation of sediment in the levees. And second, the channel is gradually filled in due to a sequence of backstepping events.

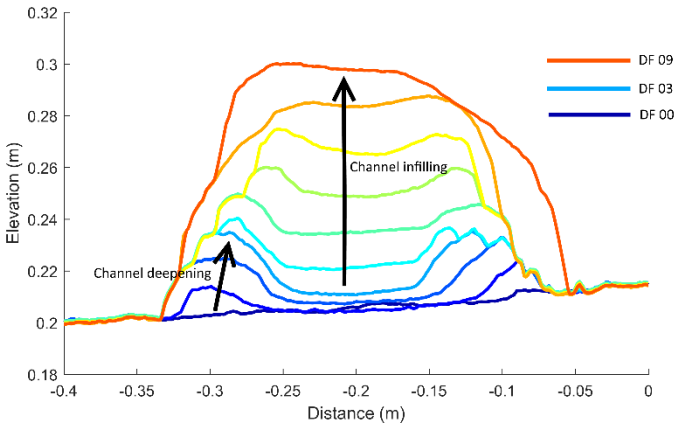

Figure 4.4: Cross-profile of DF 1 to DF 9 near the apex. A clear distinction can be made between channelization from DF 1 to DF 3 and the slower infilling of that channel from DF 4 to DF 9. Eventually a plano-convex profile remains. Profile position is depicted in figure 3.5.

DF 10 (7.4 kg; 48 vol% gravel) is able to overflow the previous debris-flow deposit completely, thereby overtopping the levees. The main locus of activity subsequently focusses to the right side of the debris-flow fan, where due to the absence of a channel a large debris flow (DF 12: 10.3 kg; 17 vol% gravel) is able to inundate a large area hence the increase in deposit width (figure 4.3c). The absence of levees on the fan and the relatively lower volume causes DF 13 (6.3 kg; 8 vol% gravel) to have a decreased runout, therefore creating a plug in the channel. This plug causes the main locus of activity to switch back to the fan midline where eventually DF 15 (11.1 kg; 0 vol% gravel) is able to create levees and to completely shut off previous avulsion. No influence of composition could be derived.

Until DF 17 (6.9 kg; 17 vol% gravel) the main locus focusses around the fan midline. DF 18 (6.5 kg; 64 vol% gravel) has slightly less volume than DF 17 but a significant larger gravel fraction. Although DF 17 is able to flow until maximum fan extent DF 18 does not even reach half of the fan thereby creating a channel plug, blocking of the main channel and initiating an avulsion (figure 4.5). Figure 4.6 shows the large difference in appearance of DF 17 and DF 18 and gives an idea how much gravel is present within a gravel-rich debris-flow. Similar to DF 4, the gravel seems to have an effective influence on channel plugging and thus on fan development. The next debris flow (DF 19; 5.9 kg; 40 vol% gravel) is able to partially erode the coarse-grained snout. But, because DF 19 is lower in volume than DF 18, the plug is not eroded completely. Perhaps if a large volume debris flow would be following, the plug would be completely eroded away. However, it shows that debris-flow deposits that are high in gravel content are susceptible to erosion.

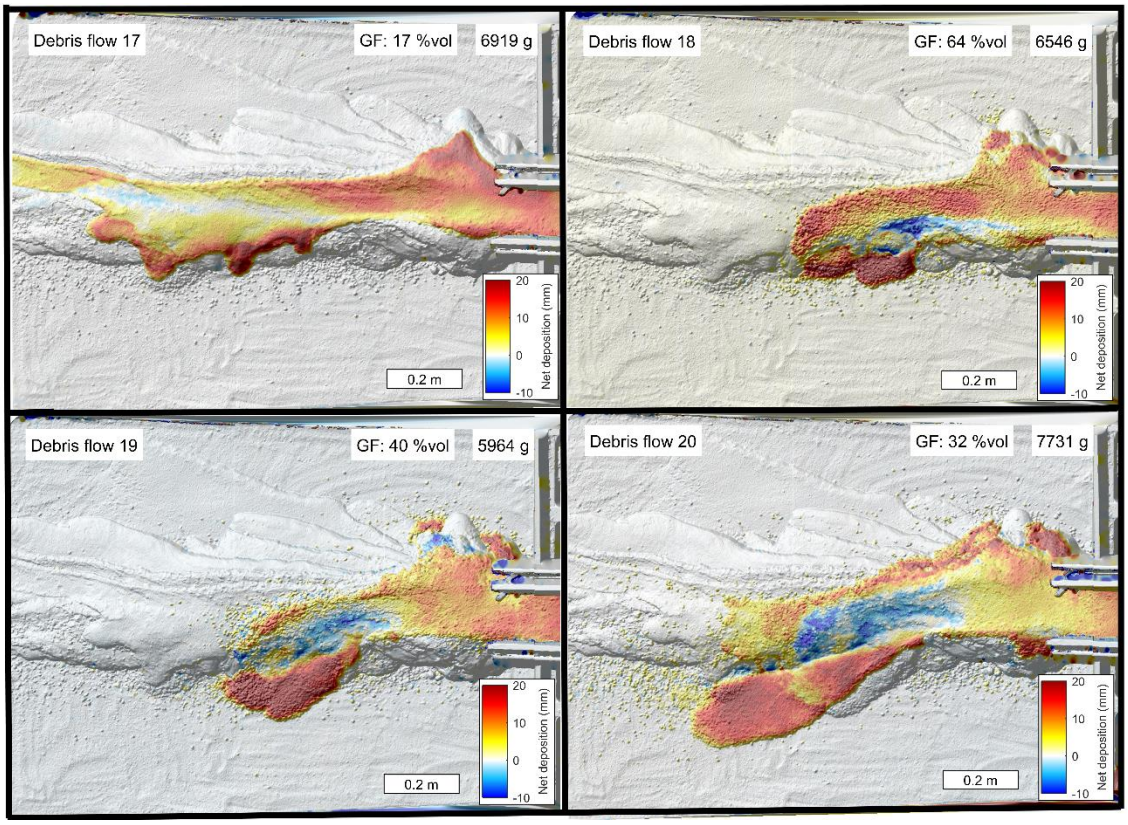

Figure 4.5: Sequence of debris flows creating a channel plug and a subsequent avulsion. Warmer colors denote deposition whereas colder colors denote erosion. High-gravel DF 18 acts as a plug initiating avulsion. During DF 20 it becomes visible that gravel-rich DF 18 is eroded away completely.

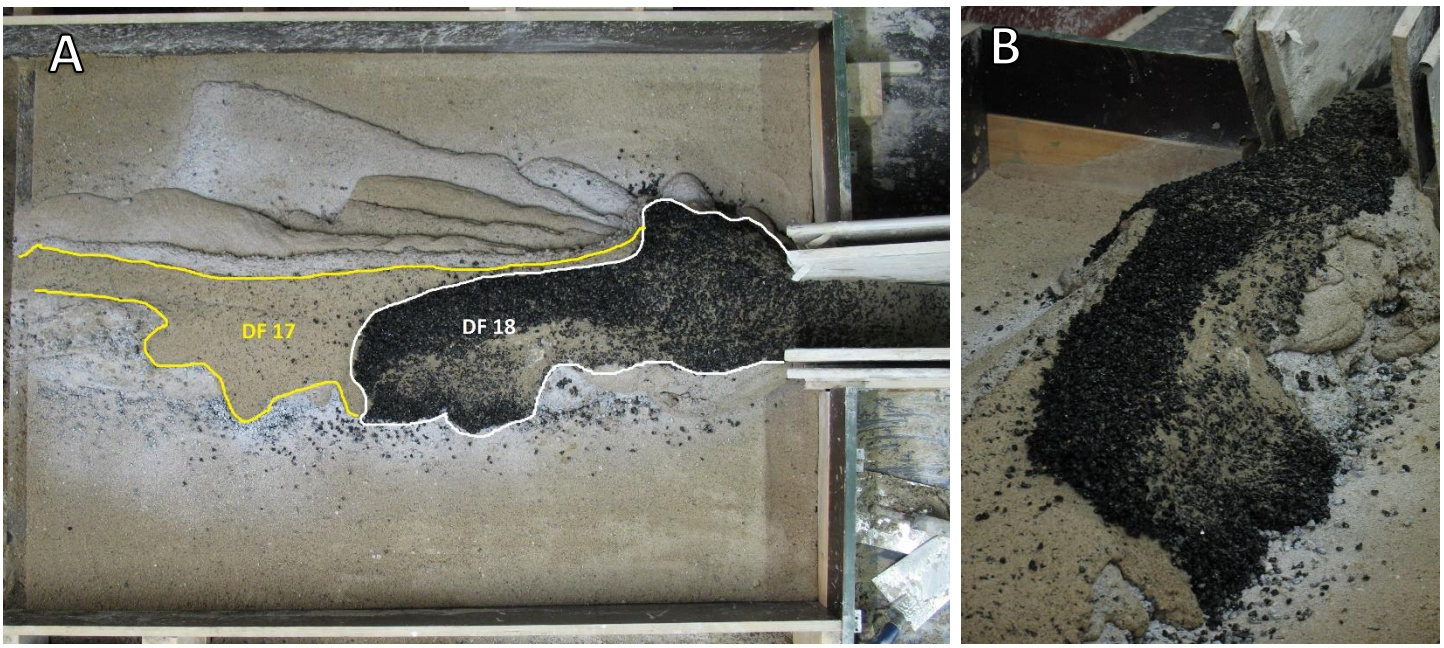

Figure 4.6: (A) Top view of the debris-flow fan shortly after deposition of DF 18. Both DF 17 and DF 18 are indicated within the figure. (B) Close-up of DF 18 where a significant increase in gravel particles is visible (black basalt particles).

Following DF 18 an avulsion cycle commences, where runout distance increases up until DF 21 (6.8 kg; 25 vol% gravel). Although DF 20 (7.7 kg; 32 vol% gravel) is larger in volume than DF 21, it is able to flow further than DF 20. This exemplifies the increased routing abilities due to channel formation. DF 22 (6.2 kg; 8 vol% gravel) on the other hand is not able to route completely (although channel depth is increasing (figure 4.3e)) until maximum fan extent and therefore creates a plug within the channel. Three possible reason can be attributed to this. (1) the decrease in volume, (2) the low amount of gravel and (3) a sudden change (decrease) in slope (figure 4.7).
In figure 4.7 it becomes evident that previous debris flows also encountered a sudden decrease in slope, however they seem less susceptible to this sudden decrease. Also, the height of the snout is much larger than previous deposits. It might be the effect of an increased cohesivity and an increased viscosity within debris flows with lower gravel fractions.

DF 23 (6.4 kg; 32 vol% gravel) and DF 24 (6.8 kg; 17 vol% gravel) are affected due to this channel plug and therefore forcing the main locus of activity to move towards the fan midline. Eventually during DF 25 (7.1 kg; 0 vol% gravel) the main locus of activity shifts to the fan midline thereby reactivating a channel formed during DF 17.

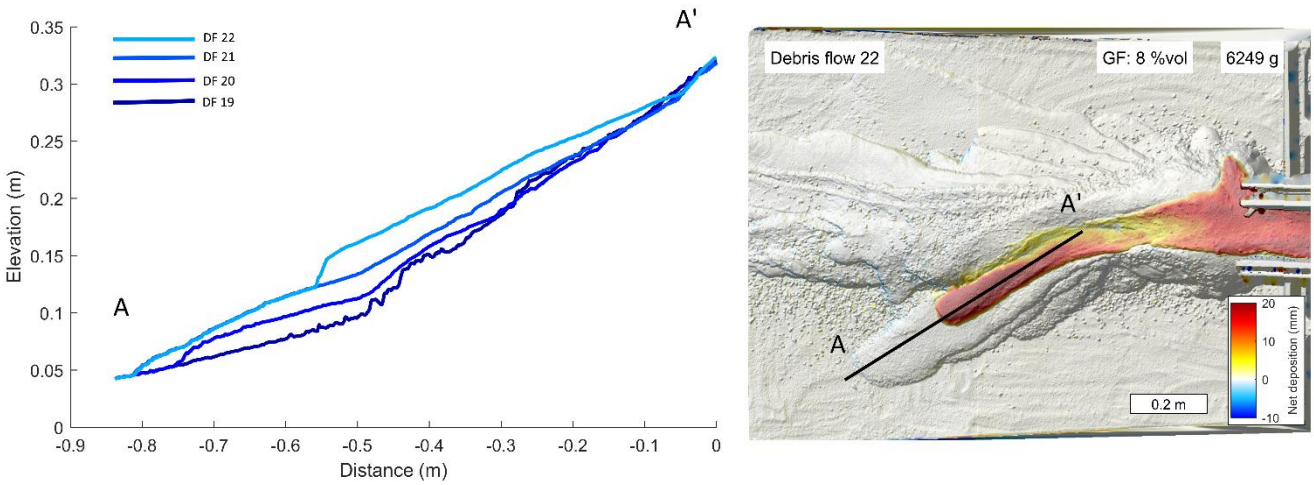

Figure 4.7: Left: synthetic cross section of DF 19 until 22 showing the plug formation. The lighter colors denote events that occurred later in time. DF 22 stops just after a sudden shift in slope topography. This sudden slope change is also seen during the previous debris-flow events. However, DF 22 seems more susceptible of this effect. Right: DF22 with erosion (warm colors) and deposition (cold colors). Position of cross section is depicted as the black line.

From DF 25 a sequence of reducing volumes up until DF 29 (respectively 7.1 kg; 0 vol% gravel, 6.9 kg; 17 vol% gravel, 6.0 kg; 8 vol% gravel, 6.2 kg; 25 vol% gravel, 5.5 kg; 32 vol% gravel), causes consecutive backstepping. No evidence is visible of direct influence of gravel fraction on this sequence. Volume changes seem to be the main driver for this backstepping sequence.

Up until DF 32 (7.3 kg; 40 vol% gravel) a clear searching phase can be distinguished where every debris-flow deposit shows several end lobes and no main channel can be characterized. From DF 33 (7.6 kg; 8 vol% gravel) the focus starts to lie on a channel left of the fan midline (figure 4.8). This channel does not exist long and soon the channel is backfilled and the main locus of activity switches to the right side of the debris-flow fan from DF 38 (5.7 kg; 48 vol% gravel) until DF 43 (8.8 kg; 25 vol% gravel). It becomes apparent that while the channel on the left side of the apex is slowly filled in, the sediment needs another way to flow through. This commences an avulsion towards the right side of the fan (also shown in figure 4.3a).

Figure 4.8 shows the sequence of debris-flow deposits with annotations of processes that occur. Although the gravel fractions range from high to low within this sequence (56 vol% to 8 vol%), no

apparent influence on fan topography becomes visible. It seems that volume difference and local topography are the main drivers for the fan evolution during this sequence. Especially because every backstepping or plugging event within one snout of the debris-flow deposit is compensated by a longer runout in another snout. Based on figure 4.1 gravel-rich debris-flow events, should potentially show reduced runout distances, but based on current sequence it can be concluded that in this case debris-flow fan evolution is rather influenced by volume change and local topography.

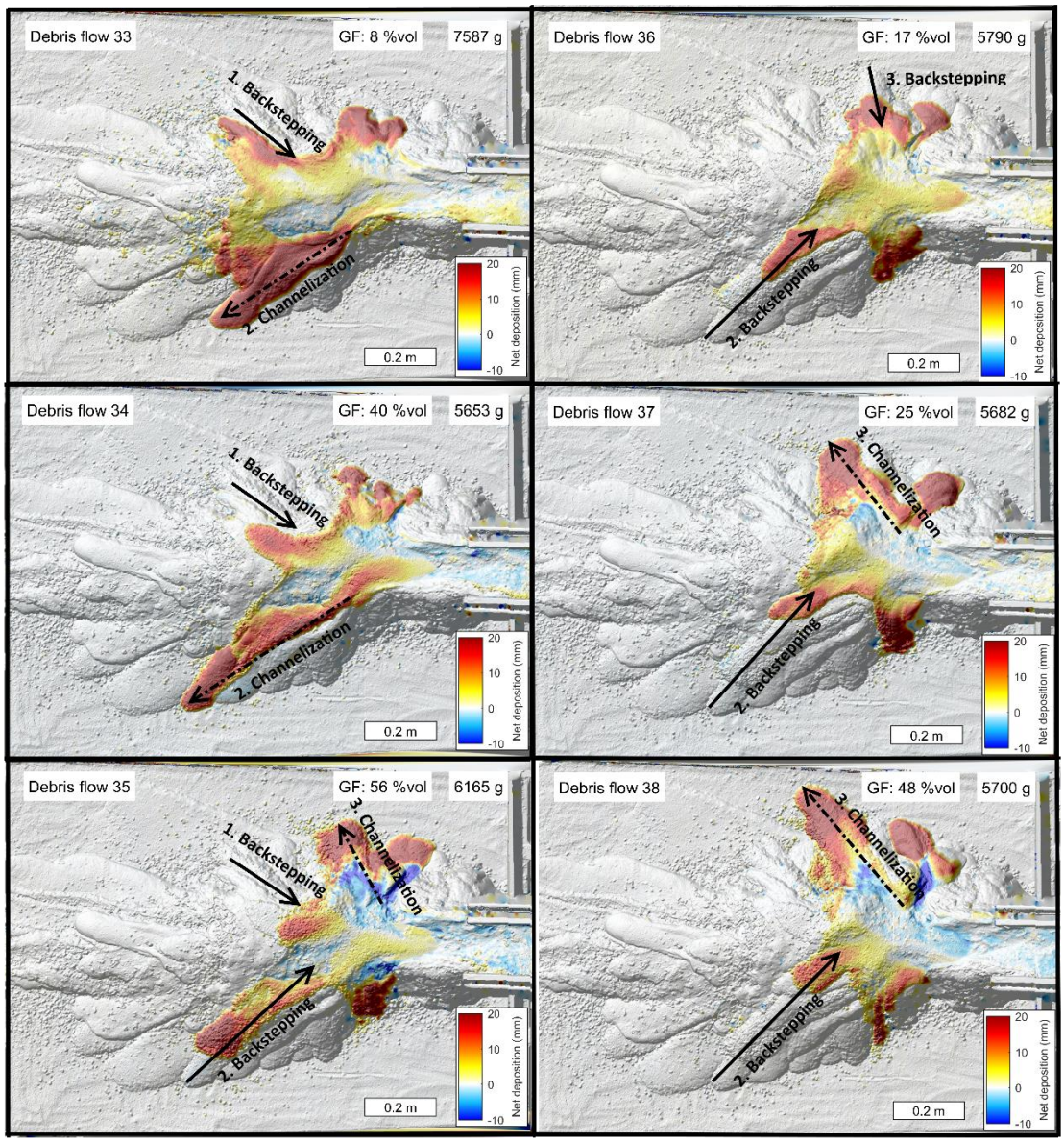

Figure 4.8: Debris-flow sequence DF 33 to DF 38. Representation of a searching phase where more debris flow snouts are present and alternate in channelization and backstepping. This figure visualizes that during this sequence, gravel fraction has little to no influence on debris-flow fan development.

After DF 38 the main locus of activity lies on the right side of the fan. Due to a drastic decrease in volume with DF 44 (5.5 kg, 17 vol% gravel) a channel plug is created, leaving a plano-convex surface (figure 4.3e). This event is followed up by a debris flow with lower gravel. Although DF 45 (7.1 kg; 8 vol% gravel) is 1.6 kg higher in volume it does not reach far on the fan. It does however have an increased width. According to figure 4.1 and previous observations (figure 4.7) it might indicate that runout is decreased due to the reduced gravel fraction, however, causes such as local topography, a decrease in gradient and the absence of a channel with levees also influence runout distance and deposit width so it would be unrealistic to say that solely gravel fraction is causing this reduced runout.

Gravel-rich DF 46 (6.0 kg; 72 vol% gravel) is not able to flow far due to this plano-convex surface created by DF 44 and DF 45. It deposits a gravel-rich plug on the plano-convex surface and subsequent trailing sediment is deflected to both sides (figure 4.9). The inability to overtop the plano-convex surface can

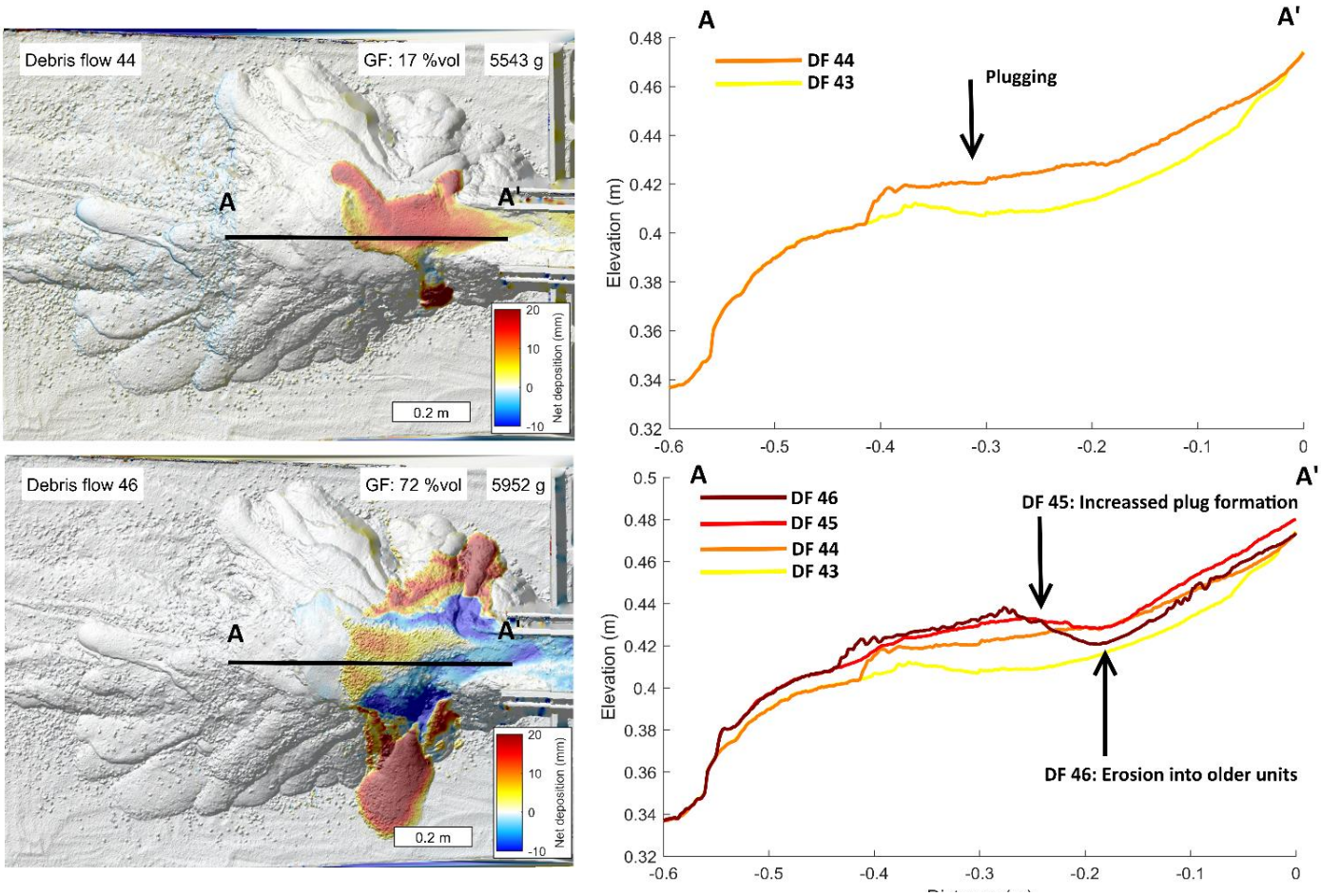

Figure 4.9: Erosion/deposition map of DF 44 and DF 46. The right side of the image contains cross profiles along the line presented in the left figure. The cross profiles show the channel plugging during DF 44 and the increased erosion during DF 46.

be attributed to the low volume but also to the reduced mobility of a gravel-rich debris flow (reference experiments; De Haas et al., 2015). Additionally, it becomes apparent that erosion is drastically increased. When looking back at figure 4.8 this same pattern emerges, that debris-flow events with higher gravel fraction show more erosion than debris-flow events with lower gravel fractions.

The erosion close to the apex creates two potential channels within the debris-flow fan. Up until DF 53 (6.0 kg; 40 vol% gravel), both depressions in fan topography are utilized for sediment flow routing. Figure 4.3a depicts that two snouts occur simultaneously and are similar in length during a few events. However, starting from DF 54 (6.9 kg; 8 vol% gravel) the right side is backfilled rapidly and the main

locus of activity start to lie at the left side of the debris-flow fan. During this increased focusing towards the left of the debris-flow fan a channel is formed, which progressively increases distance and fan extent. Finally, DF 57 (9.2 kg; 0 vol% gravel) causes the right-side channel to become completely blocked off.

DF 57 is a remarkable event. Although it contains approximately as much as 2.6 kg more volume than previous debris-flow event (DF 56: 6.6 kg; 17 vol% gravel), it is not able to reach any further than the previous flow (figure 4.10; figure 4.11). Although it would be expected that the channel in which DF 57 flows is used for flow routing therefore increasing the runout distance, especially with large flows, DF 57 does not show this. As an addition to this, deposition area is very small and lobe height is subsequently increased. A compact appearance and reduced runout distance is seen (figure 4.11) and can potentially be attributed to the low gravel fraction within DF 57.

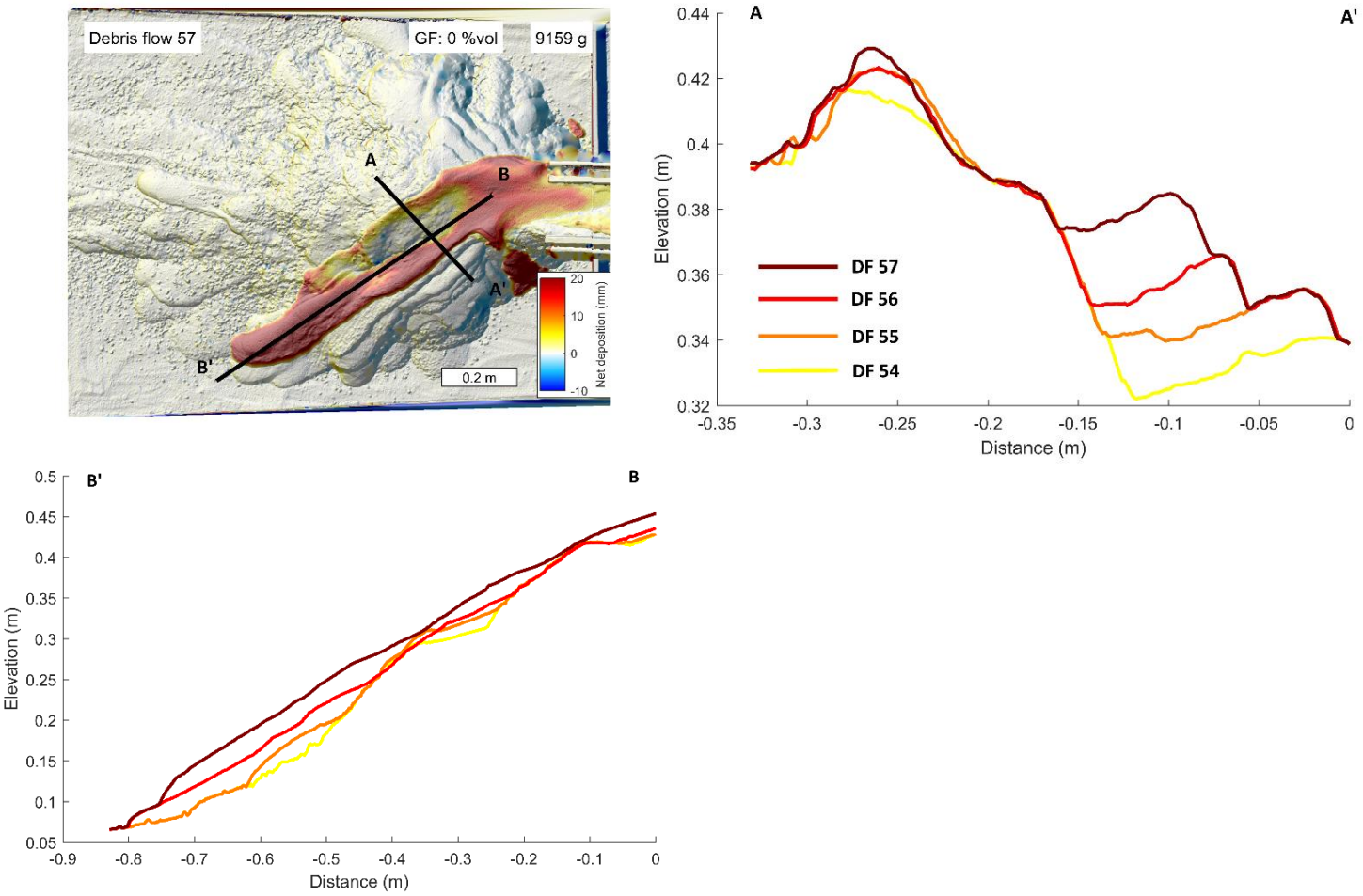

Figure 4.10: Erosion and deposition map of DF 57 with cross section and long section. DF 57 shows an increased deposition height compared to previous events. Most likely caused by the decreased deposition area related to the gravel fraction.

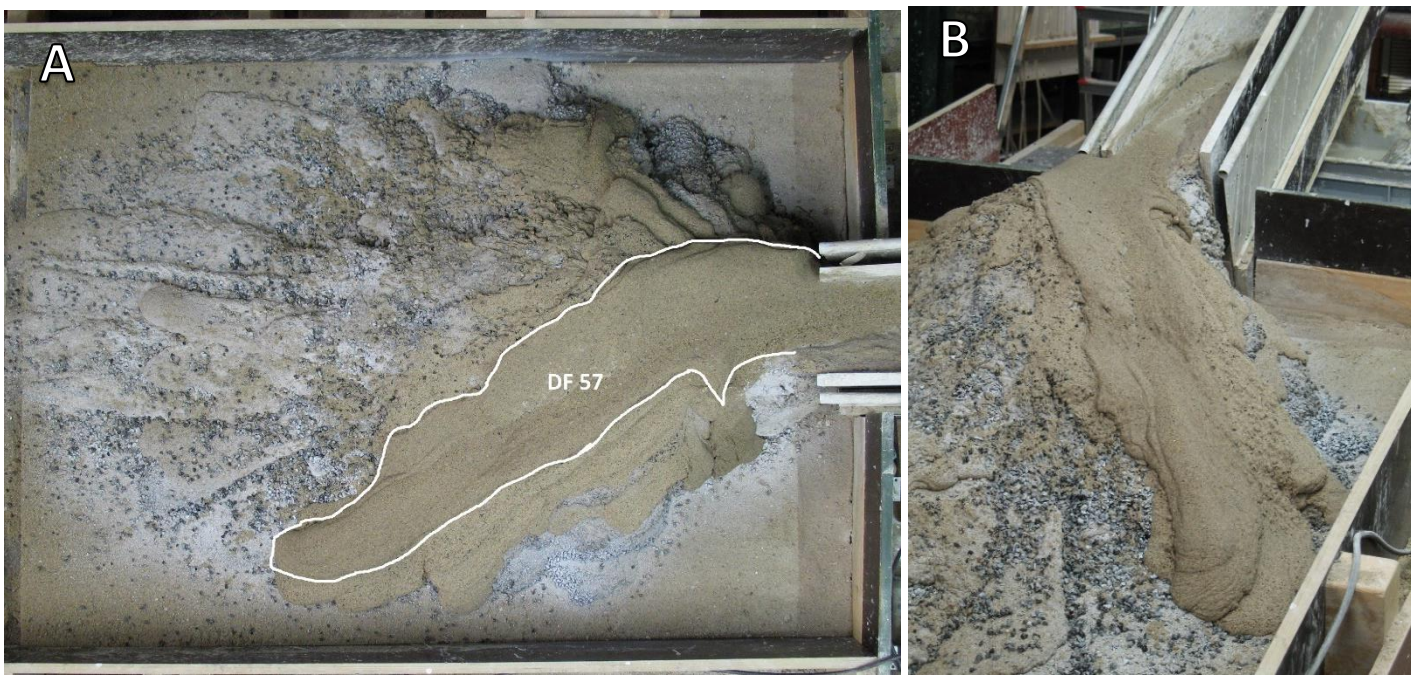

Figure 4.11: (A) Top view of the debris-flow fan shortly after deposition of DF 57. (B) Close-up of DF 57 where a clear absence of gravel particles is visible.

DF 59 (12,1 kg; 64 vol% gravel) is the largest event on this debris-flow fan. This debris flow caused a large inundated area as well as high runout. Remarkable is the high amount of erosion caused by this debris-flow event. A debris-flow event that is closest to DF 59 in volume is DF 15 (11.1 kg; 0 vol% gravel). Figure 4.12 shows both debris-flow deposits. It becomes evident that both debris flows occurred in different situations where during DF 15 the fan was not yet fully developed and therefore local topography was substantially different.

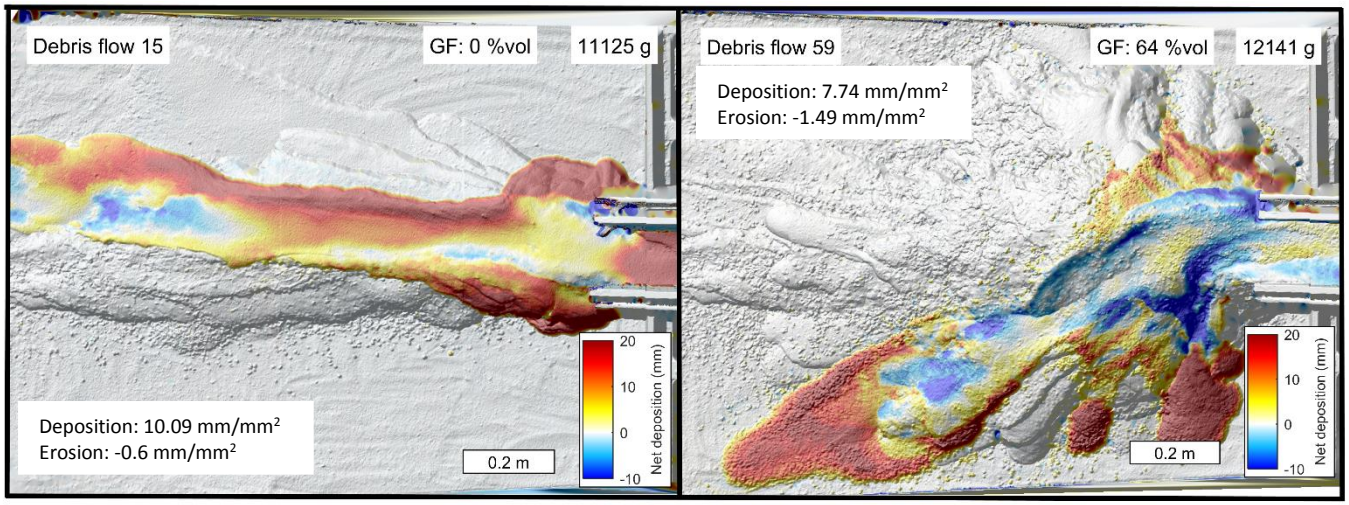

Figure 4.12: Comparison of low gravel and high gravel debris flows with comparable higher volumes. Warm colors denote deposition, cold colors denote erosion. Additionally, the deposition and erosion values per area are added to aid the conclusions. It is evident that DF 59 shows more erosion and fewer deposition. However, circumstances of deposition are slightly different, therefore it is not safe to say that solely composition change does increase erosion.

Deposition and erosion values are added, to evidently derive that erosion is higher with higher gravel fractions and deposition is higher with lower gravel fractions for these two debris-flow events. An increased erosion is visible during DF59 which might be related to gravel fraction however, this conclusion must be approached with caution as local topography might also be a controlling factor in

debris-flow deposition, routing and thus perhaps also erosion (e.g. large momentum through a small channel might enhance erosion).

DF 62 (7.3 kg; 8 vol% gravel) shows also evidence for the decrease in runout and the overall more compact appearance of lower gravel debris-flow deposits. DF 62 has 1 kg more volume than DF 61 (6.3 kg; 17 vol% gravel) however again, it is not able to overtop previous flow deposits. Also showing nearly no erosion and thicker lobe height. Next flow (DF 63 (6.9 kg; 25 vol% gravel)), being 0.4 kg lower in volume is again able to overtop previous debris-flow deposit.

Until DF 73 (6.9 kg; 17 vol% gravel), the main locus of activity lies on the fan midline. Where runout and subsequent fan evolution is governed by a change in volume rather than a change in composition. During this sequence the present channel and slope is gradually filled where eventually a plano-convex surface exists. The cross-section of figure 4.13 is taken close to the apex (as presented in figure 3.5). It becomes visible that during the sequence the slope to the left is gradually filled up, this causes the locus of activity to gradually go towards the fan-midline. As also shown in figure 4.3a. Eventually the surface is straight with nearly no sloping. At DF 74 (7.6 kg; 72 vol% gravel), this causes the debris-flow fan to enter the searching phase. The relatively immobile high-gravel debris flow is not able to run far due to the lack of a channel and its gravel content.

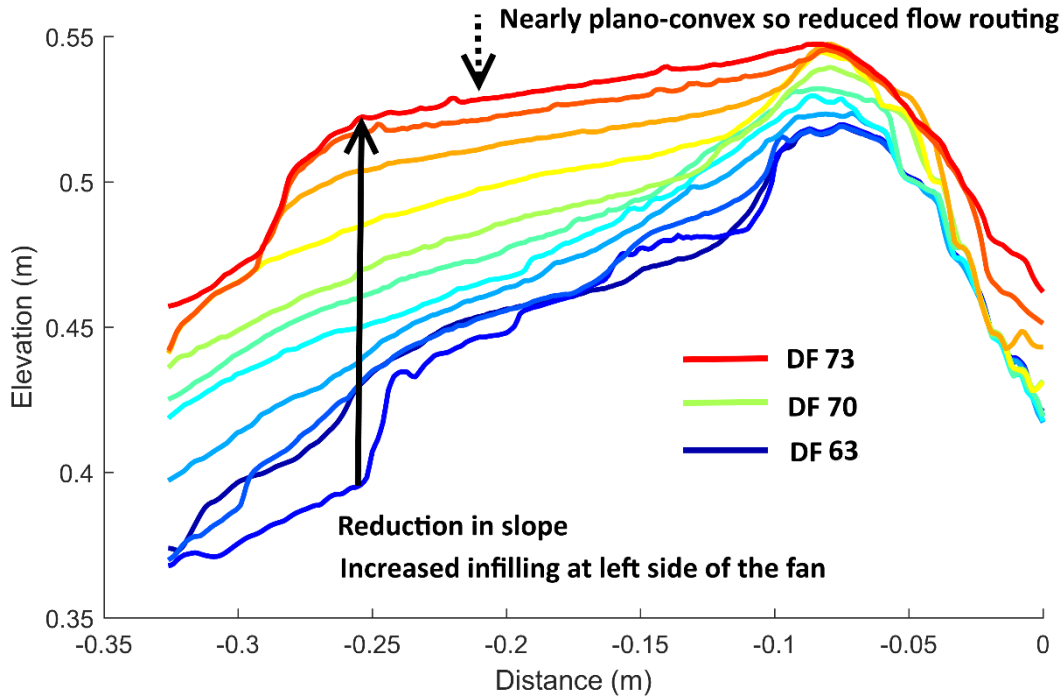

Figure 4.13: Cross-section of channel depth close to the apex. DF 63 to DF 73 warmer colors depict an increase in debris-flow events. The left side of the cross-section shows a relative larger increase in height. Main locus of activity shifts from the left to middle caused by the gradual decrease in slope. Profile position is depicted in figure 3.5

DF 74 turns out to be a highly erosive event. It causes the sudden creation of a new channel. Due to the erosive power of DF 74 the searching phase lasts only for about two debris-flow events. The new channel that is formed is subsequently channelized by an increased focus towards this path and a new avulsion cycle commences (figure 4.14). This event shows that one debris-flow event that is high in gravel content, is able to instantly create a channel that is able to route sediment of upcoming flows if conditions are favorable. This event caused similar effects as the comparable event during DF 46.

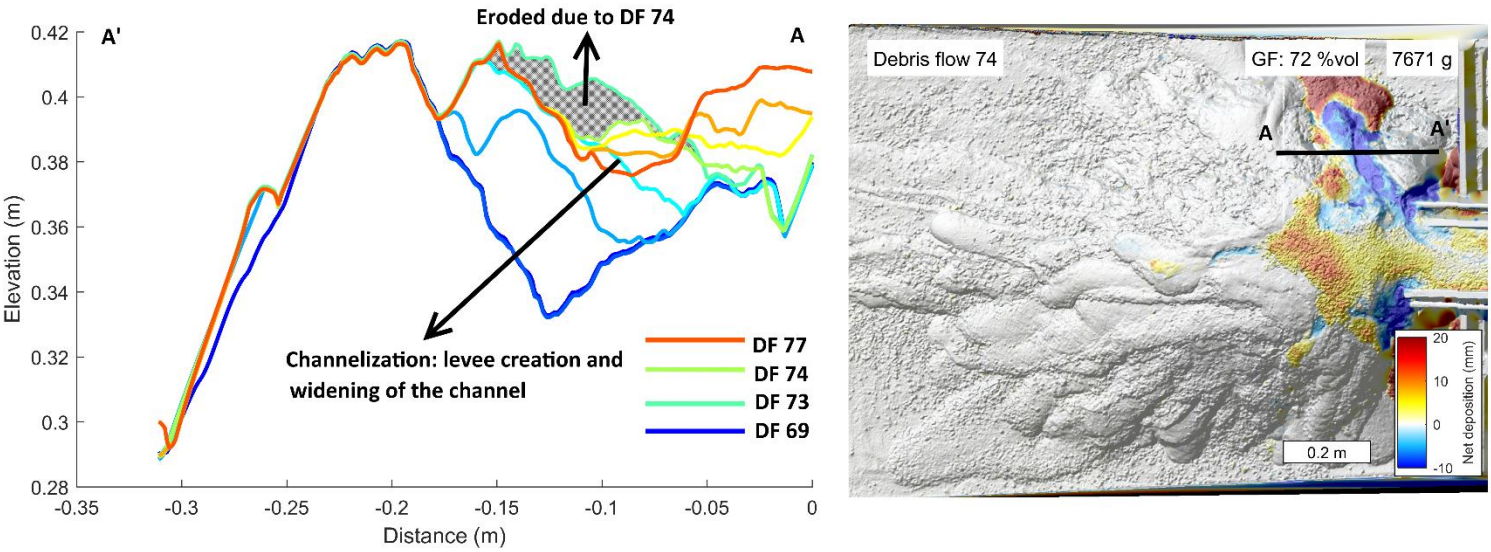

Figure 4.14: Left: cross section of DF 69 to DF 77. Right: erosion & deposition of DF 74 with the indication of cross-section position. The left image shows that DF 74 is able to erode a large portion of the prior flow deposit. This first erosion event causes next flows to be routed along this route, subsequently channelizing it; creating levees and widen it.

Overall, when focusing on the effect of gravel fraction change on the spatio-temporal patterns of fan 01, several preliminary conclusions can be made. (1) A sediment composition change within a debris flow can reduce or increase runout. However, fan topography and debris-flow volume seem to dictate mobility. (2) Gravel-poor debris-flow events show little to no erosive behavior and seem to form a more compact debris-flow deposit with high lobe thicknesses. These gravel-poor debris-flow deposits are therefore more favorable to act as channel plugs, especially in combination with lower volumes. (3) Gravel-rich debris-flow events show more erosive behavior. Due to this erosive behavior they are able to incise the debris-flow fan, subsequently creating a space to route upcoming sediment. Gravel-rich debris flows therefore seem to occasionally act as an initiator for avulsions. However, conditions must be favorable (such as in figure 4.9 & 4.14). To aid these conclusions, observation during the experiment showed that gravel-poor debris flows were effectively holding water within the deposit, whereas gravel-rich debris flows were releasing more water after and during deposition. Therefore, the debris flow looked more watery during high-gravel events and more solid during low-gravel events. These conclusions will be thoroughly tested within coming sections and Discussion chapter.

4.2.2. Fan 02

Figure 4.15 gives the summary of measurements for fan 02. During the creation of this fan only the gravel fraction sequence has been changed in comparison with fan 01. This figure alone shows a very large difference in spatial temporal evolution as compared to fan 01. In places, comparisons with fan 01 will be made to show differences or similarities between trends on the fans

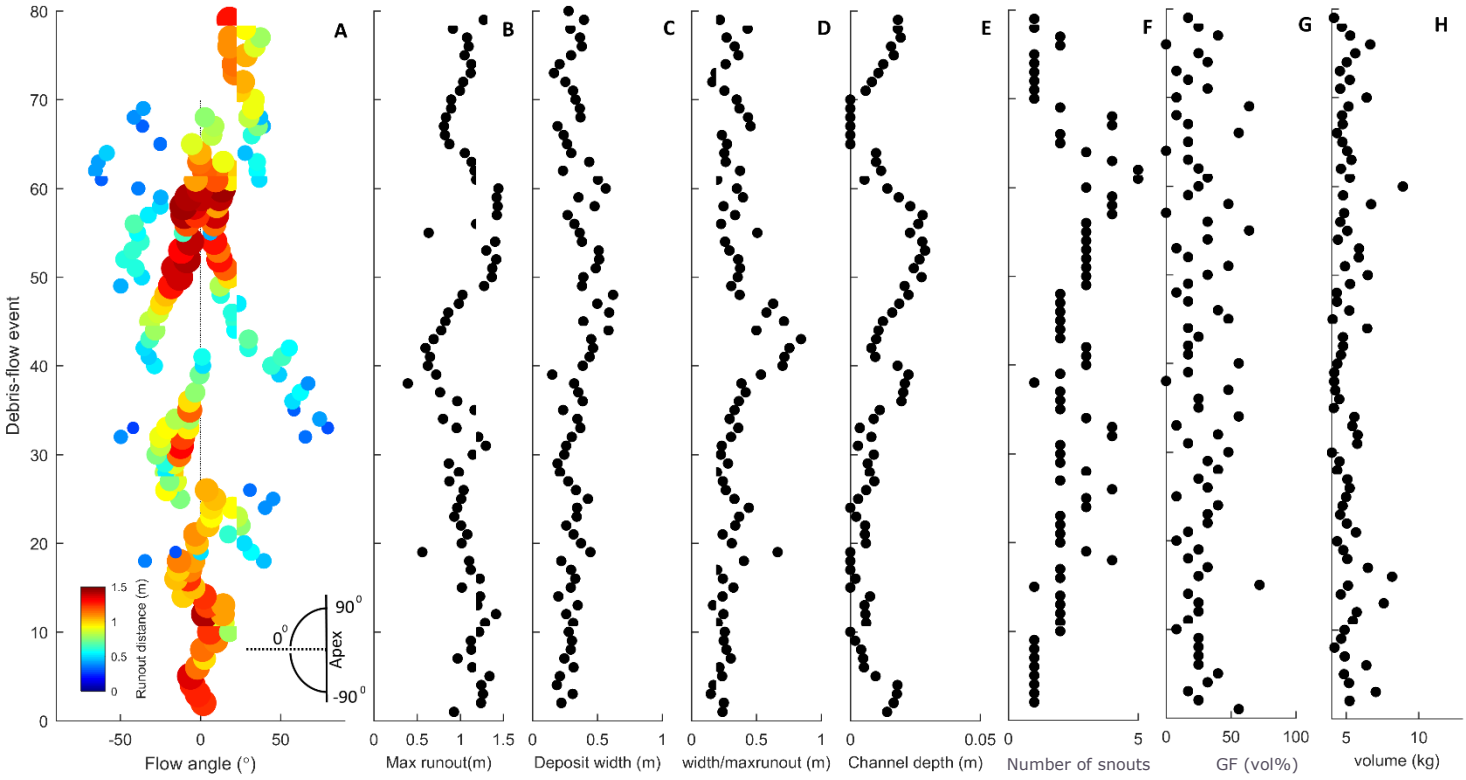

Figure 4.15: Summary of spatio- temporal measurements on fan 02. The y-axis values represent the debris-flow events for every plot whereas x-axis values differ per plot. (a) Flow angle and runout distance per snout against the debris-flow event. Multiple data points during one debris-flow event indicate multiple snouts. Warm colors denote high runout values whereas cold colors denote lower runout values. (b) Maximum runout (m) for each debris flow indicating the debris-flow snout with the largest length. (c) Deposit width (m) for each debris flow. (d) Width of the deposit divided by the maximum runout. (e) Channel depth close to the apex in order to derive sequences of backfilling and channelization. (f) Number of snouts of each debris flow. (g) The gravel fraction (vol%) of the debris-flow sediment mixture. (h) Debris-flow volumes (kg).

After the first debris-flow event, the influence of gravel fraction is directly visible. As expected (according to the reference experiments), DF 1 (7.1 kg; 56 vol% gravel) is reaching slightly further than half of the outflow plain. In comparison to the similar sized debris flow from fan 01 the runout distance is drastically reduced (figure 4.16). As DF 1 acts as a plug, the momentum of the next debris flow is reduced resulting in an increased width and shorter runout distance for DF 2 (9.6 kg; 25 vol% gravel). Evidently, in this stage, a composition change does influence local topography development. The blockage of DF 1 prohibits the debris-flow fan from reaching max extent until DF 12 (10.3 kg; 25 vol% gravel).

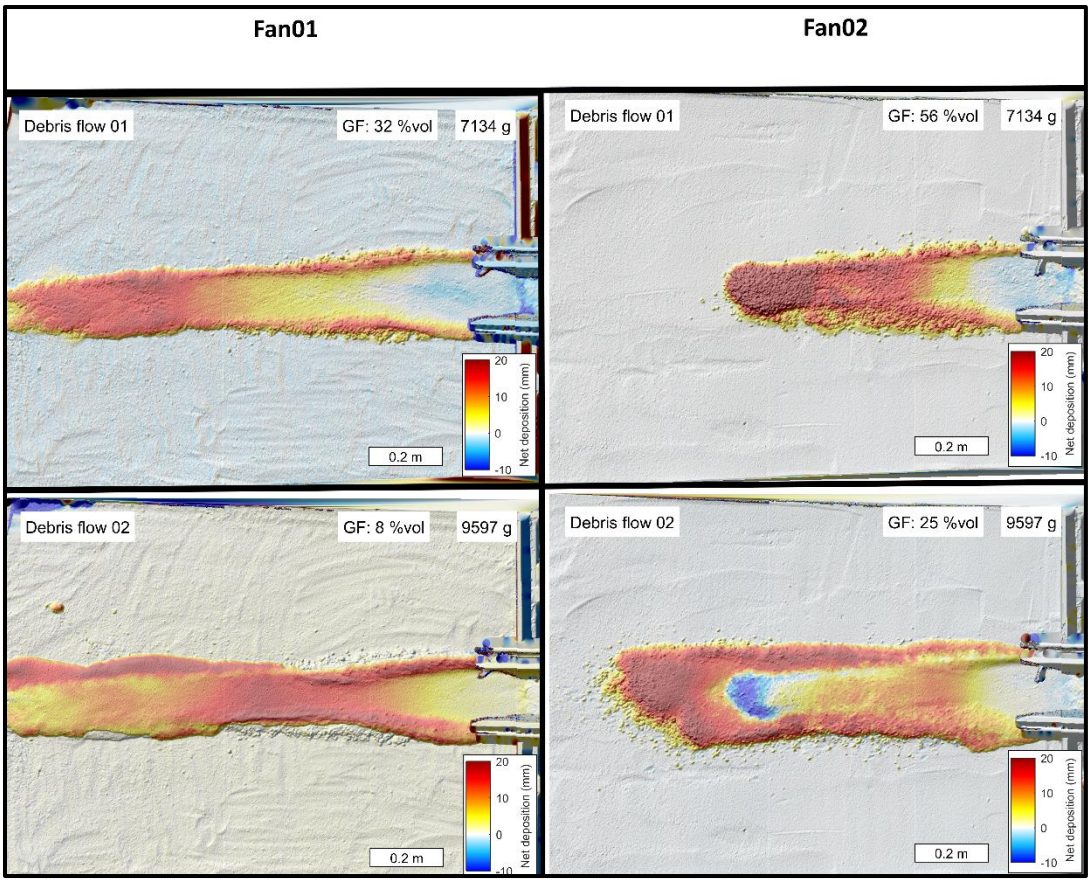

Figure 4.16: Left: Erosion and deposition image from fan 01, DF 1 (32 vol% gravel) & DF 2 (8 vol% gravel). Right: Erosion and deposition image from fan 02, DF 1 (56 vol% gravel) DF 2 (25 vol% gravel). Evidently shows the influence of composition in the early stages of fan development. High-gravel debris flows are less mobile with little to no topographic influence.

DF sequence 5 to 7 shows a backstepping sequence induced by decreasing debris-flow volume (respectively: 8.7, 6.7, 5.7 kg), regardless of a change in debris-flow composition (40, 25, 25 vol% gravel). This indicates that over such large volume changes a small composition change has little to no visible effect on fan development. Until DF 8 (6.3 kg; 25 vol% gravel) the main locus of activity lies approximately around the fan midline. The gradual filling of the main channel (also in figure 4.15) causes DF 9 (6.7 kg; 25 vol% gravel) to overtop the levees on the right side of the fan. Subsequent flow DF 10 (7.4 kg; 8 vol% gravel) is then able to flow via this route. However, this flow lacks the ability to create a channel, therefore next flows are again directed towards the fan midline. The absence of a channel for routing and the large increased deposition closer to the apex can be pointed out as cause (rather than composition change) for the prevention of avulsion development on this side of the fan. The increased deposition close to the apex is the result of a small bulge created due to the sequence of backfilling.

DF 15 (11.1 kg; 72 vol% gravel) is the largest debris-flow event occurring on the debris-flow fan and also contains the highest gravel fraction. From figure 4.15d it can be deduced that channel depth is nearly 0 when this debris-flow event occurred. Figure 4.17 shows the debris-flow deposit and shows that it was able to overtop all channel levees subsequently eroding the sides of the debris-flow fan. It becomes evident that runout distance is low relative to the volume. For example, the previous debris-flow event DF 14 (7.0 kg; 17 vol% gravel) is able to flow further. DF 15 does not have enough momentum and force to overtop the end lobe of the previous deposit although the surface is nearly flat (as visualized in figure 4.17).

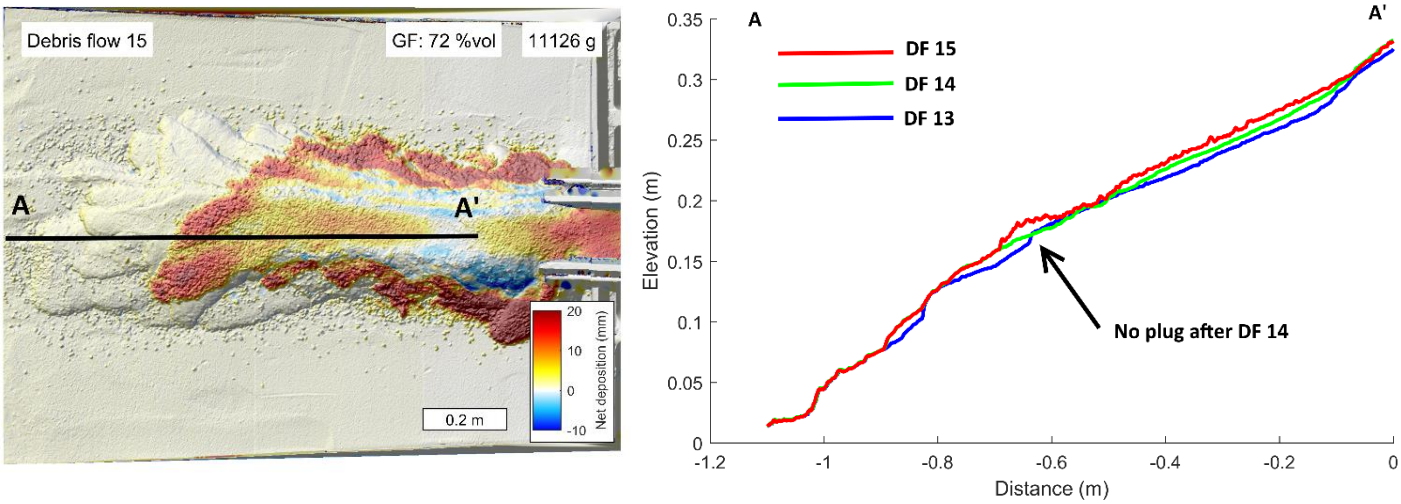

Figure 4.17: Left: Erosion and deposition image of DF 15 deposit. with indication of cross section position. Right: cross section as depicted in the left image. DF 15 snout is visible. it shows evidently that DF 14 did not leave an increased snout on the cross section indicating that DF 15 stopped due to a decrease in momentum and the lack of sufficient force to reach until max fan extent.

The geometry of this DF 15 deposit might show that, when topography is not a limiting factor, for example with the absence of a big solid plug, or a very deep channel, gravel-rich debris-flow events can sufficiently influence runout distance and therefore influence avulsion behavior of the debris-fan.

Due to the leftward orientation of the debris-flow snout of the DF 15 deposit, a small avulsion towards this side of the fan is initiated. DF 16 (8.9 kg; 25 vol% gravel) further erodes the channel levees on the left side of the fan enhancing further avulsion. Until DF 19 (6.0 kg; 25 vol% gravel) this side of the fan is used and a small channel is formed to route subsequent debris-flow events. The decreasing volumes (respectively 8.9; 6.9; 6.5 kg) prevent the avulsion from reaching larger runout distances. Also, the lack of channel levees after DF 15 leads to a number of small snouts close to the apex (figure 4.15a & 4.15f), decreasing debris-flow energy and therefore reducing maximum runout. DF 19 being smaller in size is able to route its sediment via one of these snouts on the right side of the fan creating a minor avulsion. Next flow DF 20 (7.8 kg; 8 vol% gravel) is able to overtop the channel plug that is deposited due to the avulsion in DF 19 and the main locus of activity is back on the fan midline. The debris-flow fan enters the searching phase with multiple snouts on either side of the fan until DF 26. During these flows fan evolution is driven by volume change rather than composition change.

From DF 26 (6.9 kg; 32 vol% gravel) an avulsion sequence commences. Where a clear channelization phase can be distinguished with increasing channel depths (figure 4.15e; DF 26-31). From DF 32 (7.4 kg; 40 vol% gravel) a backstepping sequence is initiated partly induced by increased erosion close to the apex. This erosion as also pointed out in figure 4.18 is caused by erosive power of trailing water after the debris-flow events. Due to the steep sides the water is able to incise deep into the debris-flow fan. This causes a sediment loss and therefore a momentum and energy loss towards the main channel along the fan midline. This event induces the backfilling of the main channel and subsequently an avulsion sequence to the right side of the fan.

Figure 4.18 depicts the two backstepping sequences from which DF 32 was the initiator, and DF 37 (5.7 kg; 48 vol% gravel) the end. The first backstepping sequence occurred during DF 32-34 and the other from 35-37. DF 35 (6.2 kg; 25 vol% gravel) is able to flow again along the fan midline and therefore can be seen as an avulsion.

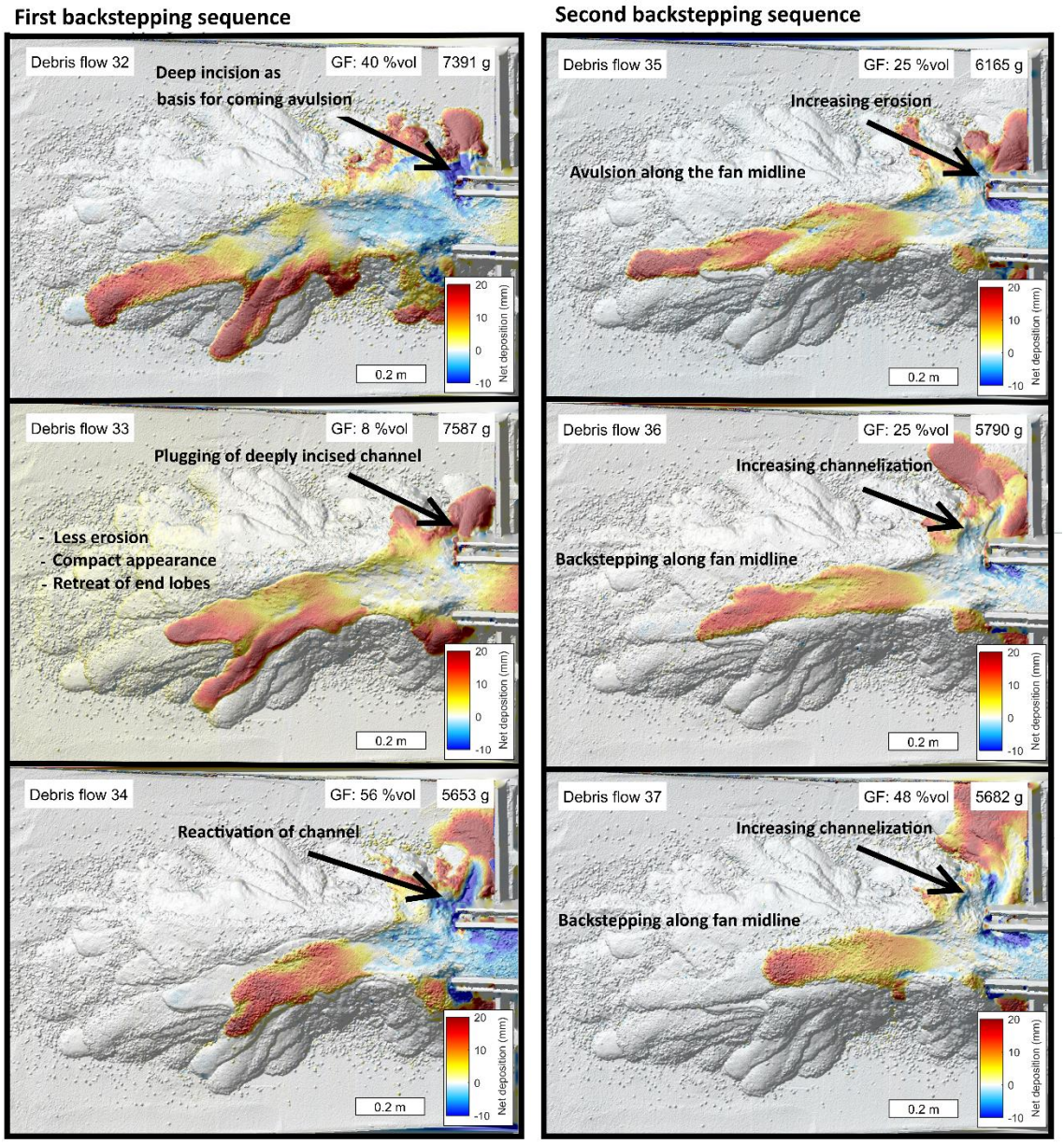

Figure 4.18: Erosion & deposition images of DF 32 to DF 37 showing two backstepping sequences with notations of process occuring during the sequence. DF 35 is the avulsion as a result of the first backstepping sequence. Red colors denote deposition. Blue colors denote erosion.

DF 33 (7.6 kg; 8 vol% gravel) is a remarkable event, where the volume is slightly higher than previous debris-flow event but it is not able to overtop previous deposit. It becomes evident from figure 4.18 that this deposit contains much less erosion and it has a much more compact appearance (e.g. less spread, lower deposit width). Also, it is able to fill in previous deep incision as depicted in figure 4.18 during DF 32. In relation to comparable results from fan 01 the processes during this event might be largely attributed to debris-flow composition. DF 33 creates a channel plug and forces the next debris-flow to stop earlier. However, as DF 34 (5.6 kg; 56 vol% gravel) already has a relatively lower volume it would be expected to have a reduced runout anyway. DF 34 being a gravel-rich debris-flow event shows substantial amounts of erosion and is therefore able to erode away the plug within the deep incision close to the apex. As also concluded on fan 01 here, the increased erosive power of gravel-rich debris-flow events is again demonstrated. So, regarding fan evolution the gravel-poor debris-flow

event DF 33 followed up by the low-volume gravel-rich debris-flow event DF 34 has little to no influence on debris-flow fan development. But, when DF 34 hypothetically contained a lower gravel fraction, the channel plug might not be eroded away and the avulsion on the right side of the fan would have never occurred. However, this is only speculation.

The main locus of activity remains on the right side of the fan until DF 43 (8.8 kg; 25 vol% gravel). Until this point gradual backfilling with approximately similar sized debris-flow events occurred (DF 40-42, respectively 6.3, 6.5, 6.5 kg). Remarkably, DF 40 (56 vol% gravel) has an increased erosion compared to DF 41 and 42 (17 vol% gravel; 17 vol% gravel). Again, gravel-rich debris flows are able to erode significantly more compared to gravel-poor debris flows.

DF 43 is able to spread along the fan, thereby blocking of the main channel and eroding the other side of the fan, acting as an initiator for next avulsion. Figure 4.15 shows that from DF 43 until DF 63 two main debris-flow snouts exist that increase in length towards the point that one is cut off and just one main channel exists. Regarding fan evolution, this is a large difference compared to fan 01 where one main channel existed and a few smaller snouts were present as well. Whereas the channel already formed at the left side of the debris-fan from DF 43, channelization starts only around DF 50 at the right side of the fan. This causes the left channel to be far more developed during DF 50 (figure 4.15: runout at the right side of the fan is slightly lower). Figure 4.19 shows a cross-sectional profile of run 43 to 64 where the development of two channels is visible.

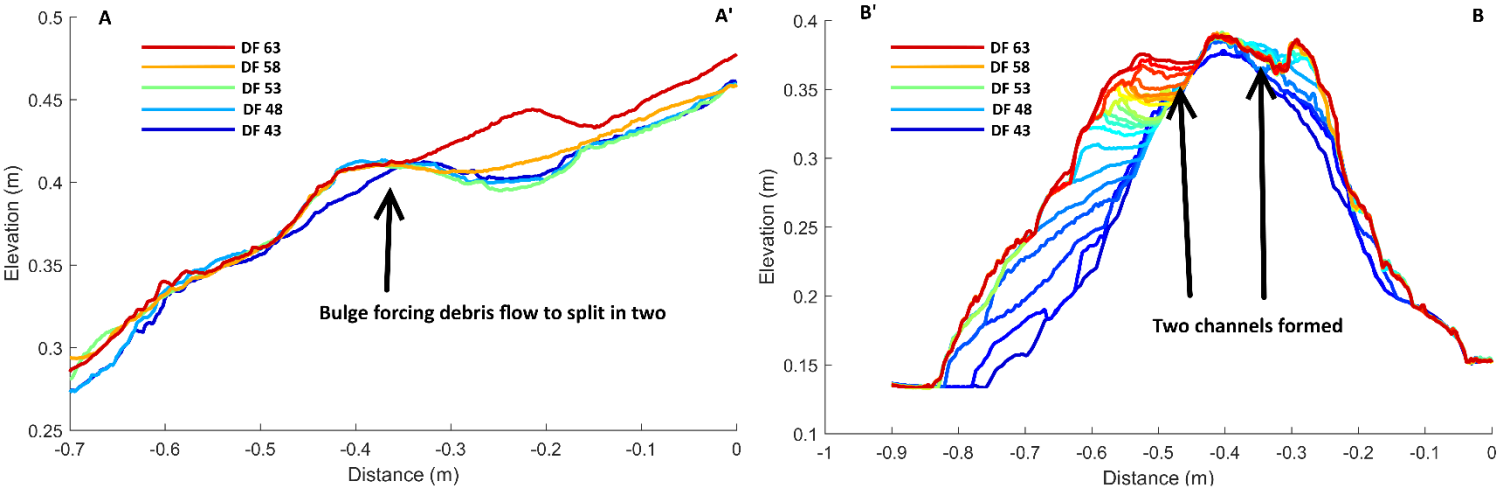

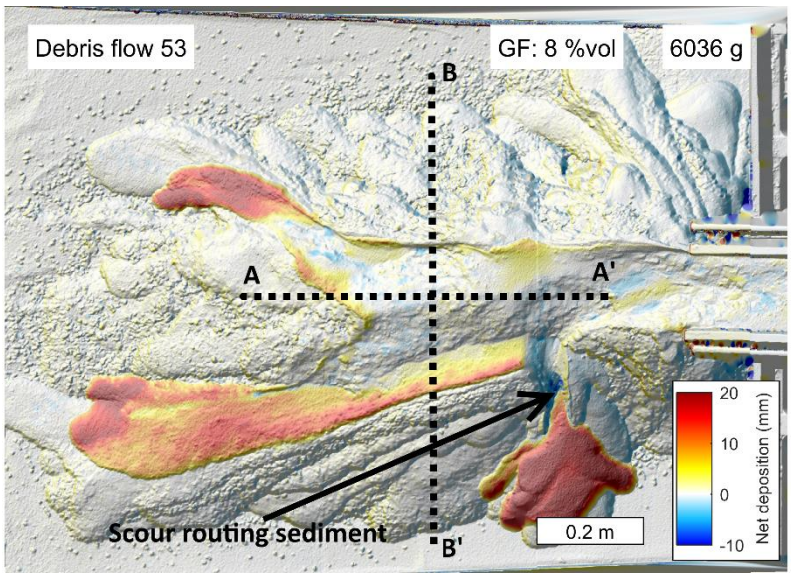

Figure 4.19: two cross-section profiles showing the development of the fan during DF 43 to DF 63, and the erosion/deposition image of DF 53 showing the position of the cross-sections. The section along the fan midline shows the bulge causing the debris flows to split and therefore the cause of the two main channels. The cross-section perpendicular to the fan midline shows the build op of the fan around this bulge. It is visible that on the left side of the fan channel formation occurred as an increasing channel levee height is visible in the later debris-flow events. On the right side of the fan increased scour causes the development of the channel starting around DF 50. On the image of DF 53 a scoured channel is visible at the left side closer to the apex, which is able to route substantial amounts of debris.

The position of the cross-section is depicted on an image of DF 53 (6.0 kg; 8 vol% gravel). This figure shows that a significant scour occurs at the left side of the debris-flow fan. This scour is routing sediment, subsequently decreasing the runout distance and volume within the main channel lobes. This scour developed since DF 43 where it started as minimal erosion. Only at DF 65 this channel is completely filled in and no debris is routed via this way anymore. This scour might be seen as an avulsion as it is able to route substantial amounts of debris via its channel. However, significant amounts of debris are still routed via the two large channels developed during the sequence of DF 43-63. It shows that the presence of channels increases the maximum runout substantially. Relatively low-volume debris-flow events were able to route until nearly maximum fan extent, while still some sediment was routed through the scoured avulsion on the left side of the fan (e.g. DF 53 – DF 56, figure 4.19; figure 4.20).

DF 55 (6.3 kg; 64 vol% gravel) is a high-gravel debris-flow event and reacts differently to the scour depicted in figure 4.19 and 4.20. For clarification DF 54 and DF 56 are also shown in figure 4.20. It becomes visible that DF 55 has a decreased momentum and is not able to overtop this scour and therefore completely routes via this channel. Observations during the experiment show that flow velocity is not sufficiently large to be able to follow the similar path as previous flows. DF 55 does have a lower volume however, keeping in mind that two fully developed channels are present which are able to effectively rout debris (as exemplified in figure 4.19 where DF 53 has a lower volume than DF 55). This is a relatively good indication of a sediment composition change affecting debris-flow runout and therefore debris-flow fan development.

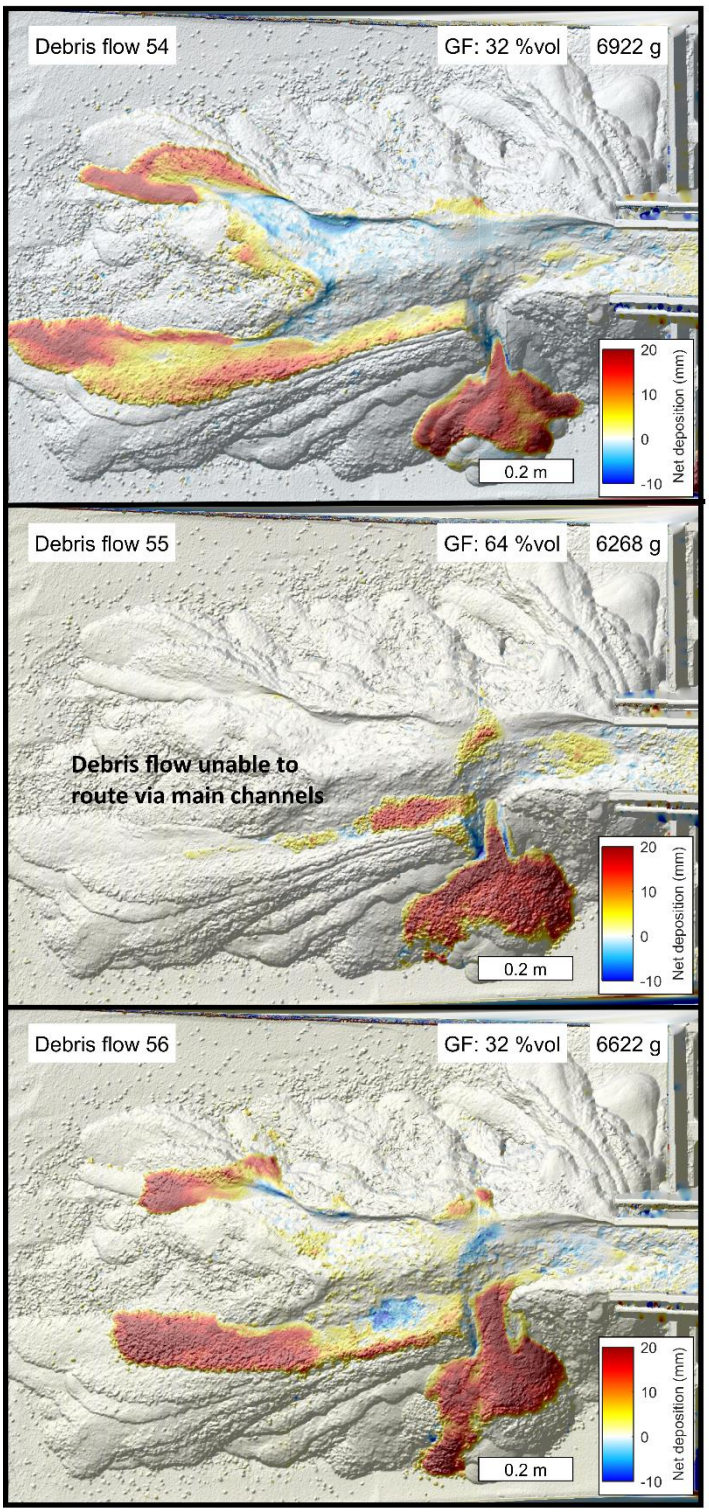

Figure 4.20: Erosion & deposition images of debris-flow sequence 54 to 56. DF 55 shows a decreased runout and a complete routing via the channel at the left side of the fan.

From DF 61 (6.3 kg; 32 vol% gravel) a backstepping sequence commences. At DF 64 (6.5 kg; 0 vol% gravel) the right channel of the two main channels is blocked and the left channel becomes the only main channel on the fan. The left channel is slightly lower than the right channel and therefore is able capture all the sediment. The backstepping sequence continues until DF 65 (6.0 kg; 17 vol% gravel). DF 66 (6.5 kg; 56 vol% gravel) then starts a new avulsion cycle towards the right side of the fan. It becomes visible that during deposition of the lobe towards the right side of the fan, a lot of erosion occurs (figure 4.21). This might have to do with the higher gravel content. It becomes evident that this commences a new channelization phase, next flow DF 67 (6.4 kg; 17 vol% gravel) uses this newly scoured pathway and further erodes it. Although lower in gravel content, this debris-flow event is also able to erode a substantial amount of the debris-flow fan. This might be a consequence of the initial erosion during DF 66 and thus a composition effect. However, this remains speculative.

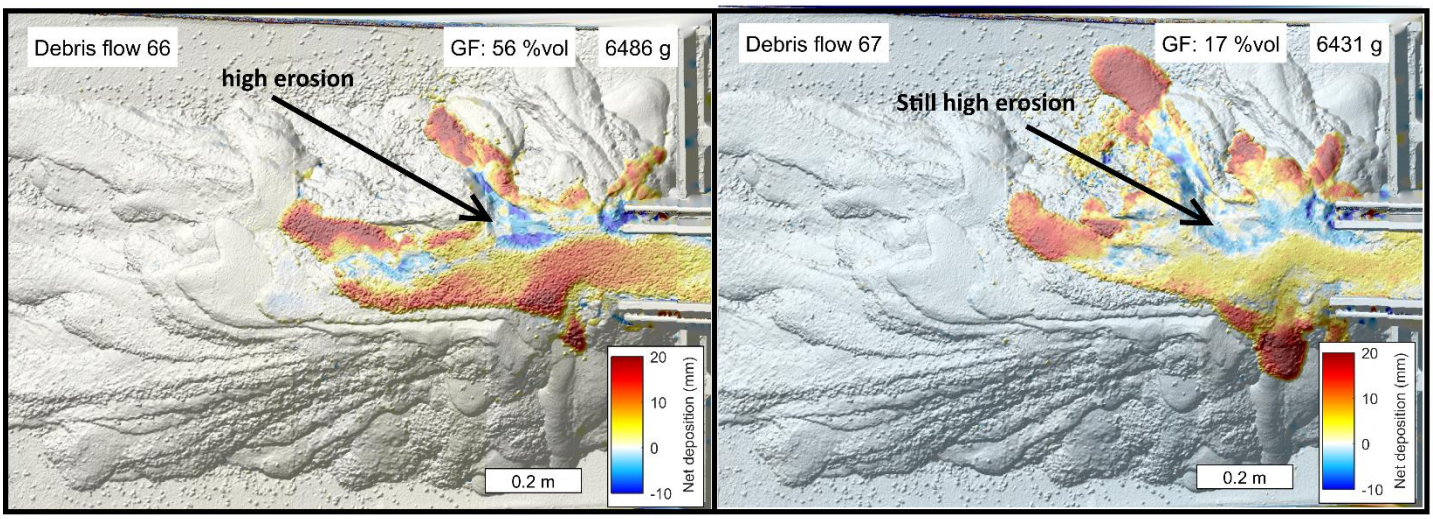

Figure 4.21 Erosion & deposition image of DF 66 & DF 67. It becomes visible that erosion is high at DF 66 when first flowing that direction. This results in DF 67 having increased erosion.

From DF 67 to DF 75 channelization causes the runout to increase slightly during each subsequent flow. Eventually from DF 75 to 79 a backstepping sequence commences. Both the channelization and backstepping sequence are mainly caused by the variability in volume.

Overall, similar trends as fan 01 can be derived. However, for this fan the influence of changing debris-flow sediment composition on debris-flow fan development seem less pronounced. In early stages of fan creation, the influence of a change in sediment composition is obvious as runout distances are decreased, but when topography becomes more complex more variables come into play which are able to affect debris-flow deposition. Gravel-rich debris flows seem to be able to exert more control on debris-flow fan behavior as opposed to gravel-poor debris flows. Namely, mobility seems drastically more decreased during gravel-rich debris-flow events than for gravel-poor debris-flow events. Also, erosive power of gravel-rich debris flows seems higher. The compactness of gravel-poor debris-flow events seem to occur on this fan, however, multiple gravel-poor debris-flow deposits did not show this behavior and thus that relationship is not as apparent as for fan 01. Next sections will go deeper into the influence of a change in sediment composition on debris-flow deposition and debris-flow fan development.

4.3. Gravel fraction effect

To investigate the effect of gravel fraction on the behavior of debris flows and thus the eventual evolution of the debris-flow fan maximum runout and snout width/height ratio are compared against the gravel fraction. According to the reference experiments snout width/height ratio is influenced by a change in gravel fraction. Snout width is excluded from this analysis as snout width is mostly dependent on topography, volume and number of snouts. Similarly, debris-flow snout height is also dependent on these factors. By taking the width/height ratio, the volume factor and the increased amount of snouts are partly cancelled out. An increase in volume causes an increase in both width and height therefore dividing them with each other cancels out this effect. Similarly, more snouts cause smaller lobes however, their relative size is expected to be similar. Width/height ratio on the other hand is still influenced by topography.

Figure 4.22a & 4.22c depict the maximum runout against the gravel fraction with volume as third variable of fan 01 and fan 02. Figure 4.22b and 4.22d depict the maximum runout against the volume with gravel fraction as third variable. The red lines in figure 4.22a and 4.22c depict the average value per gravel fraction.

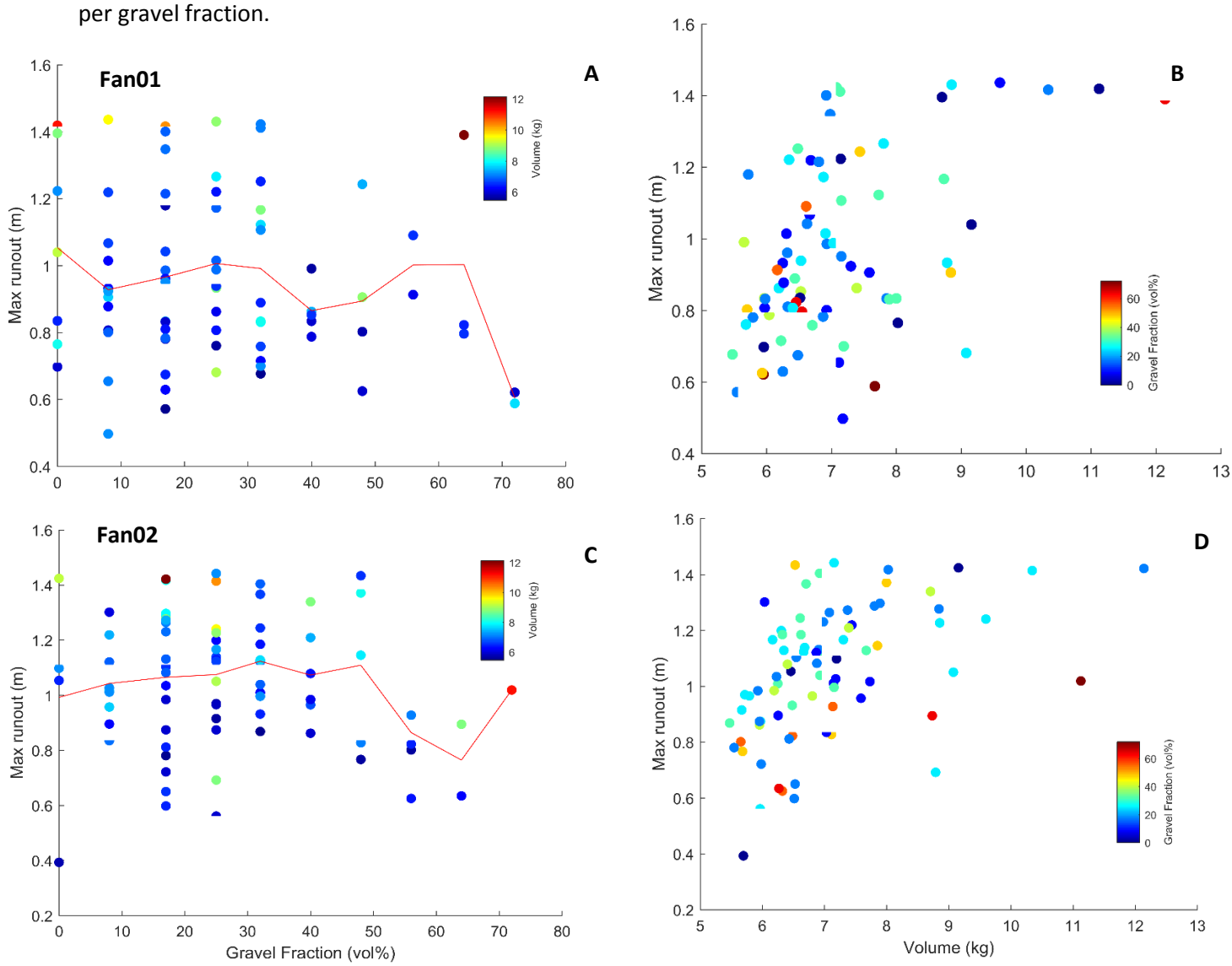

Figure 4.22: Gravel fraction and volume effect on maximum runout for fan 01 and fan 02. (A) Maximum runout (m) against gravel fraction (vol%) with volume (kg) as third value for fan 01. The red line depicts the average for each gravel fraction. (B) Maximum runout (m) against volume (kg) with gravel fraction (vol%) as third variable for fan 01. (C) Maximum runout (m) against gravel fraction (vol%) with volume (kg) as third value for fan 02. The red line depicts the average for each gravel fraction. (D) Maximum runout (m) against volume (kg) with gravel fraction (vol%) as third variable for fan 02.

Based on the reference experiments (figure 4.1) and the previous study of De Haas et al (2015) it is expected that runout is lower at lower gravel fractions, peaks around a gravel fraction of 25 to 32 vol% and then reduces towards the higher gravel fractions. In general, fan 01 does not show this trend (figure 4.22a). Only the 72 vol% gravel fraction shows a drastic decrease in runout distance. Two of the tree data points with a 64 vol% gravel fraction show a decreasing tendency however, the average trend is distorted because one of the debris-flow events with 64 vol% gravel contained the largest volume within the experiment. Therefore, it was able to have an increased runout. It must be noted that, although it was the largest volume in the experiment, it was not able to reach maximum fan extent.
For 0 vol% gravel fraction this relationship is the opposite of what is expected (based on figure 4.1) however, from figure 4.22a it can be deduced that a relatively large portion of the debris-flow events containing 0 vol% gravel also consisted of a large volume therefore distorting the trend.

In general, for fan 02 (figure 4.22c) this trend seems to follow the relationship established within the reference experiments and the experiments of De Haas et al. (2015). Both higher- and lower-gravel debris-flow events show lower average maximum runout distances. Runout distance peaks around 32 vol% and then gradually declines towards higher gravel fractions. One debris flow containing a gravel content of 72 vol% simultaneously contained one of the largest volumes during the experiment. This causes the maximum runout to be substantially increased therefore distorting the trend. It is however worthy to mention that, although it contained one of the largest volume it was not able to surpass maximum average runout. This trend gives a small indication of composition change able to influence fan evolution.

Figures 4.22b and 4.22d both show the volume against the maximum runout for fan 01 and fan 02. A relationship can be deduced from this images in which an increase in volume does seem to increase maximum runout. It indicates that in general debris-flow runout is influenced by volume. Possibly for fan 01 the influence of volume, and the influence of topography are too pronounced so that in general the effect of gravel fraction on runout diminishes.

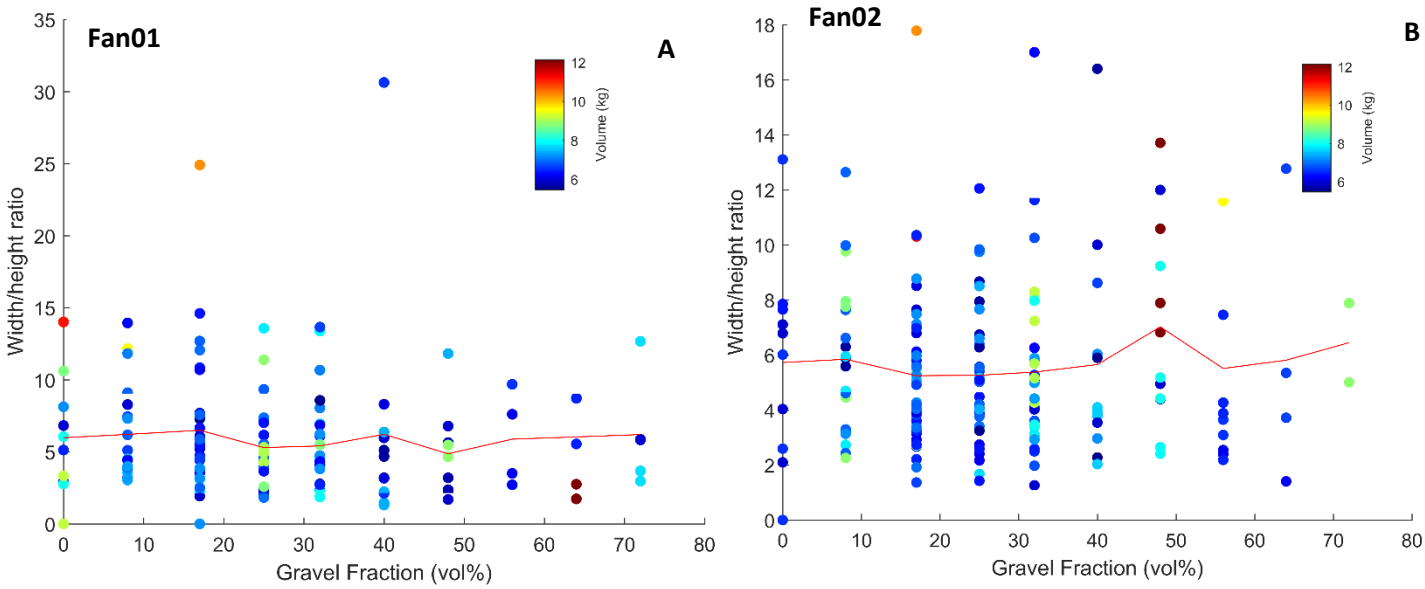

Figure 4.23: Gravel fraction against width/height ratio with volume as third variable for fan 01 and fan 02. The red line connects average values per gravel fraction.

In figure 4.23 the width/height ratio per snout per debris flow is put against the gravel fraction with volume as the third variable for fan 01 and fan 02. The red line connects the average width/height ratio values per gravel fraction. Based on the reference experiments it is expected that the width/height ratio of lower gravel fractions is relatively lower and increases slightly towards higher gravel fractions. This trend however, fluctuated heavily and should be approached with caution.

For both fan 01 and fan 02 no apparent effect of debris-flow composition can be depicted. The width/height ratio lies on average approximately around 6 for both fans and remains approximately there for every gravel fraction. Also, a decreased width/height ratio for a gravel fraction of 0 vol% as depicted in the reference experiments is not visible. When the debris-flow fan is in a channelization or a backstepping phase, width is mostly confined or at least influenced by the width of the present channel. This means that width/height ratios are subsequently affected. Local topography therefore plays an important role in deposit width and thus also height.

This result means that the snouts are not relatively bigger and therefore do not cause an increased tendency for channel plugging. However, investigation on the spatio- temporal patterns in the previous section revealed that the overall thickness of a low-gravel debris-flow seemed relatively larger. In the next section it is investigated if this trend holds for all low-gravel debris-flow events.

4.4. Deposition & erosion patterns

Two preliminary conclusions based on the spatio-temporal patterns were that gravel-poor debris-flow events show more compact and less erosive behavior compared to gravel-rich debris-flow events and gravel-rich debris-flow events show more erosive behavior than gravel-poor debris-flow events. First the deposition per debris-flow area (m/m^2) against gravel fraction (vol%) is plotted. Then the erosion per debris-flow area (m/m^2) against gravel fraction (vol%) is plotted and finally the ratio deposition over erosion per debris flow (m/m) against gravel fraction (vol%) will be plotted. All images contain volume (kg) as third variable to give extra information on the effect of volume changes on the trends. It must be noted in advance that towards lower and higher gravel fractions data points become less abundant and therefore the scatter increases.

4.4.1. Deposition

Figure 4.24a and 4.24b give the total deposition divided by the area of the debris-flow deposit (m/m^2) against the gravel fraction (vol%) for fan 01 and fan 02. For fan 01 (figure 4.24a) it becomes evident that there is a definite increase in deposition per area when having lower gravel fractions. This is in accordance with the results from the spatio-temporal patterns. This trend means that for lower gravel debris-flow events lobes will be larger in height and can therefore more easily act as plugs or increase backfilling speed.

As already expected from the observations, for fan 02, this trend is far less pronounced as for fan 01 (figure 4.24b). It seems that debris flows which are higher in mobility (e.g. GF 25 vol% & GF 32 vol %) have an increased deposition per area rather than the less mobile ones, which is counterintuitive as less mobile debris flows come earlier to a stop containing more volume within a smaller space. The trend from figure 4.22c shows that lower-gravel fractions show lower maximum runout distances, therefore it is also expected solely based on this data that total deposition should increase. According to the reference experiments this trend should especially hold for low-gravel debris-flow events as they have relatively small widths, relatively short runout distances and relatively higher snout heights (figure 4.1). However, several other factors affect the area of deposition. For example, (1) the presence of a channel, (2) the presence of a plug causing sediment to abruptly stop and accumulate and, (3) the absence of a channel causing the debris flow to spread across the total debris-fan. On fan 02 topography may have been such a controlling factor that these trends could not occur.

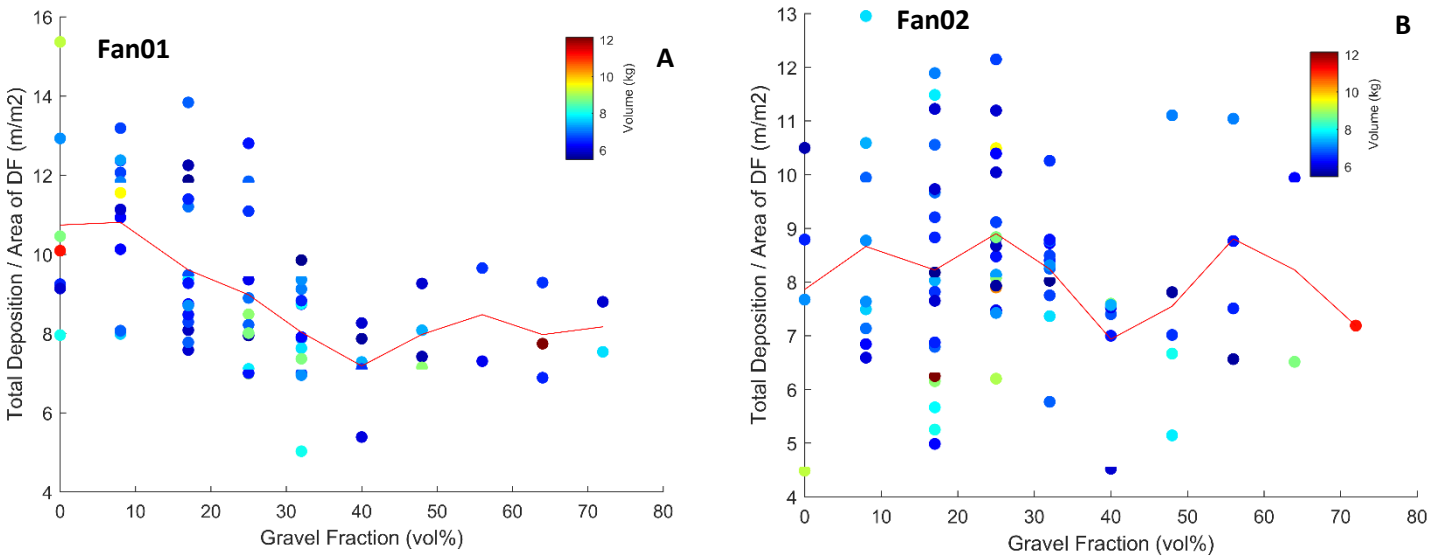

Figure 4.24: Gravel fraction (vol%) against total deposition divided by the total area (m/m2) with volume as third variable for fan 01 and fan 02. The red line connects the average values per gravel fraction

4.4.2. Erosion

Figure 4.25a and 4.25b give the total erosion divided by the area of the debris-flow deposit (m/m^2) against the gravel fraction (vol%) for fan 01 and fan 02. For fan 01 (figure 4.25a) this figure shows a strong trend of an increase in erosion towards higher gravel contents. A decreasing trend is already visible with somewhat lower gravel contents (from 25 vol% until 48 vol%). This trend implicates that debris flows with higher gravel content are able to effectively erode parts of the debris-flow fan. An increase in erosion increases the possibility of avulsion towards this incised part, as shown in the spatio- temporal patterns (Figure 4.5, 4.9 & 4.14).

For fan 02 this trend is quite similar as for fan 01 and compared to figure 4.24b far more evident than the deposition per area trend on the fan. Similar to fan 01, it becomes visible that erosion increases towards higher gravel fractions. Analysis on the spatial-temporal patterns on fan 02 did show that erosion seemed higher towards higher-gravel fractions, but the trend was far less pronounced compared to fan 01. However, the analysis in figure 4.25b shows that on fan 02 erosion is also higher towards higher gravel contents and therefore strengthens the conclusion.
Remarkably, for one debris flow containing a gravel content of 72 vol% the total erosion per area is substantially lower and therefore distorts the trend. However, this debris-flow event had a very large volume and occurred quite early in fan-development (DF 15), which means that the area was substantially larger and debris-fan steepness was not as high as for later debris-flows. This possibly caused the erosion to be limited.

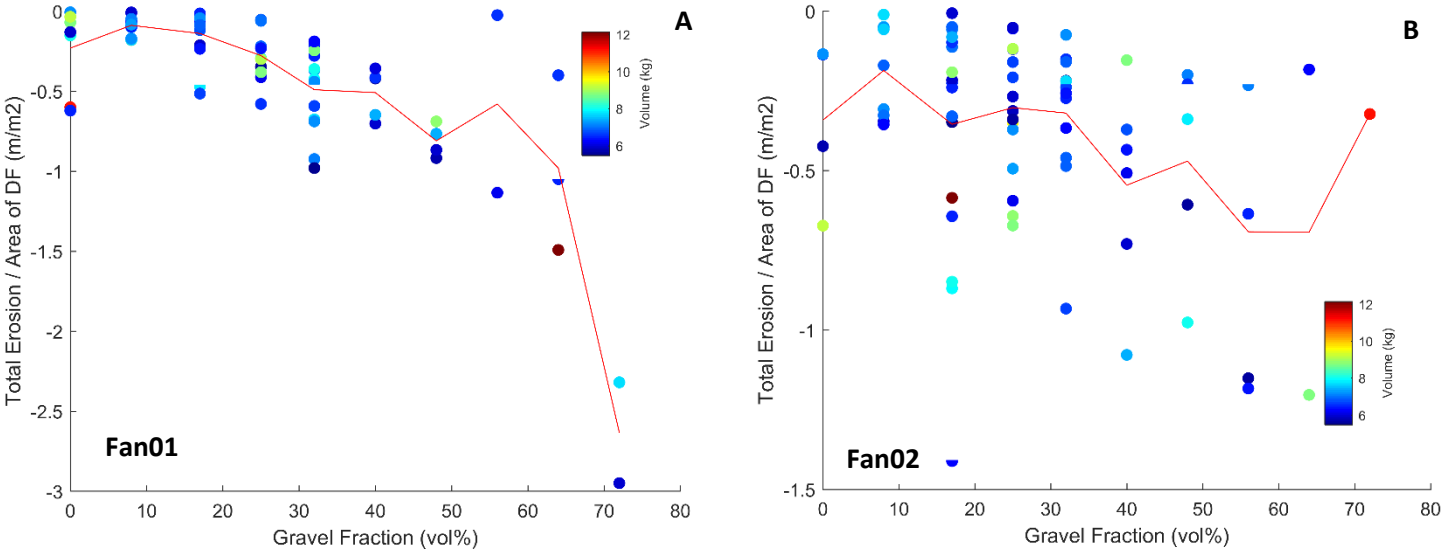

Figure 4.25: Total erosion divided by the total area per debris flow (m/m²) against gravel fraction (vol%) with volume as third variable for fan 01 and fan 02. Red line connects the average values per gravel fraction. Negative numbers indicate negative deposition and thus erosion.

4.4.3. Deposition-erosion ratio

Figures 4.26a, 4.26b and 4.26c show the deposition-erosion ratio for fan 01 and fan 02 per gravel fraction. Due to the peaks in deposition erosion ratio especially with lower gravel fractions the graph cannot be properly read, therefore in 4.24b and 4.24c the y-axis is limited to respectively 400 m/m and 250 m/m which enhances readability but a few data points are lost. Nonetheless they are taken into account during the average calculation depicted by the red line. For fan 01 it becomes evident that the ratio is very high with low gravel fraction, this possibly due to the complete absence of erosion during low-gravel debris-flow events (as dividing by a value close to 0 results in very large values). Towards higher gravel fraction the value ratio decreases meaning that deposition values are closer to erosion values indicating that deposition is lower or erosion is higher. Taking into account both figures 4.24a and 4.25a, it is evident that erosion increases over deposition so it is safe to conclude that erosion increases relative to the deposition towards higher gravel fractions on fan 01.

For fan 02 higher deposition erosion ratio values occur in the lower gravel fraction indicating that the trend is approximately higher for low-gravel fractions and lower for high-gravel fractions. The figure shows that low-gravel debris-flow deposit substantially more than they erode. However, this trend does not hold for a gravel fraction of 0 vol %. Possibly due to the influence of local topography as described in section 4.4.1. Also towards higher gravel fractions, the trend of increased erosion over deposition is less pronounced than during fan 01. It might be the consequence of an apparent reduction of influence of debris-flow composition with deposition on fan 02 (figure 4.24b). The main deduction that can be made from figure 4.26c is that in general deposition per area is larger than erosion per area during lower gravel fractions (8-32 vol%).

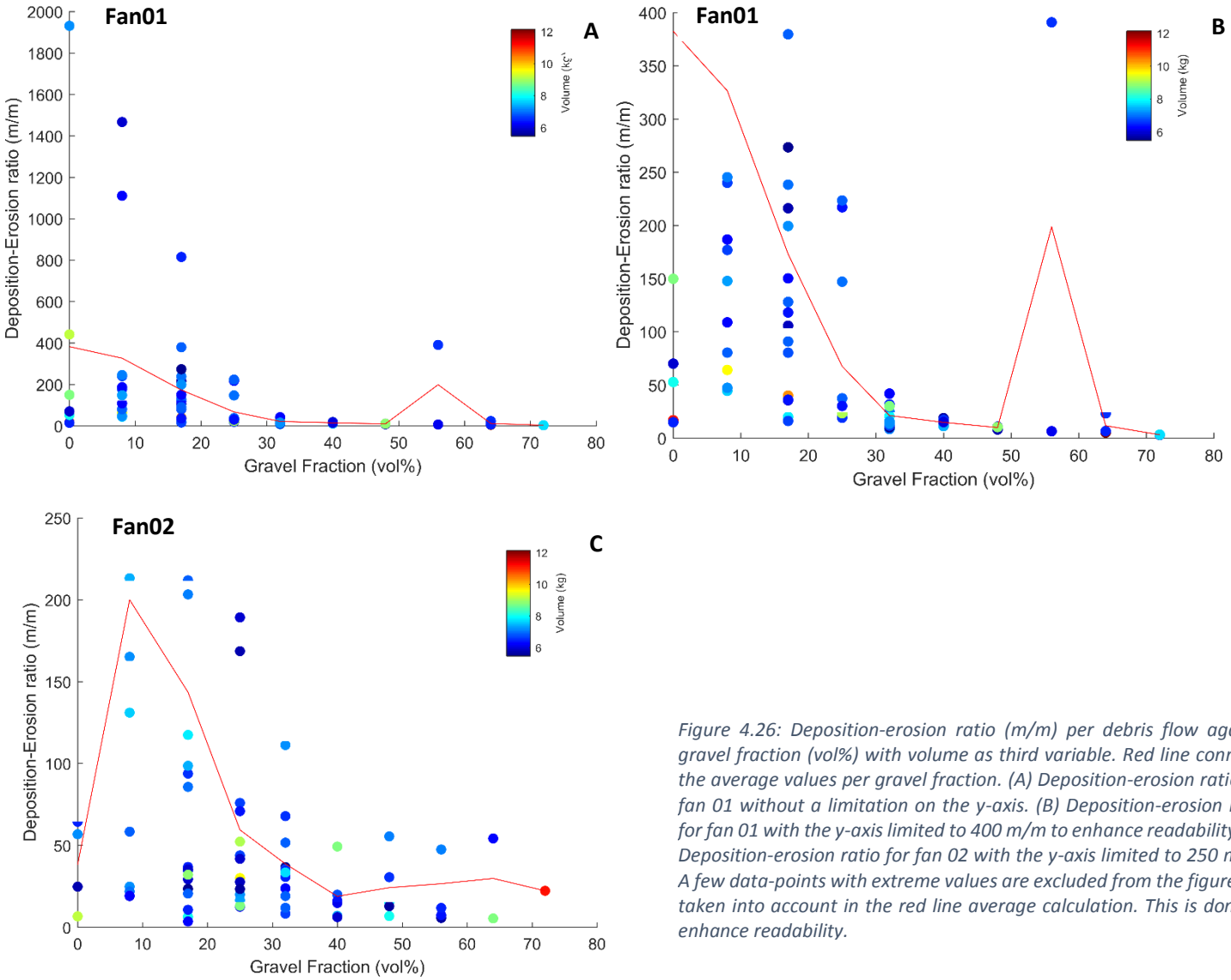

Figure 4.26: Deposition-erosion ratio (m/m) per debris flow against gravel fraction (vol%) with volume as third variable. Red line connects the average values per gravel fraction. (A) Deposition-erosion ratio for fan 01 without a limitation on the y-axis. (B) Deposition-erosion ratio for fan 01 with the y-axis limited to 400 m/m to enhance readability. (C) Deposition-erosion ratio for fan 02 with the y-axis limited to 250 m/m. A few data-points with extreme values are excluded from the figure but taken into account in the red line average calculation. This is done to enhance readability.

4.5. Hazard map

Figure 4.27 shows the hazard maps of both fan 01 (figure 4.27a) and fan 02 (figure 4.27b). The numbers within the map are percentages, where a hundred percent indicates that all debris-flow events passed that point on the map. Both these maps show that the debris-flow fan expands radially from the apex elongated along the fan midline downslope. The elongated shape can mostly be attributed to the high momentum and energy of the debris flow when it passes the apex. Due to this effect the debris-flow fan is not purely radial. However, on natural fans, this effect can also be seen (De Haas et al., 2017). On fan 01 it becomes visible that, as depicted in figure 4.27a, the right side of the fan is used less frequently as the left side. This is because of accumulation of material on this side prevented the flow to go that direction. Remarkably, this had such an impact that it caused the main direction of the flows to be slightly pointed underneath the fan midline.

In contrast to fan 01, the main direction of fan 02 is along the fan midline (figure 4.27b). It also becomes evident that runout distances are higher than for fan 01 as a result of the two main channels that occurred during fan evolution that were able to effectively route debris further downslope.

Remarkably, also an area of relatively lower number of encounters is positioned on the right side of the fan. However, far less pronounced than during fan 01. The position of the avulsion and subsequent channelization in the later stages of the fan development is also visible right from the fan midline as depicted in figure 4.27b.

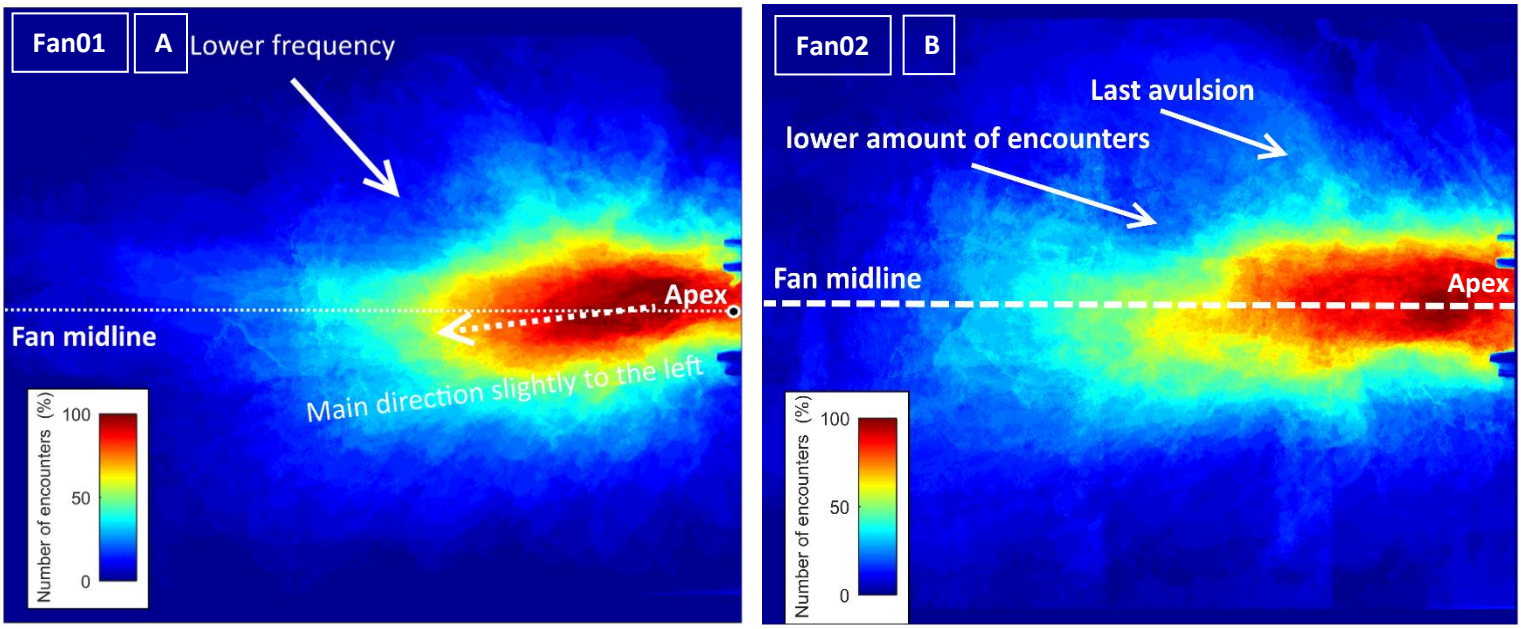

Figure 4.27: Hazard map containing the number of encounters for each spot on the outflow plain. Red colors denote a high frequency and blue colors denote lower frequencies. (A) Fan 01, (B) Fan 02

4.6. Roughness

Here a summary of surface roughness evolution will be given. Average bed roughness is put against maximum runout and width/height ratio to be able to deduce any influence of bed roughness on fan evolution and, the results of the lobe-snout bed roughness analysis will be summarized.

4.6.1. Surface roughness evolution

In figure 4.28 surface roughness evolution of fan 01 and fan 02 is depicted by consecutive plotting of every 10th debris-flow event. Starting with the 1st event in the darkest blue. Warmer colors depict later debris-flow events. Figure 4.28b and 4.28d depict the runout distances with gravel fraction to be able to relate the surface evolution to a change in runout distance and debris-flow composition. Surface roughness is calculated after every debris flow until the maximum extent of the debris-flow fan. This means that during the first debris-flow events the debris-flow fan extent is significantly smaller. Inherently to this, a small change in roughness with a smaller fan extent can therefore have a significant effect on the average surface roughness (e.g DF 1 for fan 02 in figure 4.28b). When the debris-flow fan starts to get fully developed, this effect will be much smaller. Because of this, little details are neglected and the focus lies on the general patterns visible, especially those in later stages of the debris-flow fan.

For fan 01 (figure 4.28a), the foremost trend that becomes evident is that close to the apex, the surface is less rough throughout fan development. An explanation for this occurrence might be the fact that the main channel is present here. Because the bulk of the gravel tends to focus on the front of the debris flow and in the levees as seen during the reference experiments and in De Haas et al. (2015) and Iverson (2010) it causes the occurrence of a low-gravel surface along the first meters of the debris-

flow fan. However, for fan 02 (figure 4.28b) this difference is not as pronounced. When solely focusing on the runout distance per gravel fraction from the reference experiments and De Haas et al. (2015) it is possible to assume that when the debris-flow fan is getting more developed the surface roughness will be going towards an equilibrium where the distal part of the debris-flow fan will have an average roughness representing more mobile gravel fractions, whereas proximal parts will have an average roughness representing less mobile gravel fractions. Relating to the reference experiments, it means that extremely rough debris-flow events deposit the closest to the apex and then a combination of gravel-rich and gravel-poor debris-flow events. Both fan 01 and fan 02 do not show this differential grain size distribution along the fan surface. However, due to the fact that both gravel-rich and gravel-poor debris flows are immobile it might occur that these cancel each other out so no trend becomes evident.

Fan 01 does show some large fluctuations in surface roughness in comparison with fan 02 which does not seem to fluctuate much. On fan 01 from DF 30 to DF 50 it is visible that a high peak of surface roughness is visible which seems to enlarge towards later debris-flow events. From observations during the experiments it becomes evident that for the most part a searching phase was active during this debris-flow sequence. This led to maximum debris-flow runouts approximately reaching halfway the fan (figure 4.28b; figure 4.29). High-gravel debris-flow events within the searching phase did not always have a clear snout and lobe structure, but were a bit more spread out. This caused gravel at the edges of the debris-flow deposit to be ejected and carried downslope by gravity rather than due to the carrying capacity of water (figure 4.29). Eventually an accumulation of coarser material occurred a bit downslope leading to an average increase in surface roughness.

Both fans do not show any significant trend, possibly due to the number of debris-flow runs. But most likely due to the absence of water-fraction change within the debris-flows. As Whipple & Dunne, (1992) attribute the grain size segregation mostly to the change in water volume within the debris-flow events (further elaborated on in Discussion).

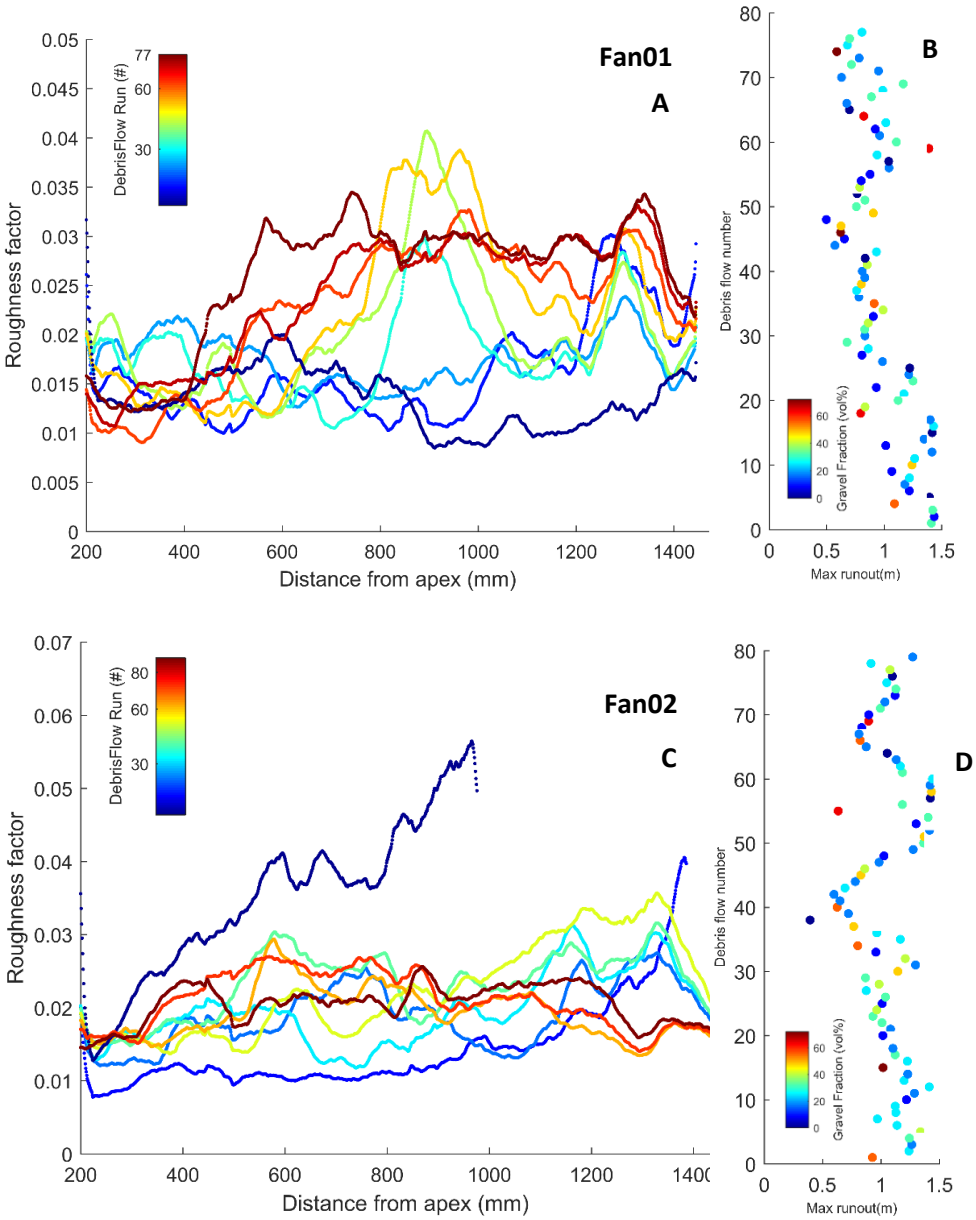

Figure 4.28: Surface roughness evolution for fan 01 and fan 02. Every 10th DF is plotted starting with the first event in dark blue. Warmer colors depict later debris flow events. Part C & D depict the maximum runout (m) against the debris-flow number with gravel fraction as third variable. This, to be able to better relate surface evolution with maximum runout and gravel fraction.

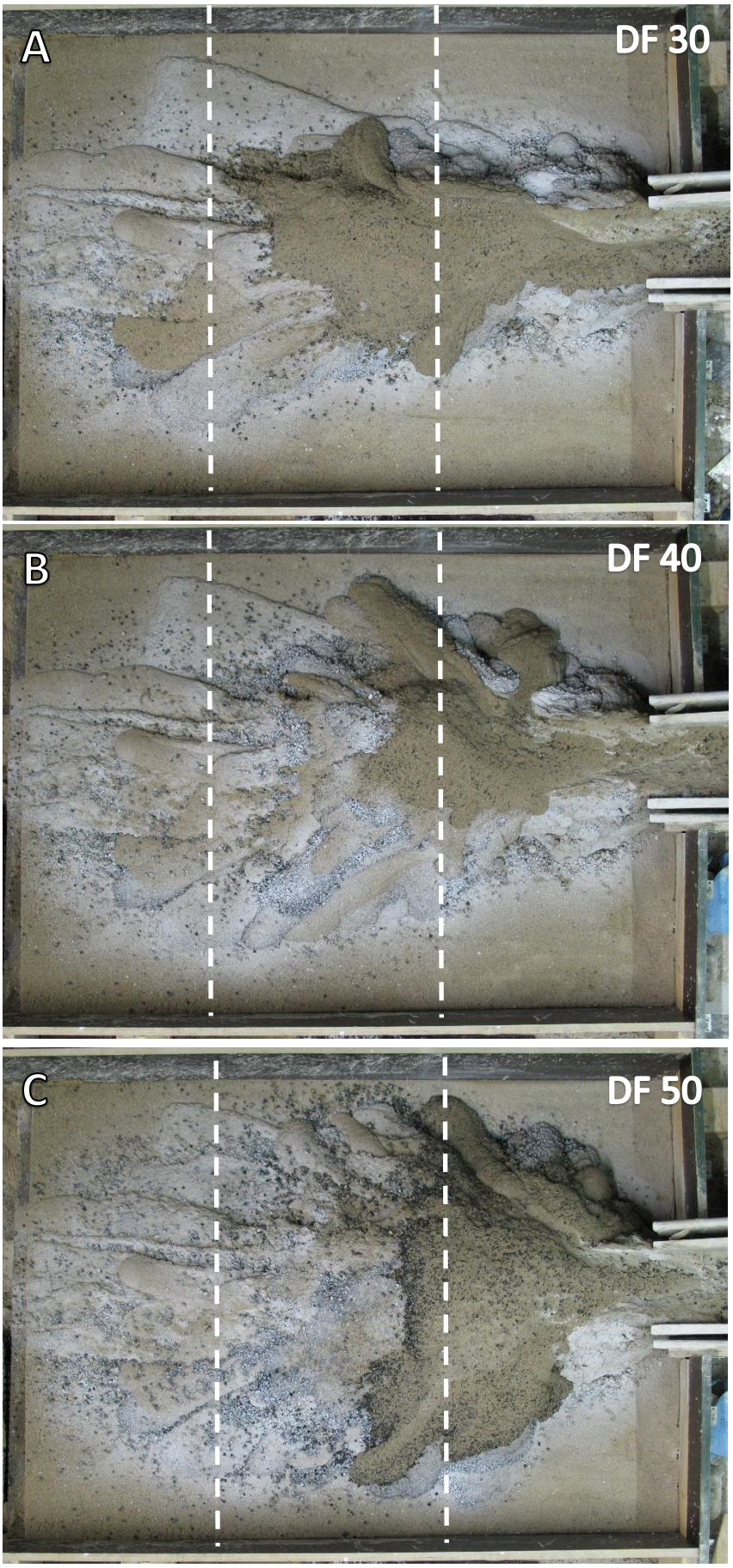

Figure 4.29: Top down view of the surface of fan 01 after (A) DF 30, (B) DF 40, (C) DF 50. An increase in loose gravel particles is seen mid-fan due to the ejection of particles from the debris flows (area between the white dashed lines). The debris-flow fan shows a white glow, which is caused by spraypaint needed for proper DEM extraction. Both DF 30 and DF 50 show a large width due to the debris-flow fan, being in a long-lasting searching phase.

4.6.2. Average bed roughness

The average bed roughness value is a quite simplistic value that represents the average bed roughness that is underneath the debris-flow deposit. Local variation within the bed roughness is neglected, but comparing the average bed roughness underneath a debris-flow deposit, with its snout width/height ratio and maximum runout might reveal any general relationships.

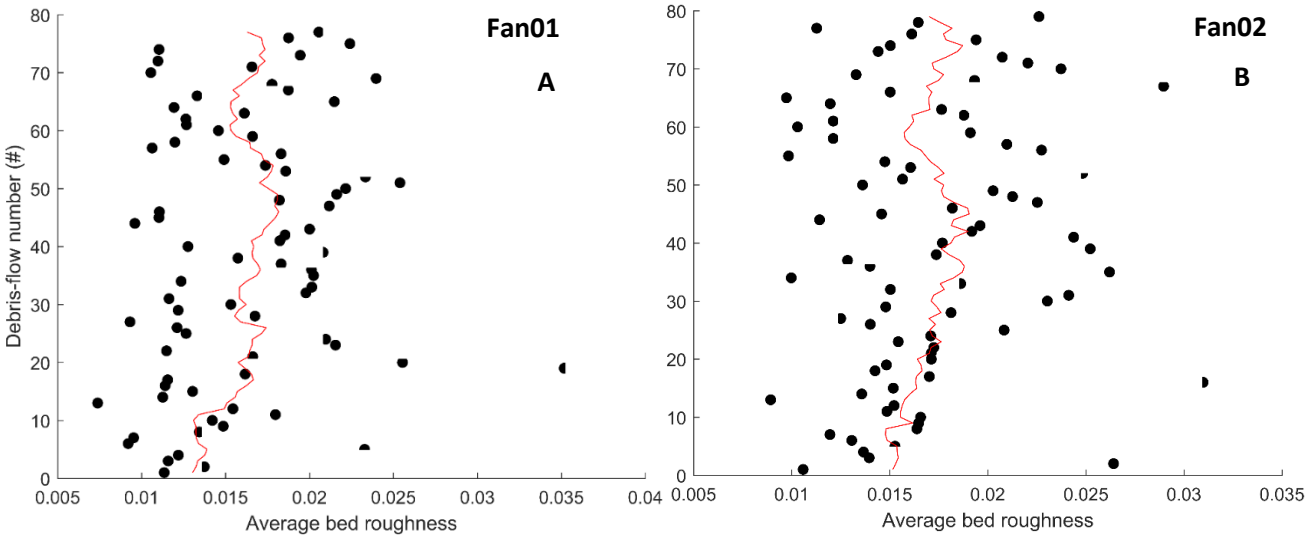

Figure 4.30: Average bed roughness underneath the debris-flow deposit against debris-flow number for fan 01 (A) and fan 02 (B). The red line indicates the moving average with a kernel size of 15 values.

Figure 4.30 puts the debris-flow number against the average bed roughness for fan 01 and fan 02. The red line depicts the moving average with a kernel size of 15 values so local variation are neglected and the main trend becomes clear. For both fan 01 and fan 02 there is an increase in average bed roughness with increasing fan development. For fan 01 this increase is visible until DF 30. After that debris-flow event the average bed roughness varies more or less around the same value. A small dip occurs between DF 60 and DF 70, as a result of a backstepping sequence which caused in-channel deposition. Bed roughness in a channel is mostly lower than surrounding parts. When a backstepping sequence occurs the debris flows are mainly deposited within the channel and therefore bed roughness is reduced.

For fan 02 the average bed roughness increases until approximately DF 45. Then the average starts to decrease again where it again starts to rise around DF 63. Remarkably, this decrease in bed roughness coincides with the avulsion creating the two main channels. Debris flows were mainly routed through the main channels, as channel beds are mostly smooth, average bed roughness is subsequently reduced.

Figure 4.31 shows the average bed roughness against the maximum runout of the debris-flow event, with the volume as third variable. For both fan 01 and fan 02, no relationship can be deduced. Iverson (2010) and De Haas et al. (2015) concluded that bed roughness has an effect on runout as described earlier. However, based on this figure, it seems that on a small-scale debris-flow fan, volume has more influence on maximum runout especially for the larger volume events. Some medium-sized debris flows (represented as green to yellow dots in this image) seem to be having variable maximum runouts, ranging from low to medium length. However, these debris flows are most likely influenced by other factors, such as local topography and number of snouts of the debris-flow deposit and also the gravel fraction.

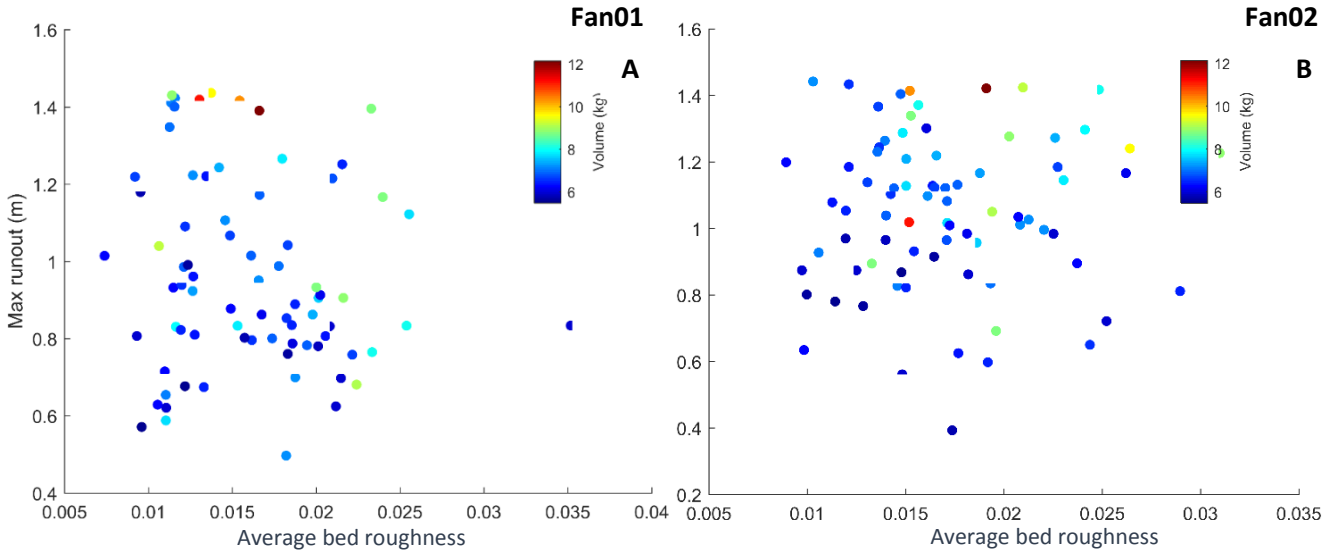

Figure 4.31: Average bed roughness underneath the debris-flow deposit against the maximum runout per debris-flow event for (A) fan 01 and (B) fan 02. Colors of the data dots depict the volume.

Figure 4.32 shows the average bed roughness underneath the debris-flow deposit against the width/height ratio of each snout. For fan 01 a trend is visible in which an increase of width/height ratio seems to occurs towards lower bed roughness's. For fan 02 this trend is not that clear. Because of the fact that multiple factors influence the width/height ratio, including gravel fraction (see reference experiments) and local topography no substantial bed roughness effect can be derived from both these figures.

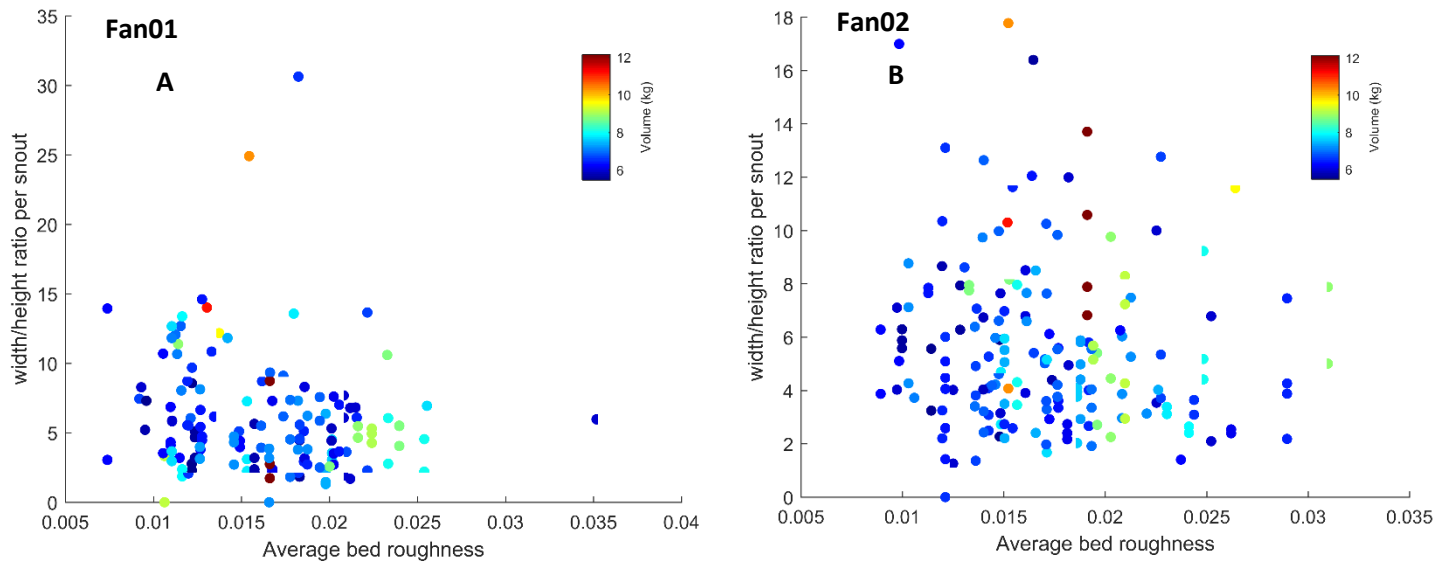

Figure 4.32: Average bed roughness against width/height ratio per snout with volume as third variable for (A) fan 01 and (B) fan 02.

4.6.3. Body-snout comparison

To get a more detailed insight in the influence of bed roughness on the runout of the debris-flow event, the average bed roughness per area underneath the snout is divided by the average bed roughness per area underneath the body. If it turns out that bed roughness is higher underneath the snout than underneath the body, this might indicate that debris flows runout is decreased when encountering a rougher bed. Figure 4.33 shows the results of this analysis.

For fan 01 it becomes visible that approximately two-third of the debris-flow snouts stops at a rougher bed. It is a result that should be approached with caution. First, the trend is not very convincing as still one-third stops at a less rougher bed. And second, when relating it to the surface roughness evolution graph (figure 4.28a), which displays a roughness increase towards distal parts of the fan. Given the fact that the snout lies further away from the apex than the body. This lower surface roughness area close to the apex decreases the average body bed roughness and therefore gives a distorted view. Also in consideration with the fact that the maximum runout is not affected by bed roughness the given results presented in figure 4.33a should be approached with care.

Similar to fan 01, the majority of debris-flow snouts on fan 02 tend to stop on a rougher bed. In fact, apparently during fan 02 the number even increased compared to fan 01. According to figure 4.28c no significant roughness change is occurring along to fan towards the distal parts. This leads to the idea that bed roughness is evenly spreaded along the fan. Therefore, the fact that the majority of the snouts have a rougher bed than their body has a little more added value as it seems that although no apparent difference downstream occurs, debris-flow events tend to stop on rougher bed. However, the results should again be approached with care as figure 4.31b shows that maximum runout is not affected by bed roughness and also the area of calculation for the average roughness within the body or the snout significantly differs. Where larger body values potentially tend to have more similar roughness values as a small change in bed roughness does not influence the total body as much as a similar sized change in bed roughness would affect the average bed roughness within the snout having a much smaller area.

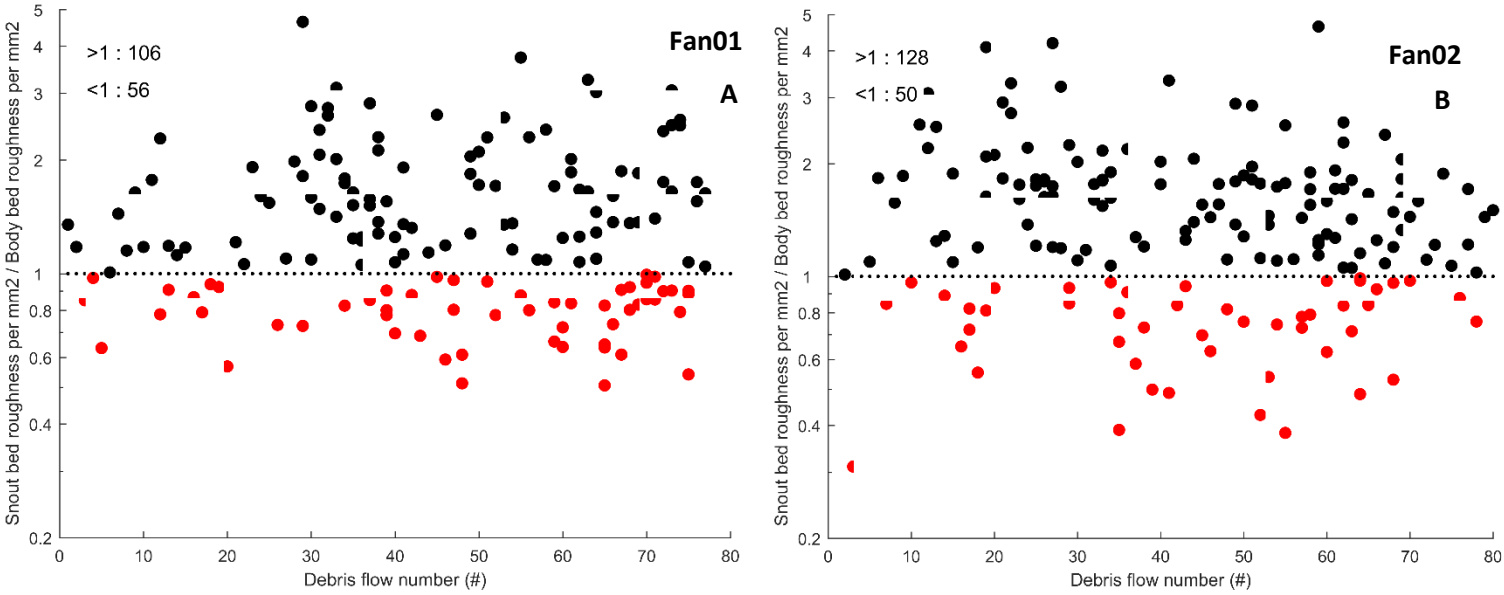

Figure 4.33: Average bed roughness per mm² of the debris-flow deposit snout divided by the average bed roughness per mm² of the debris-flow deposit body. The Y-axis is a log-scale. A value higher than 1 indicates rougher bed underneath the snout and vice versa. Red colors indicate data with values lower than 1. (A) Fan 01, 106 snouts have higher roughness than their bodies. 56 snouts have lower bed roughness than their body. (B) Fan 02, 128 snouts have higher roughness than their body. 50 snouts have lower bed roughness than their body.

During the experiments, no significant effect of sieving due to a matrix-poor bed, as described by Hooke (1967) and Milana and Tietze (2002) and observed in the field by Milana (2010), could be observed. Hooke (1967) mentions that sieve deposits tend to occur when little to no finer material is present within the debris flow. During this experiment matrix-poor deposits mostly occurred when debris flows contained very high gravel fraction (72 vol% gravel). However, these high-gravel debris-flow deposits were usually followed by more matrix-rich lower-gravel debris flows, so effective sieving could not occur. Also, these high gravel debris-flow deposits were more easily eroded by the subsequent debris-flow events due to lack of cohesivity. This caused the gravel-rich debris-flow deposits to rather be eroded than to cause any significant sieving. Also, no winnowing of matrix due to infiltrating water could be observed. Additionally, when taking into account that bed roughness did not show any significant effect in general, and a questionable effect on runout distance as revealed with the lobe-snout analysis, the effect of sieving does not become clear.

5. DISCUSSION

In this section, both experimental debris-flow fans are compared and discussed. First the effects of surface roughness and gravel fraction on avulsion behavior and fan evolution is discussed. A relation will be made with the experiments of De Haas et al. (*in review*) of which the thin double-pareto magnitude-frequency distribution used during the fans in this study corresponds to a fan in that study. Then, the processes as deduced from the experimental fans will be related to natural debris-flow fans. Secondly, the effects of the smaller scale within this experiment will be analyzed to ascertain comparability with natural debris-flow fans. And thirdly, implications will be made for mitigation of debris-flow hazards.

5.1. Effects of surface roughness and gravel fraction on avulsion behavior and fan evolution.

5.1.1. Gravel fraction

In this section the general trends in relation to gravel fraction as depicted in the results section are discussed. Results are related to literature and the usefulness for hazard mitigation is derived.

5.1.1.1. Surface roughness evolution

Surface roughness evolution of both fans did not show a particularly pronounced differential grain size distribution along the fan surface based on the mobility of the debris flows. Fan 01 did show a peak in roughness approximately halfway the fan from DF 30 to DF 50. However, this occurred due to the fact that the fan was in searching phase with increased number of snouts and a decrease in maximum runout where gravel was ejected from the debris flow downslope rather than being transport as part of a fluid (as explained in section 4.6.1). Distribution of debris flows based on their mobility was therefore limited by local topography. On fan 02 such a long-lasting searching phase did not occur, possibly explaining the lack of such a high peak in surface roughness. Observations on the experimental fans within this study are in contrast with observations of Whipple & Dunne (1992) and Blair & McPherson (1998), who observed a decrease in roughness towards more distal parts of the Owens Valley natural debris-flow fans. However, they concluded that water content in a debris flow on a debris-flow fan in the Owens Valley has a significantly larger effect on runout distance than a variation in grain-size. In addition, De Haas et al. (2015) also showed a significant effect of water fraction change on runout distance. During this study water fraction remained the same for every debris-flow event and based on the results, no influence of gravel fraction on the evolution of the surface roughness can be deduced. In relation to the results of De Haas et al. (2015) and Iverson (2010) and the natural debris-flow fans in the Owens valley (Whipple & Dunne, 1992; Blair & McPherson, 1998), this strongly suggests that on both natural and experimental debris-flow fans water fraction has a strong influence on surface evolution and a change in gravel fraction alone is not able to significantly change surface roughness evolution and enhance differential grain size distribution on a debris-flow fan. To create an experimental fan with variable water content, would possibly aid this discussion.

5.1.1.2. Maximum runout and width/height ratio

Whipple & Dunne (1992) attribute the evolution of morphology of the fan to two key features. The physical properties of the debris flow and the fan topography (presence of channels, slope, etc.). De Haas et al. (2017) divides the cause of avulsion behavior and the spatio- temporal evolution in processes occurring on a debris-flow timescale and processes occurring on multiple debris-flow timescales. In which local topography and debris-flow mobility are the key features on a single debris-flow timescale and the compensation tendency of the system is the key feature on the multiple debris-flow scale.

On a debris-flow fan, debris-flow runout is partly related to the mobility of the debris-flow event. The effect of gravel fraction on mobility on a single debris-flow scale becomes apparent in this study (reference experiments and occasionally on the experimental fans as depicted in the spatio- temporal

pattern section) and several other studies (Major, 1997; Iverson, 2010; De Haas et al., 2015). However, relating the maximum runout to the gravel fraction per debris flow gives different trends for fan 01 and fan 02 (figure 4.22). For fan 01 this trend is far less pronounced than for fan 02. Fan 01 however, had a searching phase which lasted approximately 20 debris flows (DF 30-50). This had a significant effect on the fan topography and thereby affected the course of multiple subsequent debris flows. This becomes apparent from the total hazard map where debris-flow events are directed with an angle to the fan midline. For fan 02 such a long-lasting searching phase did not occur. On this fan, a long-lasting channelization phase in which two main channels were present occurred (also approximately 20 debris-flow events, DF 43-63). Debris flows were routed through these channels and were therefore able to reach their full potential distance. The long-lasting channelization phase, and the lack of other strong topographical features obstructing debris flows during fan 02 results in a maximum runout trend that better represents the mobility of the debris flows with compositions (reference experiments).

These results suggest that when topography is sufficiently complex gravel fraction has less influence on runout distances. In relation to the observations, this suggest that on the scale of multiple debris-flow events, it is very much dependent on the evolution of the topography to which extent gravel fraction is able to influence runout distance.
It must be noted that volume also has an obvious effect on mobility, as the trend of higher runout distances with higher volumes is also apparent (figure 4.22b & 4.22d). The thin double-pareto magnitude-frequency distribution as used during the experiment of De Haas et al. (*in review*) is used during my experiments. However, when a change in magnitude-frequency occurs, this trend might be very different, as different volumes have different effects on local topography. It is therefore of importance to test the effect of a gravel fraction change with different magnitude-frequency distributions.

Width-height ratios of debris-flow snouts do not show any trend towards different debris-flow compositions (figure 4.23). In the reference experiments, although not very evident, a slight increase towards higher gravel fractions is seen, and a significant decrease with 0 vol% gravel (figure 4.1). The lack of trend suggests that the width-height ratio is not influenced by gravel fraction at all on the debris-flow fan scale. As debris-flow deposition is mostly confined to the channel when in channelization and backstepping phase, and when in searching phase to a lesser extent, to the present topography at the edges of the debris-flow fan. This result relates to the observations of Whipple & Dunne (1992) and De Haas et al. (2017) that debris-flow deposition is dependent on the present topography during deposition.

Based on these results, it shows that the effect of a change in sediment composition on the debris-flow mobility is dependent on local topography, and that on the debris-flow fan scale, a change in sediment composition does not show a pronounced influence on the debris-flow fan development. However, the key feature that should be understood is how this topography is formed. Based on observations and general trends derived from all the measurements, this trend might not be visible, but if conditions are favorable one debris-flow event might initiate an avulsion, or a long-lasting searching phase, which is subsequently able to influence the topography as a whole. This emphasizes the significance of the behavior of a single debris-flow events in relation to fan development, which is later elaborated (section 5.1.3).

5.1.1.3. Deposition and erosion

A more clear, general trend can be deduced from the erosion per mm^2 and deposition per mm^2 analysis. Fan 01 shows an increase in deposition per mm^2 towards lower gravel fractions and an increase in erosion per mm^2 towards higher gravel fractions. Fan 02 does not show an increased

deposition towards lower gravel fractions but does show an increase in erosion towards higher gravel fractions. This relationship of gravel fraction and bed scour is in accordance with other experimental flows (Egashira et al., 2001; De Haas & van Woerkom, 2016). An increase in debris-flow grain size causes an increase in erosion as the ratio between the debris-flow grain size and the bed grain size becomes larger (Egashira et al., 2001; De Haas & van Woerkom, 2016). The lack of erosion with gravel-poor debris flows on the other hand can possibly be accounted to a decrease in grain collisional forces and an increase in viscous flow behavior (Ancey, 2001; Iverson, 2010; De Haas & van Woerkom, 2016).

Additionally, when combining these results with the observations that low-gravel debris-flow deposits were able to retain their internal water for a longer period than high-gravel debris-flow deposits, it suggests that within this experiment high-gravel debris-flow events more easily lose their internal water. In gravel-rich debris flows there is an abundance of large intergranular pores, which imply the existence of hydraulic diffusivities (according to Iverson, 2010). These high diffusivities facilitate dissipation of excess pore fluid pressure and drainage of pores (Iverson, 1997; Iverson, 2010). The increased dissipation of internal water within gravel-rich debris-flow events potentially causes the watery tail as seen with gravel-rich debris flows thus explaining the increased erosion. Also, this might explain the lack of erosion within lower-gravel debris-flow events. When no draining occurs due to the lack of large intergranular pores as is the case for low-gravel debris flows, the tail is not fed by any surplus of water, resulting in a more solid tail, which potentially explains the compact appearance and thus the increased deposition per mm^2. Again, both deposition per mm^2 and erosion per mm^2 are dependent on the topography. The presence of a well-developed channel can increase runout of relative immobile debris flows, therefore decreasing the average deposition per mm^2. The presence of two well-developed channels on fan 02 during approximately 20 debris flows might have had an influence on the trend as presented in figure 4.24b. Also, volume has an impact on this trend, which becomes visible an average decrease in erosion for fan 02 goes hand in hand with a substantial increase in volume. Although these factors also play a role within this analysis, the established trend of increased erosion towards higher gravel fractions and an increased deposition towards lower-gravel fractions seems quite evident.

5.1.2. Bed roughness

In this section the general trends in relation to bed roughness as depicted in the results section are discussed. Results are related to literature and the usefulness for hazard mitigation is derived.

5.1.2.1. Average bed roughness

Results from this study show that for both fans average bed roughness increases during fan development. Obviously due to the continuing supply of gravel via the debris-flow events. The average bed roughness is calculated for the maximum extent of the fan, meaning that for the first debris flow, the maximum extent just comprised the area of that debris-flow event. This does mean that especially during the first debris-flow events one debris flow is able to completely change average bed roughness, as their relative area compared to the maximum fan area is significantly larger. Iverson (2010) and De Haas et al. (2015) emphasize that bed roughness is an important factor controlling grain-size segregation and granular agitation within a debris flow, where grain-size segregation promotes levee formation and eventually the debris-flow mobility. Iverson (2010) and Johnson (2012) elaborate that bed roughness causes basal shear influencing the velocity profile of the debris flow where velocity increases towards the top and does show shear and basal slip at the bottom. One might think that a change in velocity profile is able to affect debris-flow levee formation and thus also debris-flow runout distances. However, the results show that debris-flow behavior is largely unaffected by bed roughness and is most likely dependent on other factors such as topography and debris-flow volume.

5.1.2.2. Maximum runout and width/height ratio

In this study no increase or decrease in runout distance is visible towards higher and lower bed roughness's. The maximum runout seems largely unaffected by the change in bed roughness. Similarly, the width/height ratio per snout, especially for fan 02 remains unaffected. For fan 01 a decrease in bed roughness seem to increase width/height ratio. This means that for lower bed roughness's width is larger than height. This result would in fact follow the theory of Iverson (2010) and Johnson (2012) and the experimental results of De Haas et al. (2015) that a decrease in average bed roughness decreases internal grain-size segregation and therefore a less efficient levee formation, which in its turn might cause more sediment to deposit in a smaller area causing this increased width/height ratio. However, this would also affect runout distance and because no trend becomes apparent from that relation, the width/height ratio results should be approached with caution. Additionally, during most of the debris-flow events a channel already exists, therefore the sediment is already routed within a confined space, therefore the less efficient levee formation might be cancelled out by the routing ability of the present channel. It also must be considered that average bed roughness is a very simplistic value that is the average of all the bed roughness values underneath the complete debris-flow deposit. Bed roughness does show heterogeneity along the fan, which might influence debris-flow deposition. Therefore, this value should also be approached with caution

Also, no extra effect due to sieving is observed. A lack of matrix-poor deposits might be attributed to this (Hooke, 1967). However, when a gravel-rich matrix-poor debris flow deposited, the snout of that debris-flow eroded rather than to cause any enhanced infiltration due to sieving (as explained in section 4.6.3).

5.1.2.3. Body-snout analysis

The lobe-snout analysis shows for both fans on average, a higher roughness underneath the snout compared to the roughness underneath corresponding lobe. This might indicate that snouts favorably stop on rougher surface as the collisional effect of a rough bed with the debris flow increases energy dissipation and thus an early halt of the debris flow (De Haas & van Woerkom, 2016). But, there are many factors that influence this trend. For fan 01 this is the fact that roughness is higher towards more distal parts of the fan. When calculating the average bed roughness of the body this lowers the average to such an extent that dividing the snout with the lobe generally gives a value higher than 1. Also, debris-flow bodies regularly deposit within a channel, except during the searching phases. Because the debris-flow body mainly contains less gravel due to the internal grain size segregation causing gravel particles to be deposited in the front of the lobe or the levees, in-channel deposits are generally less rough. Indicating that channel beds generally have lower bed roughness's. This automatically implies that higher bed roughness's in the snouts are expected. The lobe-snout analysis might indicate that rougher bed does influence debris-flow deposition however, the relative influence of different factors is not established, therefore the true influence of bed roughness remains uncertain

Also, it must be considered that debris flows with different gravel fraction react differently to the bed. De Haas & van Woerkom (2016) mention that scour depth decreases towards lower gravel fraction due to more viscous behavior. This might also indicate the fact that viscous flow is less influenced by a rougher bed due to the decrease collisional effect and the subsequent dissipation of energy.

The bed roughness results within this study show no significant trend on the larger scale. The relative contribution of different factors also influencing the relationships must first be established to solely conclude anything about the effect of bed roughness on the fan evolution. It must be considered that a small disturbance might propagate through fan development it is therefore important to know the

exact effect of bed roughness on a single debris-flow behavior scale. It is also important to get to know the behavior under several morphologies, such as a present channel, steep sides etc. as topography is able to effectively influences debris-flow behavior.

5.1.3. Grain-size sequences favoring or inhibiting avulsion.

During this section, both fans will in places be related to the fan of the study of De Haas et al. (*in review*) with a similar sequence of magnitude of debris-flow events. The debris-flow fan avulsion cycle model as proposed by De Haas et al. (2016) (figure 2.7) holds also for the experimental fans in this study. During the spin-up phase debris flows were stacked on top of each other before the alternating channelization, searching and backstepping phases could occur. This is also seen during previous experiments that used the same experimental setup (De Haas et al. 2016; *in review*). Similarly, when the debris-flow fan grew more developed an increase in snouts became visible, especially during the searching phase (figure 4.3f & 4.15f). This number decreased during channelization phase where mostly just one or two channels were occupied.

Due to natural variance it is expected that the debris-flow fan in this study is superficially different from the fan in De Haas et al. (*in review*), however fan development and general processes occurring as depicted by De Haas et al. (*in review*) are expected to be the same. Due to the lack of more experiments containing the thin double-pareto magnitude-frequency distribution, this remains an assumption. Also, when taking into consideration this natural variation and the small differences in runout distances as depicted in the reference experiments between gravel fractions, 17 vol% and 48 vol%, the focus lies on the effects caused by the very low or very high gravel fractions. As it is hard to deduce if natural variation can be accounted or the effect of a small gravel-fraction in- or decrease.

In this section, first the effects of composition favoring or inhibiting avulsion are discussed for fan 01 and fan 02, then the magnitude sequences favoring or inhibiting avulsion as observed by De Haas et al. (*in review*) are viewed and the effect of the sediment composition on that sequence is discussed.

The main effect that becomes visible for both fan 01 and fan 02 is that the course of the debris flow is very much dependent of the volume, however extreme changes in debris-flow composition are able to affect debris-flow behavior. Gravel-rich debris-flow events seem to lose internal fluid faster (Iverson, 1997; 2010), which evidently reduces mobility and increases the chance of creating a channel plug or a decreased slope when no channel is present (Fan 01: DF 18; DF 46; DF74. Fan 02: DF01; DF15; DF 34; DF 69). Similar for gravel-poor debris-flow events, occasionally runout is reduced and a channel plug is deposited (Fan 01: DF22; DF 55. Fan 02: DF 33). Also in combination with the increased erosion during gravel-rich debris flows and the compactness of low-gravel debris flows the effect of debris-flow composition on fan evolution is noteworthy.

Local topography is also of importance to assess the effect of debris-flow sediment compositions on debris-flow behavior. For example, during the late stages of the backstepping phase, a plano-convex surface is present close to the apex (observed during experiments, and in the avulsion cycle model of De Haas et al., 2016). The lack of a pronounced channel with levees causes especially gravel-rich debris flows to stop rather early in relation to similar sized lower-gravel debris-flows. On Fan 01 this can be seen with DF 46 (6 kg; 72 vol% gravel) and DF 74 (7.7 kg; 72 vol% gravel). On Fan 02 this can be seen with DF 1 (7.1 kg; 56 vol% gravel) and DF 15 (11.1 kg; 72 vol% gravel). In all these situations the presence of a plano-convex profile causes the debris flow to stop early and to deflect trailing sediment to the sides of the debris-flow fan. Subsequently high amounts of erosion take place due to the trailing water. These high amounts of erosion can, when topography is favorable (large accommodation space on both sides of the apex), initiate a new avulsion cycle.

The in- or decreased mobility of a debris flow caused by its gravel fraction can be diminished when the debris-flow fan is in a searching phase of the avulsion cycle. For example, during the long-lasting searching phase on fan 01 (DF30-50) where debris-flow deposits contained multiple snouts, the effect of a change in sediment composition did not significantly affect debris-flow fan development. DF 33 (7.6 kg; 8 vol% gravel) having a low gravel fraction did show more compact behavior and less erosion, but it behaved quite similar to DF 32 (7.4 kg; 40 vol% gravel) which contained similar volume and also deposited when the fan was in its searching phase. DF 35 (6.2 kg; 56 vol% gravel), which according to the reference experiments is expected to have a decreased runout distances because of its higher gravel fraction, similarly showed a lack of influence on mobility due to this gravel fraction as on two of the four deposited snouts backstepping occured whereas on the other two still channelization occured. Although the effect of the searching phase diminishes the influence of gravel fraction on the mobility of the debris flow, the increased erosion for higher gravel fractions debris flows does still apply (figure 4.9). The results show that when deposition takes place on a confined space with multiple channels a change in debris-flow composition is not able to abruptly change the course of the debris-flow fan. However, the sediment composition effects such as decreased erosion and increased deposition per area for gravel-poor debris flows and the increased erosion for gravel-rich debris flows can subtly influence the course of the debris-flow fan. In light of propagation of a disturbance along the fan, a small increase in erosion can favor channelization potentially favoring an avulsion towards that side, whereas an increased deposition can create a small bulge, where a continuous supply of sediment potentially can turn this small bulge into a larger topographic high. This did not seem the case during the searching phase of fan 01, however it must be taken into mind. On fan 02 a long-lasting searching phase did not occur, so this trend cannot be deduced from fan 02.

The effect of a change in debris-flow sediment composition on avulsion behavior can also be derived when relating debris-flow sediment composition to sequences that favor avulsion. De Haas et al. (*in review*) observed that sequences of similar sized flows or flows with progressively decreasing size favor avulsion (DF 15-19; DF 25-29) and a channel plug sequence (DF 35-36) favored avulsion. Obviously, the effects of these sequences are different for each fan. For fan 01 the DF 15-19 sequence is quite interesting. Up until DF 17 the fan was in channelization phase, where debris-flow events were able to reach max fan extent. However, suddenly due to the decrease in size and possibly also due to the increased gravel fraction, DF 18 was not able to reach until half of the fan. Following debris flow, DF 19, was not able to overtop this plug due to the decrease in volume and therefore an avulsion was initiated. For the DF 25-29 sequence continuous channelization occurred up until DF 21, but due to the decrease in volume and the decrease in gravel-fraction within the debris flow a solid plug was formed that deflected subsequent debris-flow events and inhibited further avulsion.
On fan 02 also a backstepping sequence is found during DF 15-19 and DF 25-29, however gravel fractions were approximately around 25 vol% and 32 vol% without a significant change and therefore no effect of gravel fractions on that sequence could be deduced.

It becomes evident that debris-flow behavior depends on an interplay between volume, composition and topography of the debris flow and the debris-flow fan, where the volume of the debris flow affects the main behavior of the debris flow and composition can diminish or enhance this behavior based on the mobility of the sediment composition. Where the influence of composition over the influence of volume changes also depends on the topography at time of deposition.
It is therefore of importance to derive the magnitude-frequency distribution of a debris-flow fan system, then derive the sediment composition of the catchment to be able to predict debris-flow sediment composition. And then it is of importance to derive the current state of development of the debris-flow fan and the local topography. All these factors influence debris-flow behavior and fan evolution. It must be mentioned that on this experimental fan, the effect of debris-flow composition became the clearest when a change in gravel fraction was substantial. A small change in gravel fraction might also influence the course of the debris-flow however, due to the lack of comparative material

and the subtle influence of multiple factors such as local topography, local roughness and natural variability, this small change does not become visible.

5.1.4. Debris-flow composition affecting avulsion behavior and fan evolution on natural debris-flow fans

Studies on natural debris-flow fan avulsion behavior and evolution are scarce. The recent study of De Haas et al. (2017) claims to be the first systematic study of avulsion mechanisms on natural debris-flow fans. That study aims to identify generic spatio-temporal patterns controlling avulsions on debris-flow fans. They conclude that the magnitude-frequency distribution largely controls avulsion behavior. However, they weren't able to deduce any trends related to debris-flow compositions. As discussed earlier, to be able to derive any effects caused by debris-flow composition it is necessary to look at the effect it has on a sequence of several debris flows instead of the general patterns on the complete fan. When looking at single debris flows on natural debris-flow fans the influence of debris-flow sediment composition on mobility and the comparability with the constructed experimental fans becomes visible. As an example, observations on the Kamikamihori fan showed a debris flows that formed a matrix-poor boulder dam at its flow front, due to relatively immobile behavior. This caused deposition close to the apex, creating a channel plug and deflecting subsequent flows (Okuda et al., 1981; Suwa et al., 2009). In comparison with the experimental fans the same becomes visible, where a plano-convex surface in combination with a relative immobile gravel-rich debris flows created a plug subsequently deflecting its own watery tail to the sides as well as the sediment of subsequent flows.

Deriving sediment composition from debris flows during monitoring of natural debris flows on a debris-flow fan would possibly aid this discussion and give more insight into avulsion behavior and evolution of debris-flow fan

5.2. Scale effects.

Small-scale experimental debris flows exhibit disproportionately large effects of fluid yield strength, viscous flow resistance and grain inertia, while exhibiting disproportionately little effect of pore fluid pressure which caused runout distances to be relatively short compared to natural debris flows (Iverson, 1997; 2010; De Haas et al. 2015; 2016). Nevertheless, the typical debris-flow depositional features were formed (coarse grained levees, coarse grained snout, channel), which evidently shows that grain-size segregation and the increased buoyance of larger clasts are present (Johnson, 2012). De Haas et al. (2015) even concluded that the inundated area and channel width/depth ratio of debris flows within this experimental setup compared relatively to natural debris flows.

The two experimental fans that were created for this study encountered a few additional scale effects that should be considered. The first one being the fact that close to the apex extreme slopes could occur, especially during the early stages of fan development. Staley et al. (2005) did a survey of surficial patterns on 19 debris-flow fans and measured that mean fan gradient was at its highest close to the apex (up to 40 degrees), but values as high as seen during the experiments were not present (nearly vertical). The experimental results show that when the debris-flow fan showed a plano-convex curvature close to the apex due to a backstepping sequence sediment was routed to both the sides of the fan. Because this occurred due to a gravel-rich debris-flow event this was accompanied by high amounts of erosion. One can imagine that erosion due to trailing water is significantly higher on steep slopes than on shallow slopes. These extreme slopes were then eroded unrealistically deep. This deeper erosion lead to an increased focus toward that side of the fan. Concluding from both experimental fans, it is expected that subsequent sediment is direct toward the sides of the fan.

However, this deep incision potentially causes an increase in focus, meaning that the avulsion develops faster than it should due to this scale effect.

Time might also be an essential part during debris-flow fan development. Beaty (1970) estimated a debris-flow fan in White Mountains, California, U.S.A to be approximately 700.000 years old. During this period weathering of the surface might take place subsequently changing the surface morphology, especially on parts of the fan that encounter very little debris-flow activity. This might influence debris-fan development in the long run. Additionally Blair & McPherson (1994) concluded that reworking of surface morphology can be substantial when recurrence intervals of deposition are low and rates of reworking are high.

Although the experimental debris-flow fan might be influenced by the scale effects, the results show that the general expected trends are present and the similarities between the experimental and natural debris flows allow for quasi-realistic interactions between debris flows and evolving fan morphology. Therefore, the avulsion mechanisms and tendencies can be studied and broad comparisons with natural debris-flow fans can be made (cf. Paola et al., 2009 De Haas et al., 2016; 2017).

5.3. Implications for debris-flow hazard mitigation

The results of the experimental fans show that avulsion behavior and debris-flow fan development remains subjected to natural variability and multiple other factors of which the exact effects are not yet constrained (e.g. effect of bed roughness, topography). This causes the exact effect of composition on avulsion behavior and debris-flow fan development to remain somewhat concealed. An increase in availability of comparative studies on the effect of sediment composition on debris-flow fan development and avulsion behavior will potentially help reveal more information on the exact effect of a sediment composition change on debris-flow fan development and avulsion behavior. However, the two experimental fans clearly showed that both high- and low-gravel debris-flow composition influence the debris-flow behavior. For debris-flow hazard mitigation the importance lies in the prediction of avulsion behavior. De Haas et al. (*in review*) provided some guidelines for debris-flow hazard mitigation based on the magnitude-frequency distribution. They depict a sequence of moderate-sized debris flows to be an important possible avulsion trigger when followed by a larger-sized event. Additionally, they mention that large-volume debris flows are able to breach levees and create new channels during overbank surges. The results of my study can provide additional information to enhance these guidelines.

The results of this study show that a change in debris-flow sediment composition can enhance a backstepping sequence if it coincides with multiple low-mobility debris-flow sediment compositions. On the other hand, it can diminish the backstepping sequence when composed of multiple high-mobility debris-flow sediment compositions. However, for this situation it remains of importance to detect for channel plugs, as a volume change in combination with a channel plug remains animportant cause of avulsion during these sequences.

To predict impeding avulsions, it is of importance to map out topography and derive in which phase within the avulsion cycle (as proposed by De Haas et al. (2016)) the debris-flow fan is present (searching, backstepping, channelization). During the presence of a plano-convex surface close to the apex after a backstepping sequence, the conceptual model of De Haas et al. (2016) predicts that a searching phase initiates. However, this study shows that when a gravel-rich debris flow occurs during this stage, avulsion might occur within one debris-flow as gravel-rich debris flows stop early, subsequently deflecting the trailing watery body to the sides. This can create small channels where subsequent debris-flows are routed through.

Also, due to the increased erosive power of high-gravel debris flows compared to gravel-poor debris flows, the ability of large-volume debris flows to breach levees and create new channels during overbank surges is increased. High-volume debris flows seem to cause higher erosion when containing more gravel on the experimental fans (figure 4.12). These results are in accordance with experimental results from (De Haas & van Woerkom, 2016).

Concluding, to be able to correctly predict avulsion behavior, four factors should be constrained or estimated for the debris-flow fan system. (1) The magnitude-frequency distribution, (2) the grain-size distribution of the catchment and the sediment composition distribution for the debris flows, (3) the current phase within the avulsion cycle (channelization, backstepping, searching) in which the debris-flow fan is present and (4) the relatable local topography.

It must be stressed that during this study only a thin-double pareto magnitude-frequency distribution is used. The effects of composition on debris-flow fan development and avulsion behavior with different magnitude-frequency distributions might be different (De Haas et al., 2017; *in review*). Also, a change of water fraction did not occur within this experiment. As the effect of an in- or decrease of water fraction can be significant for both single debris-flow events and on debris-flow fan development (Whipple & Dunne, 1992; Iverson,2010; De Haas et al., 2015) it should be investigated further. Therefore, the need for further study is required.

6. CONCLUSION

In this study the effect of sediment composition change on avulsion behavior and debris-flow fan development is investigated. During this study, two experimental debris-flow fans are created, where the sequence of volumes corresponds to a fan from De Haas et al. (*in review*) where magnitude-frequency is distributed along a thin double-pareto distribution with an average of 5 kg sediment weight. The composition change on both experimental fans is distributed along a heavy-tailed double-pareto distribution where the average gravel fraction lies approximately around 25 vol% gravel. The sequence of compositions differs for both experimental fans, and are randomly taken from this distribution.

After consecutive stacking of debris-flow deposits during the spin-up phase, the avulsion cycle patterns as proposed by De Haas et al. (2016) are clearly visible. For both fan 01 and fan 02 general trends derived from the complete fan occasionally reveal some relationships. Most noteworthy is the effect of a sediment composition change on the erosion and deposition per mm^2. On the fan-scale, gravel-poor debris flows, reveal to be less erosive and more compact, showing an increased deposition per mm^2 towards low-gravel fractions. This only applies for fan 01, as other factors are able to influence the general deposition trends during fan 02 so that this trend does not become visible (e.g. long-lasting channelization phase). Vice versa, debris flows with higher amounts of gravel, reveal to be much more erosive. This trend is seen for both fan 01 and fan 02. Bed roughness does not show a pronounced effect on debris-flow behavior, which is most likely attributed to the large quantity of other factors controlling debris-flow behavior (topography, volume, sediment composition). Additionally, no sieving by gravel-rich deposits is visible on the experimental debris-flow fan.

The effect of a sediment composition change on avulsion behavior and debris-flow fan development is best seen on a timescale of a couple of debris-flow events. Three main conclusions can be established. (1) Debris-flow sediment composition is able to enhance or diminish the mobility of a debris flow with a given volume, where the volume dictates the main mobility of the debris flow but the mobility is influenced by related debris-flow sediment composition. In this study, a sudden increase in gravel fraction during a sequence of decreasing volume is able to instantly initiate an avulsion, whereas a more gradual transition is expected when composition remains similar. (2) The effect of debris-flow sediment composition on mobility is influenced by local topography. With a complex topography a change in composition does not significantly change runout. With a plano-convex surface close to the apex, the effect of a sediment composition is enhanced (best seen for gravel-rich debris flows). (3) An increase in erosion is seen with gravel-rich debris-flows. These are able to effectively enhance channelization. This increased erosion can act as initiator for avulsions, especially in cases where topography and fan development are favorable (e.g. steep slopes). Vice versa, gravel-poor debris flows are more likely to create a channel plug or deposit a solid body thereby influencing subsequent debris flows.

The results show that rather than a composition sequence favoring avulsion, avulsion behavior on the experimental fans is controlled by an interplay between volume sequence, fan topography and debris flow composition. For hazard mitigation it is therefore of importance to derive (1) the magnitude frequency distribution, (2) the grain-size distribution of the catchment and the composition of distribution for the debris flows, (3) the current development phase in which the debris-flow is present and (4), the local topography. Although the experimental fans in this study are only formed with the thin double-pareto magnitude-frequency distribution and a set of predetermined compositions, natural debris-flow fans might display different behavior. To increase understanding of the influence of debris-flow sediment composition on debris-flow fan development and avulsion behavior it is advised to derive composition from natural debris flows during monitoring of natural debris-flow fans.

REFERENCES

Addison, K. (1987). Debris flow during intense rainfall in Snowdonia, North Wales: a preliminary survey. Earth Surface Processes and Landforms, 12(5), 561-566.

Ahnert, F. (1970). Functional relationships between denudation, relief, and uplift in large, mid-latitude drainage basins. *American Journal of Science*, *268*(3), 243-263.

Ancey, C. (2001). Role of lubricated contacts in concentrated polydisperse suspensions. *Journal of Rheology*, *45*(6), 1421-1439.

Beaty, C. B. (1963). Origin of alluvial fans, White Mountains, California and Nevada. *Annals of the Association of American Geographers*, *53*(4), 516-535.

Beaty, C. B. (1968). *Sequential study of desert flooding in the White Mountains of California and Nevada*. MONTANA UNIV MISSOULA DEPT OF GEOGRAPHY.

Beaty, C. B. (1970). Age and estimated rate of accumulation of an alluvial fan, White Mountains, California, USA. *American Journal of Science*, *268*(1), 50-77.

Beaty, C. B. (1990). Anatomy of a White Mountains debris-flow—the making of an alluvial fan. *Alluvial Fans: A Field Approach. Wiley, New York*, 69-89.

Blair, T. C., & McPherson, J. G. (1992). The Trollheim alluvial fan and facies model revisited. *Geological Society of America Bulletin*, *104*(6), 762-769

Blair, T. C., & McPherson, J. G. (1994). Alluvial fans and their natural distinction from rivers based on morphology, hydraulic processes, sedimentary processes, and facies assemblages. *Journal of sedimentary research*, *64*(3).

Blair, T. C., & Mcpherson, J. G. (1995). Alluvial Fans and Their Natural Distinction from Rivers Based on Morphology, Hydraulic Processes, Sedimentary Processes, and Facies Assemblages: REPLY. *Journal of Sedimentary Research*, *65*(4).

Blair, T. C., & McPherson, J. G. (1998). Recent debris-flow processes and resultant form and facies of the Dolomite alluvial fan, Owens Valley, California. *Journal of Sedimentary Research*, *68*(5).

Blair, T. C., & McPherson, J. G. (2009). Processes and forms of alluvial fans. In *Geomorphology of Desert Environments* (pp. 413-467). Springer Netherlands.

D'Agostino, V., Cesca, M., & Marchi, L. (2010). Field and laboratory investigations of runout distances of debris flows in the Dolomites (Eastern Italian Alps). *Geomorphology*, *115*(3), 294-304.

Dowling, C. A., & Santi, P. M. (2014). Debris flows and their toll on human life: a global analysis of debris-flow fatalities from 1950 to 2011. *Natural hazards*, *71*(1), 203-227.

Dühnforth, M., Densmore, A. L., Ivy-Ochs, S., Allen, P. A., & Kubik, P. W. (2007). Timing and patterns of debris flow deposition on Shepherd and Symmes creek fans, Owens Valley, California, deduced from cosmogenic 10Be. *Journal of Geophysical Research: Earth Surface*, *112*(F3).

Egashira, S., Honda, N., & Itoh, T. (2001). Experimental study on the entrainment of bed material into debris flow. Physics and Chemistry of the Earth, Part C: Solar, Terrestrial & Planetary Science, 26(9), 645-650.

Friele, P. A., & Clague, J. J. (2005). Multifaceted hazard assessment of Cheekye fan, a large debris-flow fan in south-western British Columbia. In Debris-flow Hazards and Related Phenomena (pp. 659-683). Springer, Berlin, Heidelberg.

Haas, T., Ventra, D., Carbonneau, P. E., & Kleinhans, M. G. (2014). Debris-flow dominance of alluvial fans masked by runoff reworking and weathering. Geomorphology, 217, 165-181.

Haas, T., Braat, L., Leuven, J. R., Lokhorst, I. R., & Kleinhans, M. G. (2015). Effects of debris flow composition on runout, depositional mechanisms, and deposit morphology in laboratory experiments. *Journal of Geophysical Research: Earth Surface*, *120*(9), 1949-1972.

Haas, T., Berg, W., Braat, L., & Kleinhans, M. G. (2016). Autogenic avulsion, channelization and backfilling dynamics of debris-flow fans. *Sedimentology*, *63*(6), 1596-1619.

De Haas, T., Densmore, A. L., Stoffel, M., Suwa, H., Imaizumi, F., Ballesteros-Cánovas, J. A., & Wasklewicz, T. (2017). Avulsions and the spatio-temporal evolution of debris-flow fans. Earth-Science Reviews.

Haas, T., Kruijt, A., Densmore, A.L. (*in review*) Effects of magnitude-frequency distribution on debris-flow avulsions and fan development. *Earth Surface Dynamics*

Helsen, M. M., Koop, P. J. M., & Van Steijn, H. (2002). Magnitude–frequency relationship for debris flows on the fan of the Chalance torrent, Valgaudemar (French Alps). *Earth Surface Processes and Landforms*, *27*(12), 1299-1307.

Hobson, R. D. (1972). Surface roughness in topography: quantitative approach. Methuen.

Hooke, R. L. (1967). Processes on arid-region alluvial fans. *The Journal of Geology*, *75*(4), 438-460.

Hooke, R. L., Blair, T. C., & McPherson, J. G. (1993). The Trollheim alluvial fan and facies model revisited: Discussion and reply. *Geological Society of America Bulletin*, *105*(4), 563-567.

Hoefling, R. (2004, May). High-speed 3D imaging by DMD technology. In Machine Vision Applications in Industrial Inspection XII (Vol. 5303, pp. 188-195). International Society for Optics and Photonics.

Hungr, O., Evans, S. G., Bovis, M. J., & Hutchinson, J. N. (2001). A review of the classification of landslides of the flow type. *Environmental & Engineering Geoscience*, *7*(3), 221-238.

Iverson, R. M. (1997). The physics of debris flows. *Reviews of geophysics*, *35*(3), 245-296.

Iverson, R. M., Logan, M., LaHusen, R. G., & Berti, M. (2010). The perfect debris flow? Aggregated results from 28 large-scale experiments. *Journal of Geophysical Research: Earth Surface*, *115*(F3).

Jakob, M. (2005). Debris-flow hazard analysis. In Debris-flow hazards and related phenomena (pp. 411-443). Springer Berlin Heidelberg.

Jakob, M., Hungr, O., & Jakob, D. M. (2005). Debris-flow hazards and related phenomena (Vol. 739). Berlin: Springer.

Jakob, M., Stein, D., & Ulmi, M. (2012). Vulnerability of buildings to debris flow impact. *Natural Hazards*, *60*(2), 241-261.

Larsen, M. C., Wieczorek, G. F., Eaton, L. S., Morgan, B. A., & Torres-Sierra, H. (2002). *Natural hazards on alluvial fans; The Venezuela debris flow and flash flood disaster* (No. 103-01).

Lin, C. W., Shieh, C. L., Yuan, B. D., Shieh, Y. C., Liu, S. H., & Lee, S. Y. (2004). Impact of Chi-Chi earthquake on the occurrence of landslides and debris flows: example from the Chenyulan River watershed, Nantou, Taiwan. Engineering geology, 71(1-2), 49-61.

Major, J. J. (1997). Depositional processes in large-scale debris-flow experiments. *The Journal of Geology*, *105*(3), 345-366.

Marchi, L., Arattano, M., & Deganutti, A. M. (2002). Ten years of debris-flow monitoring in the Moscardo Torrent (Italian Alps). *Geomorphology*, *46*(1), 1-17.

McCoy, S. W., Kean, J. W., Coe, J. A., Staley, D. M., Wasklewicz, T. A., & Tucker, G. E. (2010). Evolution of a natural debris flow: In situ measurements of flow dynamics, video imagery, and terrestrial laser scanning. *Geology*, *38*(8), 735-738.

Milana, J. P., & Tietze, K. W. (2002). Three-dimensional analogue modelling of an alluvial basin margin affected by hydrological cycles: processes and resulting depositional sequences. *Basin Research*, *14*(3), 237-264.

Milana, J. P. (2010). The sieve lobe paradigm: Observations of active deposition. *Geology*, *38*(3), 207-210.

Okuda, S., Suwa, S., Okunishi, K., & Yokoyama, K. (1981). Depositional processes of debris flow at Kamikamihori fan, Northern Japan Alps. *Trans. Japan. Geomorph. Union*, *2*(2), 353-361.

Olaya, V. (2009). Basic land-surface parameters. Developments in Soil Science, 33, 141-169.

Paola, C., Straub, K., Mohrig, D., & Reinhardt, L. (2009). The "unreasonable effectiveness" of stratigraphic and geomorphic experiments. *Earth-Science Reviews*, *97*(1-4), 1-43.

Pederson, C. A., Santi, P. M., & Pyles, D. R. (2015). Relating the compensational stacking of debris-flow fans to characteristics of their underlying stratigraphy: Implications for geologic hazard assessment and mitigation. *Geomorphology*, *248*, 47-56.

Pierson, T. C. (2005). *Distinguishing between debris flows and floods from field evidence in small watersheds* (No. 2004-3142). US Geological Survey.

Ritter, J. B., Miller, J. R., Enzel, Y., & Wells, S. G. (1995). Reconciling the roles of tectonism and climate in Quaternary alluvial fan evolution. *Geology*, *23*(3), 245-248.

Santi, P. M., Hewitt, K., VanDine, D. F., & Cruz, E. B. (2011). Debris-flow impact, vulnerability, and response. *Natural hazards*, *56*(1), 371-402.

Savage, W., & Baum, R. (2005). Instability of steep slopes. Debris-flow hazards and related phenomena, 53-79.

Schwanghart, W., Kuhn, N. J. (2010): TopoToolbox: a set of Matlab functions for topographic analysis. Environmental Modelling & Software, 25, 770-781. [DOI: 10.1016/j.envsoft.2009.12.002]

Sharp, R. P., & Nobles, L. H. (1953). Mudflow of 1941 at Wrightwood, southern California. Geological Society of America Bulletin, 64(5), 547-560.

Shieh, C. L., Chen, Y. S., Tsai, Y. J., & Wu, J. H. (2009). Variability in rainfall threshold for debris flow after the Chi-Chi earthquake in central Taiwan, China. *International Journal of Sediment Research*, *24*(2), 177-188.

Staley, D. M., Wasklewicz, T. A., & Blaszczynski, J. S. (2006). Surficial patterns of debris flow deposition on alluvial fans in Death Valley, CA using airborne laser swath mapping data. Geomorphology, 74(1-4), 152-163.

Straub, K. M., Paola, C., Mohrig, D., Wolinsky, M. A., & George, T. (2009). Compensational stacking of channelized sedimentary deposits. *Journal of Sedimentary Research*, *79*(9), 673-688.

Suwa, H., & Okuda, S. (1983). Deposition of debris flows on a fan surface, Mt. Yakedake, Japan. *Z. Geomorphol. Suppl*, *46*, 79-101

Suwa, H., Okano, K., & Kanno, T. (2009). Behavior of debris flows monitored on test slopes of Kamikamihorizawa Creek, Mount Yakedake, Japan. *International Journal of Erosion Control Engineering*, *2*(2), 33-45.

Suwa, H. I. R. O. S. H. I., Okano, K. A. Z. U. Y. U. K. I., & Kanno, T. A. D. A. H. I. R. O. (2011). Forty years of debris flow monitoring at Kamikamihorizawa Creek, Mount Yakedake, Japan. In *5th international conference on debris-flow hazards mitigation: mechanics, prediction and assessment. Casa Editrice UniversitaLa Sapienza, Roma* (pp. 605-613).

Takahashi, T. (1981). Debris flow. *Annual review of fluid mechanics*, *13*(1), 57-77.

Takahashi, T. (2014). Debris flow: mechanics, prediction and countermeasures. CRC press.

Totschnig, R., Sedlacek, W., & Fuchs, S. (2011). A quantitative vulnerability function for fluvial sediment transport. *Natural Hazards*, *58*(2), 681-703.

Van Asch, T. (2013). *Mountain risks: from prediction to management and governance*. J. Corominas, S. Greiving, J. P. Malet, & S. Sterlacchini (Eds.). Springer-Verlag.

Ventra, D., & Nichols, G. J. (2014). Autogenic dynamics of alluvial fans in endorheic basins: Outcrop examples and stratigraphic significance. *Sedimentology*, *61*(3), 767-791.

Whipple, K. X., & Dunne, T. (1992). The influence of debris-flow rheology on fan morphology, Owens Valley, California. *Geological Society of America Bulletin*, *104*(7), 887-900.

Wohl, E. E., & Pearthree, P. P. (1991). Debris flows as geomorphic agents in the Huachuca Mountains of southeastern Arizona. *Geomorphology*, *4*(3-4), 273-292.

Xiong, M., Meng, X., Wang, S., Guo, P., Li, Y., Chen, G., ... & Zhao, Y. (2016). Effectiveness of debris flow mitigation strategies in mountainous regions. *Progress in Physical Geography*, *40*(6), 768-793.

SUPPLEMENTARY MATERIAL

Movie S1: Movie of top-down pictures taken after each debris flow on fan 01.

Movie S2: Movie of top-down pictures taken after each debris flow on fan 02.

Movie S3: Movie of top-down images of net deposition after each debris flow on fan 01.

Movie S4: Movie of top-down images of net deposition after each debris flow on fan 02.

Movie S5: Movie of 3D surface plots with net deposition after each debris flow on fan 01.

Movie S6: Movie of 3D surface plots with net deposition after each debris flow on fan 02.

Folder 'Photos & Videos RE': Folder containing photos and videos taken after each debris flow during the reference experiments.

Folder 'Photos & Videos fan 01': Folder containing photos and videos taken after each debris flow on fan 01

Folder 'Photos & Videos fan 02': Folder containing photos and videos taken after each debris flow on fan 02.